HYPORHEIC ZONE PROCESS CONTROLS ON DISSOLVED ORGANIC CARBON QUALITY

by

Paul James Gabrielsen

Submitted in partial fulfillment

of the requirements for the degree of

Master of Science in Hydrology

Department of Earth and Environmental Science

New Mexico Institute of Mining and Technology

Socorro, New Mexico, USA

May 2012

To Bethany, who deserves more credit for this than I do and who never let me quit.

ABSTRACT

Hyporheic zones (regions of streamwater-groundwater interaction) play a significant role in stream nutrient and dissolved organic carbon (DOC) processing. The nature of seasonal hyporheic DOC dynamics (in a meander bend of the East Fork Jemez River in northern New Mexico) and the processes behind them (in a new model of DOC transformation) were examined in this thesis. Two DOC flushing events were observed during the field study, during snowmelt and monsoon seasons. DOC quality provided evidence of hyporheic exchange during pre-monsoon months. To address mechanisms of DOC quality evolution, a new agent-based model (where DOC molecules are represented as individual agents) couples fluid dynamics with chemical and biological transformation of DOC in a porous medium. At the pore scale, size-dependant diffusion and variation in DOC source composition emerged as controls on DOC quality. This work represents a step toward understanding seasonal hyporheic zone DOC dynamics and the parameters controlling DOC transformation.

Keywords: dissolved organic carbon; hyporheic zone; agent-based modeling; NetLogo; excitation-emission matrices

ACKNOWLEDGEMENTS

Many thanks for the patient mentorship of my advisors, John Wilson and Michael Pullin, and for the insight and advice offered by my committee members Fred Phillips and Cliff Dahm. I would like to thank my colleagues who provided field assistance, data, figures, and insight: Jesús Gómez (who has contributed extensively to understanding the hydrology of the field site), Jevon Harding, Brian Cozzens, Carlos Ramírez-Torres, David Krzesni, Yaika Echevarría-Román, Asitha Cooray, and Ryan Schwingle. Thanks also to colleagues at the University of New Mexico: Laura Crossey and Lauren Sherson for sharing samples and data, and Steve Cabaniss for his insight into agent-based modeling and for his comments on my work. Thanks to my professors at Brigham Young University, especially Barry Bickmore and Steve Nelson who taught me how to approach a problem experimentally and John Bennion who taught me how to write and revise. Also thanks to my parents; my father's career inspired me to pursue hydrology and my mother suffered through her own graduate school experience alongside mine. Most especially, thanks to my wife Bethany and our daughters Grace and Alice for their unending patience and support. This work was supported by New Mexico EPSCoR (NSF Grant #0814449) and by a National Science Foundation Graduate Research Fellowship.

TABLE OF CONTENTS

LIST OF TABLES

LIST OF FIGURES

INTRODUCTION

Dissolved organic carbon (DOC), consisting of water-soluble organic molecules and byproducts of organic decomposition and chemical degradation processes, constitutes a critical link in carbon and nutrient cycles. The quality, or chemical and physical character, of DOC affects the degree to which it is transformed by biological and chemical processes. In turn, DOC quality affects microbial ecology, metal mobilization in streams, and anthropogenic organic contaminant solubility. This study investigates factors affecting DOC quality changes in hyporheic zones (HZs), areas of groundwater-stream water interactions that are hotspots of DOC processing.

I. Dissolved Organic Carbon

DOC is ubiquitous in natural waters and ranges in concentrations from ~0.5 mg/L in sea water to upwards of 30 mg/L in peat bogs (Thurman, 1985). It is operationally defined as the amount of organic carbon passing through a 0.45 μm filter (although other pore sizes, such as 0.7 μm and 0.2 μm, are often used). Fractions of DOC can be divided into humic acids, insoluble below pH = 2, and fulvic acids, soluble regardless of pH.

DOC is not a homogeneous substance; rather it is composed of a complex, heterogeneous mixture of organic molecules. The chemical composition and characteristics of DOC can

change independent of its quantity (Lutz et al., 2012), and can provide information about DOC source (McKnight et al., 2001) and history (Klapper et al., 2002). In this thesis, DOC chemical composition, measured through several metrics consistently used in the literature, defines DOC quality. Changes in DOC quality affect its bioavailability (Amon & Benner, 1996; Cabaniss et al., 2005; Chappelle et al., 2009) and metal binding properties (Cabaniss, 2008; Pullin et al., 2004). While DOC is ubiquitous in natural waters this study will focus on its role in hyporheic zones.

II. DOC in Hyporheic Zones

Hyporheic zones (HZs) in sediments adjacent to streams are usually defined one of three ways (Tonina & Buffington, 2009). In the geochemical definition, a hyporheic zone must contain at least 10% surface water (Triska et al., 1989). This surface water delivers nutrients, including DOC, to hyporheic sediments. The influx of nutrients from surface waters is reflected in the biological definition, in which the presence of macroinvertebrate riverine fauna delinates the hyporheic zone (Stanford & Ward, 1988). This faunal population is distinct from typically subterranean species (ibid.). The hydraulic definition includes a return of hyporheic water (and solutes) to surface water, encompassing hydrologic flowpaths that begin and end in the stream (Tonina & Buffington, 2007). In this thesis, the hyporheic zone is defined according to the hydraulic definition.

As a source of organic carbon, DOC is both consumed and produced by biota in streams and HZs, and can be a limiting factor in ecosystem metabolism (Wetzel, 1992; Wetzel, 1995; Baker et al., 1999). DOC transformative processes, notably microbial processing and photodegradation, can occur in the stream channel, but HZ nutrient processing is so significant in riverine DOC metabolism that HZs have been dubbed “the river’s liver”

(Fischer et al., 2005) and are generally considered a sink of DOC (Findlay et al., 1993). Interactions between surface water and groundwater serve as a "control point" for nutrient fluxes (Hedin et al., 1998) with a variety of terminal electron accepting processes active in HZs such as denitrification, iron and sulfate reduction, and methanogenesis (Baker et al., 1999; Zarnetske et al., 2011). In semiarid catchments with highly variable hydrology, DOC export and biogeochemical activity can be controlled by the degree of connectivity between groundwater and surface water (Brooks & Lemon, 2007).

III. DOC Quality Implications

Given the long residence times and significant biogeochemical activity in HZs (Fischer et al., 2005), it is essential to understand how HZ processes affect DOC quality.

Aqueous metal geochemistry is strongly affected by the presence of DOC. Metal solubility and mobility is enhanced by DOC (Davis & Leckie, 1978); however, DOC binding to soluble metals reduces metal bioavailability, competing with biological uptake ligands (Di Toro et al., 2001). DOC quality significantly affects metal binding affinity (Bartschat et al., 1992). For example, higher phenol and carboxylic acid content leads to increased copper binding affinity (Cabaniss et al., 2007).

Solubility of xenobiotic contaminants can also be affected by DOC quality. Adsorption of hydrophobic organic compounds (Chiou et al., 1986; Li & LeBoeuf, 2010) and dissolved pharmaceuticals (Pan et al., 2009) has been shown to be affected by the presence of humic material, with phenol and carboxyl groups and lignin decomposition products providing preferential binding sites (Thiele-Bruhn et al., 2004).

Xenobiotic degradability also may be indirectly related to environmental DOC quality. Microbial communities can acclimate to changes in their environment, including changes in organic carbon quality (Chappelle, 1993). It is not unreasonable to speculate, then, that a microbial community would be better able to biodegrade a xenobiotic organic contaminant with similar characteristics to the DOC the community is used to consuming. Thus, environmental DOC quality may help or hinder natural bioremediation capacity.

IV. Possible Climate Change Effects on DOC Quality

Since HZ size and water residence time are dependent on stream hydrology (Cardenas, 2009), hydrological changes due to climate change have the capacity to alter HZ effects on stream biogeochemistry.

In the desert southwest of the United States, climate change is projected to develop a hotter, drier climate with less precipitation falling as snow (USGCRP, 2009), earlier peak runoff, and extended periods of low flow in streams (State of New Mexico, 2005). The effect of climate change on monsoonal precipitation is currently unknown (USGCRP, 2009).

The impact of these climatic changes on DOC quality is difficult to forecast. Higher CO_2 levels may drive plant growth (Ainsworth & Long, 2005), while warmer temperatures may speed organic decomposition and microbial activity (Andrews et al., 2000). A decline in snowpack and snowmelt events could change the timing and magnitude of DOC transport to streams (Brooks et al., 1999), while extended periods of low stream flow in summers would affect the extent of hyporheic flow (Wroblicky et al.,1998).

Projections of future stream DOC quality require a thorough understanding of current DOC controls. HZ DOC processing is a focus of this research area. Recently, Wong & Williams (2009) investigated seasonal patterns of DOC dynamics in a streambed hyporheic zone in Guelph, Ontario, Canada. Tracking aromaticity, molecular weight, and fluorescence properties, they observed seasonal changes in surface water and hyporheic zone DOC, attributed to changing DOC inputs and microbial activity.

As observed by Baker et al. (2000), Dahm et al. (2003), and Wong & Williams (2009), stream DOC quality varies seasonally in response to hydrological and ecological variation. This thesis investigates the role of the hyporheic zone in controlling DOC quality, particularly under transient seasonal conditions in which source DOC quality and hyporheic environmental conditions vary.

V. Research Questions

The primary research question of this thesis is:

How do hyporheic zone physical, chemical, and biological processes interact with and control DOC quality (physical and chemical characteristics) in stream ecosystems?

Reactive transport modeling is employed along with field data to answer this question.

To examine the seasonal dynamics of DOC in a natural system, a meander bend of the East Fork Jemez River was sampled for groundwater and surface water DOC during the fall of 2010 and during spring, summer, and fall of 2011. DOC quality metrics, inorganic chemistry, and physical hydrology were used to investigate the seasonal hydrology of the meander and the nature and extent of associated groundwater-surface water interactions. DOC chemical transformations were modeled using an agent-based modeling approach to

investigate factors affecting changes in DOC quality, including variation in DOC source composition.

Throughout this thesis, the following metrics were used to assess DOC quality, in addition to dissolved organic carbon concentration:

- Molecular weight averages. Generally, fulvic acid molecular weights follow a log-normal distribution (Cabaniss et al., 2000) described by a number average (M_n) and a weight average (M_w).
- Fluorescence Index (FI), a ratio of fluorescent emission at 450 nm to that at 500 nm (excited at 370 nm) is correlated to DOC source (McKnight et al., 2001).
- Aromaticity, or percentage aromatic carbon. Molar absorptivity at 280 nm (ε280) is an excellent proxy for aromaticity (Chin et al., 1994).
- Parallel Factor Analysis (PARAFAC), a statistical decomposition technique used to discern and quantify fluorophores, chemical structures which absorb and re-emit light, (Mopper et al., 1996) contributing to the spatial and/or temporal variation in DOC fluorescence (Stedmon and Bro, 2008).

The remainder of this thesis consists of three chapters.

Chapter 2, Dissolved Organic Carbon Dynamics in a Meander of the East Fork of the Jemez River, examines hydrological effects on DOC in a meander bend aquifer in the Valles Caldera National Preserve in northern New Mexico, including effects of seasonal snowmelt and monsoon events.

Chapter 3, Modeling Environmental and Chemical Effects on Subsurface Dissolved Organic Carbon Transformation, investigates what factors in the subsurface environment or in precursor DOC quality affect abiotic and biotic DOC processing.

Finally, a concluding synthesis chapter integrates the lessons learned through these activities.

CHAPTER 2: DISSOLVED ORGANIC CARBON DYNAMICS IN A MEANDER OF THE EAST FORK OF THE JEMEZ RIVER

I. Introduction

To examine hydrologically-influenced dynamics of DOC quality within hyporheic ecosystems, a field study was conducted at a meander-induced hyporheic zone on the East Fork Jemez River (in the Valles Caldera National Preserve, Sandoval County, New Mexico, see Figure 1) to observe changes in DOC quality over temporal and spatial scales in both stream waters and shallow (hyporheic) groundwaters.

This field study primarily investigates the role of hydrology as a control on DOC quality in a hyporheic zone. However, the hydrology of this site informs DOC biogeochemistry and vice versa: DOC quality data provide dynamic information about site hydrology in addition to conventional hydrologic measurement techniques. We propose that DOC quality can act as a tracer (albeit a reactive, non-conservative tracer) between the stream and the groundwater, providing information on the timing, nature, and extent of groundwater-surface water interactions.

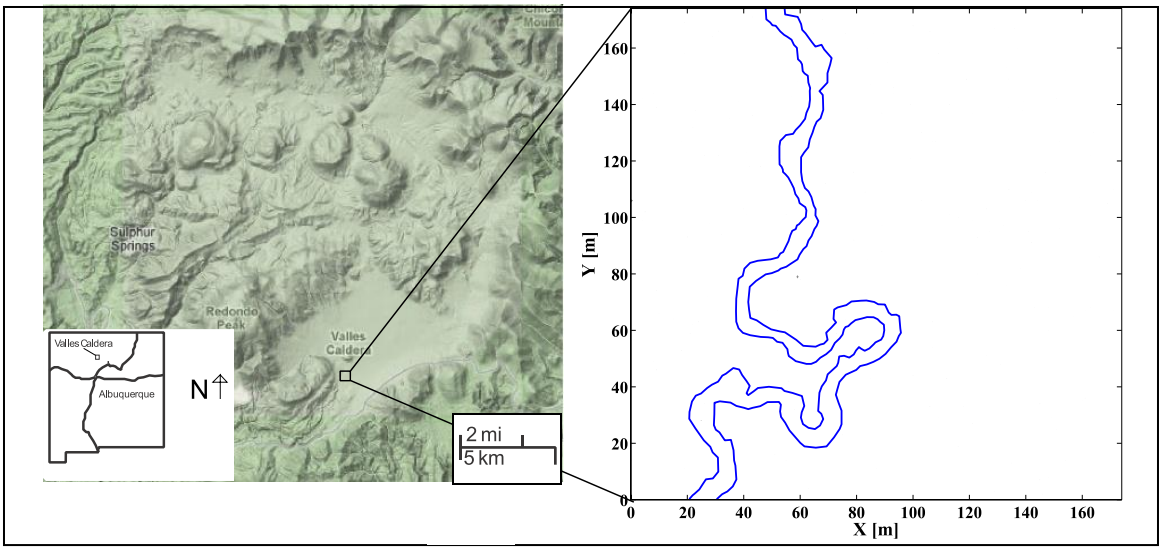

Figure 1. Location of Jemez River meander site within Valles Caldera National Preserve in northern New Mexico. The site is located within an elk exclosure fence with an extent corresponding to the boundary of the rightmost figure.

In mountain stream systems, pulses of DOC are connected to hydrological events, i.e. snowmelt (Hornberger et al., 1994) and monsoonal precipitation (Brooks et al., 2007). Brooks et al. (2007) studied the semiarid San Pedro River in Arizona, which does not experience snowmelt. They found that 96% of annual organic carbon export occurred during the monsoon season, with 92% of that carbon in particulate form. In the San Pedro, DOC dominated carbon export during non-monsoonal periods while particulate organic carbon (POC, defined as greater than 0.7 μm in diameter) dominated during the monsoon.

Hydrological controls mobilize previously generated DOC pools during snowmelt events (Brooks et al., 1999). In areas susceptible to drought, DOC can build up in aerated soils during low water table times and be available for flushing when the water table recovers (Dahm et al., 2003). DOC export in snowmelt-dominated systems is controlled by over-winter heterotrophic activity that generates a mobile organic carbon pool available for flushing to streams (Brooks et al., 1999).

Kostrzewski (2005) observed a DOC pulse during snowmelt and none during the monsoon season in Valles Caldera streams, concluding "that both hydrologic and biogeochemical controls are weak during snow accumulation in winter, hydrologic controls become dominant during the snowmelt period and biogeochemical controls are stronger than hydrologic controls during the summer monsoon" (quoted in Liu, 2008). In this study, during the 2011 field season, both snowmelt and monsoonal pulses of DOC were observed (see Chapter 2). Through multi-metric analysis, this field study strives to understand the origin and characteristics of seasonal DOC dynamics, including the two observed DOC pulses.

In addition to dissolved organic carbon concentration, several other metrics were used in this study. Ultraviolet absorbance data were used to calculate molar absorptivity at 280 nm (ε280), a proxy for DOC aromaticity (Chin et al., 1994). DOC fluorescence was used to calculate the fluorescence index (FI), a measure of DOC origin (McKnight et al., 2001). High pressure size exclusion chromatography (HP-SEC) generated distributions of molecular weight, from which three metrics were derived: the number average molecular weight (M_n), weight average molecular weight (M_w) and polydispersity, the latter being a ratio of M_w/ M_n and an indicator of the distributions' shape. Parallel Factor Analysis (PARAFAC) was used to statistically decompose fluorescence data into fluorophore components (Stedmon & Bro, 2008).

II. Field Site

Field activities were carried out at an instrumented meander of the East Fork Jemez River in Valles Caldera National Preserve, Sandoval County, New Mexico (35.841, -106.501), hereafter referred to as the Jemez River meander. The meander is located in the Valle

Grande, a broad 7.00 km x 4.33 km meadow within the larger rhyolitic Valles Caldera structure. The caldera lies along the Jemez Lineament that last erupted catastrophically 1.25 million years ago, forming the welded tuff deposits visible throughout the Jemez mountains (Smith et al., 1970; Phillips, 2004). More recent volcanic activity is evidenced by resurgent domes and a high temperature geothermal system within the caldera (Goff & Gardner, 1994). The Valle Grande was formed as lacustrine deposits filled the caldera between 1.25 Ma and 55 ka (Goff et al., 2005).

The East Fork Jemez River drains a 114 km^2 area of 50% evergreen forests, 41% grassland, 9% shrubland and less than 1% deciduous forest (New Mexico Environment Department, 2006). Grasslands, primarily within the Valle plains, are Parry's oatgrass (*Danthonia parryi*), Arizona fescue, Idaho fescue (*Festuca arizonica, F. idahoensis*), and Kentucky bluegrass (*Poa pratensis*), among others. Sedges (*Carex* spp.) are plentiful along stream banks (Parmenter, pers. comm.). Dominant tree species in the Preserve are Ponderosa pine (*Pinus ponderosa*), white fir (*Abies concolor*), Douglas fir (*Pseudotsuga menziesii*), Engelmann spruce (*Picea engelmannii*), aspen (*Populus tremuloides*), southern white pine (*Pinus monticola*), and corkbark fir (*Abies lasiocarpa*; ibid). Mean annual air temperature is 9°C and precipitation averages 476 mm/yr (Bowen, 1996). Snowfall, between October and April, comprises 40% of annual precipitation, and snowmelt drives peak stream flow between late March and mid-May (Rodriguez & Moser, 2010). Monsoonal precipitation in July, August, and September comprises another 50% (Bowen, 1996) of annual precipitation. An elevated water table, due to hydrological events, results in surface ponding and expansion of saturated areas in the Valle Grande, including at the Jemez River meander site. A hydrograph of the Jemez

River discharge during 2010 and 2011, measured at USGS gauge 08324000 below the confluence of the Jemez River and San Antonio Creek (several km downstream of the Jemez River meander), appears in Figure 2, showing effects of snowmelt and monsoon events on stream discharge. Discharge during the monsoon season (July – Nov, both years) is punctuated by sudden strong discharge events. The connection of these events to precipitation events will be addressed in Section V.

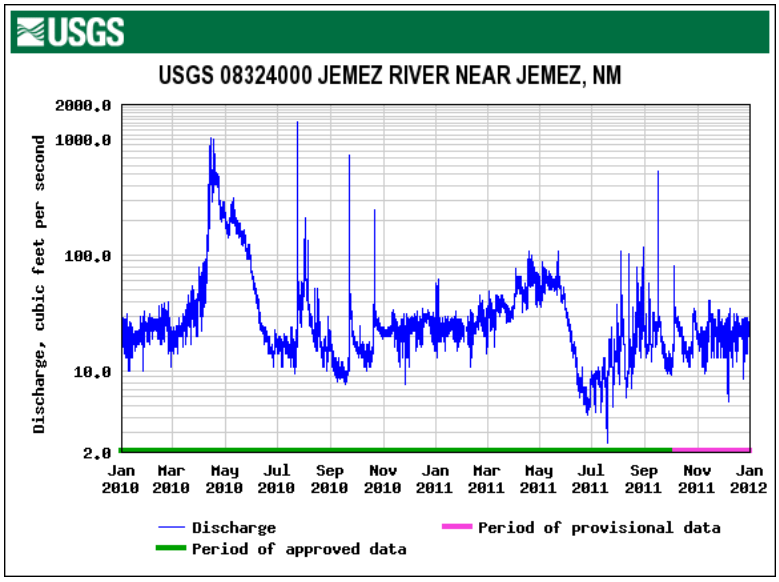

Figure 2. Stream discharge data at USGS stream gauge several km downstream of Jemez River meander site for 2010 and 2011. Note snowmelt events beginning in Mar 2010 and Feb 2011 and monsoonal floods in late summer and early fall, both years. Data and figure from US Geological Survey National Water Information System (nwis.waterdata.usgs.gov, accessed 27 Mar 2012).

The Jemez River meander is located within a fenced square elk exclosure (160 m on a side) constructed by the Valles Caldera National Preserve. Well logs from shallow groundwater well installation (see Appendix C) show that the top two feet of sediment at the meander site consist of silty loam (Rodriguez & Moser, 2010), underlain with poorly sorted gravels ranging in size from coarse sand to coarse sub-rounded gravel. Streambed sediments are comprised of medium to coarse sub-angular gravel. Turbidity progressively

increases along the length of the East Fork Jemez. This has been attributed to the influence of fine clay-like ash particles in the lacustrine sediments of the Valle Grande (Rodriguez & Moser, 2010).

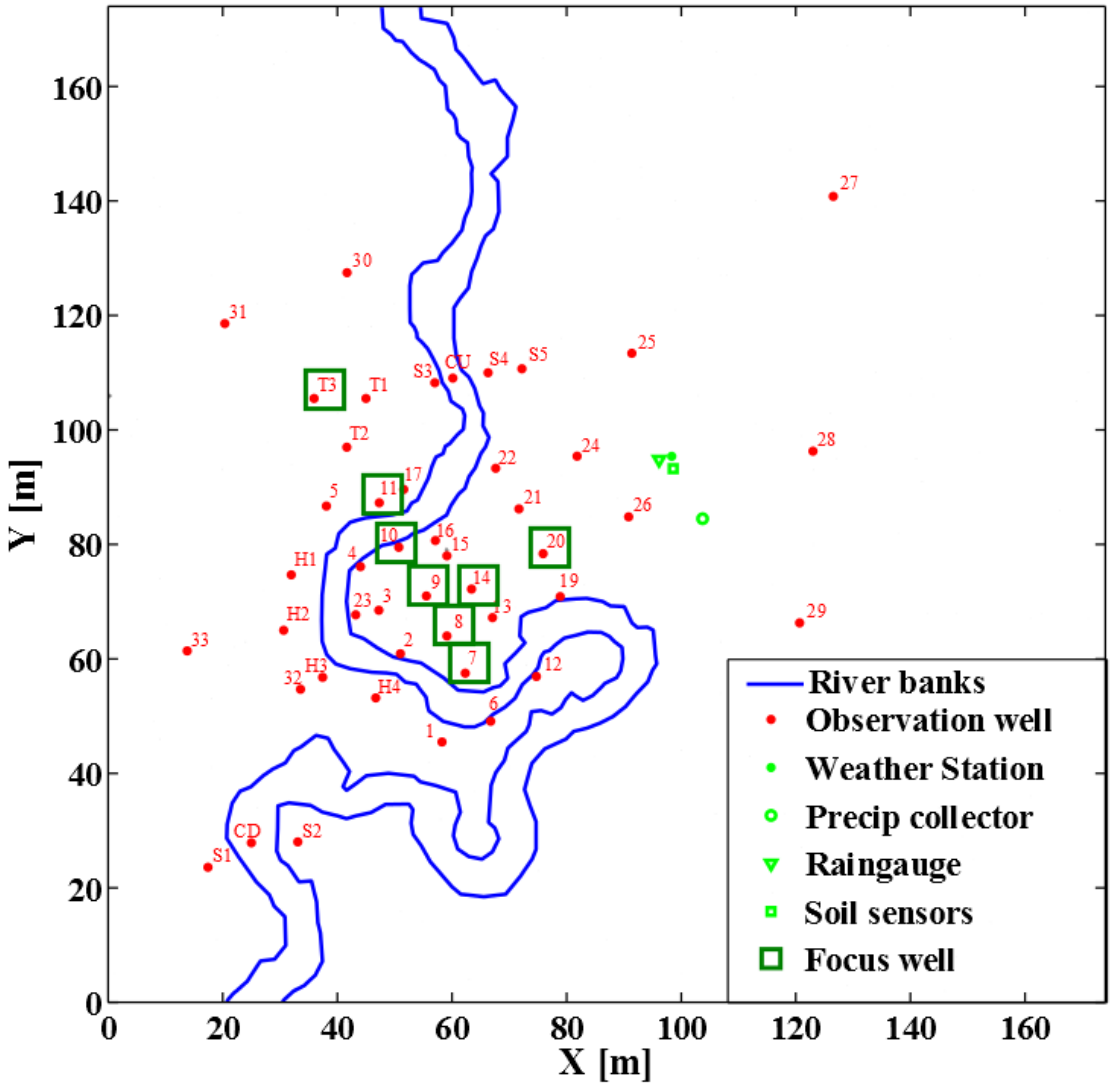

Figure 3. Map of Jemez River meander field site. Modified from figure by Jesus Gomez.

Thirty-three PVC monitoring wells (5 cm diameter) were installed at the site in June 2010, and ten more were installed in June 2011. A map of the field site, including well placements, appears in Figure 3. A typical well construction diagram appears in

Appendix C. Twenty-nine wells were instrumented with HOBO U20 (Onset Computer Corp., Bourne, MA) pressure transducers reporting pressure and temperature. Fourteen wells were instrumented with LTC Leveloggers (Solinst, Georgetown, ON) reporting pressure, temperature, and conductivity. Wells 3 and S2 contain YSI (YSI Inc., Yellow Springs, OH) slim sondes reporting temperature, conductivity, pH, dissolved oxygen, and oxidation-reduction potential. Thirty-two stainless steel piezometers (2.5 cm diameter) are installed in the streambed between in-stream monitoring wells CU and CD (see Figure 3, piezometer locations not pictured). Eight piezometers are instrumented with HOBO U12 4-channel data loggers measuring temperature at 10 cm vertical intervals within the piezometer to assess seasonal upwelling or downwelling at the streambed (Gomez, pers. comm.). A meteorological station (Campbell Scientific, Logan, UT) is also present at the site.

In summer 2011, the East Fork Jemez watershed was impacted by the Las Conchas fire, which ultimately burned 160,000 acres, 30,000 of which were within the Valles Caldera National Preserve boundaries (http://vallescaldera.com/archives/date/2011/07, accessed 1/5/2012). The fire actively burned from June 26, 2011 to August 3, 2011 (http://inciweb.org/incident/2385/, accessed 1/5/2012). Burned areas included the headwaters of the East Fork Jemez River and middle portions of Jaramillo Creek, which is a tributary of the East Fork Jemez above the Jemez River meander. The catchment area of La Jara Creek, another East Fork Jemez tributary, was unaffected, as were the headwaters of Jaramillo Creek (see Figure 4).

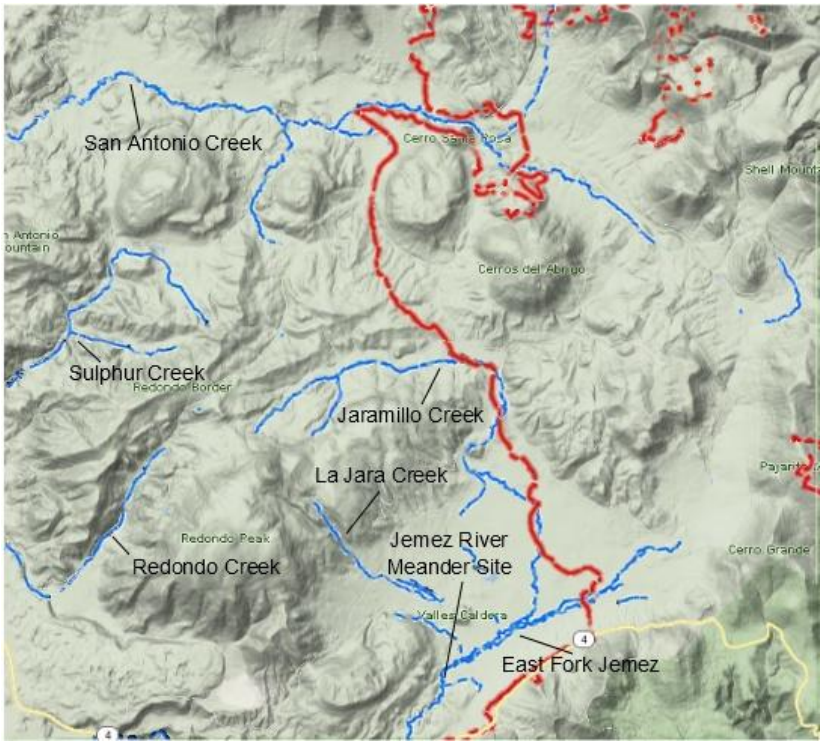

Figure 4. Major streams in the Valles Caldera National Preserve. The red line indicates the westward extend of the area burned by the 2011 Las Conchas fire.

III. Methods

Hydrology

Water level meters installed in September 2010 continuously recorded water level at 15-minute intervals in all wells and in two in-stream monitoring wells, upstream and downstream of the well field (labeled as CU and CD, respectively, in Figure 3). Pressure transducer measurements were corrected for atmospheric pressure, calibrated to water level measurements taken by hand with a Solinst 101 Water Level Meter and interpolated by kriging to produce water level maps.

DOC Sample Collection

The Jemez River meander groundwaters and surface waters were sampled ten times between July 2010 and September 2011. Details of sampling methods appear in Table 1.

Table 1. Sampling and analytical methods for each sampling event at the Jemez River meander.

Sample Date	Well Purge Time	Filter Size	Sample Acidification	Approx. Pump Rate
22 Jul 2010	~2 min	0.7 µm	Yes	Not measured
30 Oct 2010	5 min	0.7 µm	Yes	Not measured
13 Nov 2010	5 min	0.7 µm	Yes	Not measured
16 Apr 2011	5 min	0.7 µm	Yes	0.13 L/min
18 May 2011	5 min	0.7 µm	Yes	0.12 L/min
15 Jun 2011	10 min	0.2 µm	Yes	0.17 L/min
19 Jul 2011	10 min	0.2 µm	Yes, with unacidified duplicates	0.10 L/min
17 Aug 2011	10 min	0.2 µm	No	0.12 L/min
23 Sep 2011	10 min	0.2 µm	No	0.11 L/min

The number of wells sampled varied from event to event depending on available resources (battery life of the peristaltic pump) and field conditions (sampling was halted during afternoon thunderstorms during monsoon season). See Appendix B for which wells were sampled on which dates. On average, ten wells were sampled at each event. Eight wells were sampled at least 4 times throughout the sampling period: T3, 7, 8, 9, 10, 11, 14, and 20 (see Figure 3). These wells are referred to as "focus wells" and are examined in further detail in Section V.

Samples for DOC analysis were collected in 500 mL acid washed, pre-combusted (450° C, overnight – conditions used consistently throughout this work) clear glass bottles (Wheaton Science Products, Milville, NJ) with Teflon-lined lids. Samples were collected with a peristaltic field sampling pump (Masterflex, Vernon Hills, IL) and acid-washed

Masterflex Tygon tubing. At each well, tubing was lowered into the well casing and positioned approximately six inches above the bottom of the well. After the appropriate purging time, sample bottles were triple-rinsed with well water and the outflow tubing was placed at the bottom of each bottle. Bottles were allowed to overflow for approximately 30 seconds after filling, and then were capped with triple-rinsed caps. Bottles were then placed into an ice-filled cooler for preservation and transportation to the lab. A trip blank, consisting of a 500 mL bottle filled with deionized water ($\geq$ 18.2 MΩ, $\leq$ 4 ppb DOC; hereafter referred to as "MilliQ" water), was included in each sampling trip.

Low-flow sampling was employed to prevent disruption of flow fields, to prevent pumping wells dry, and to facilitate sampling of more wells at a single event. In a low-flow sampling approach, wells are pumps at rates between 0.1 and 0.5 L/min (Puls & Barcelona, 1996) until water quality parameters stabilize, indicating that formation water is being sampled. At flow rates typical to the peristaltic pump (ranging from 0.1 to 0.16 L/min), 5 minutes of pumping purged approximately 0.6 L of water. To increase this purge volume to approximately 1.2 L, purge time was increased to 10 min on June 15, 2011 and at all subsequent events. At the August 2011 sampling event, Well 10 was sampled at 10 mins and at 18 mins, which purged three well volumes from the well, to verify that water produced during low-flow sampling and water produced after purging three well volumes were sufficiently similar. Results are displayed in Table 2.

Table 2. Results from low-flow sampling tests conducted at the July and August 2011 sampling events. Results show that 10 minutes of purging produces water sufficiently similar to a three well-volume purge. DOC = dissolved organic carbon. TN = total nitrogen. FI = fluorescence index.

Sample	Pump time (min)	DOC (mg/L)	TN (mg/L)	pH	FI
W10	10	3.13	0.45	8.31	1.58
W10-3V	18	3.12	0.42	8.31	1.59

Sample filtration was performed within twelve hours of sample collection in the laboratory at New Mexico Tech. Prior to June 15, 2011, samples for DOC analysis were filtered through 0.7 µm Whatman GF/F filters held in precombusted glass filtration apparatus. Nalgene polycarbonate filtration apparatus were occasionally used as well, following determination that organic carbon leaching from these apparatus was negligible. Filters were rinsed with 100 mL MilliQ water before sample filtration. Filter blanks were collected at each sampling event to ensure that contamination from the filters and the filtration process was negligible relative to DOC concentrations present in the samples. Actual filter blank samples contained DOC concentrations between 0.05 and 0.29 mg/L (July 2011 and May 2011 sampling dates, respectively, MilliQ blank subtracted), representing between 1.9% (July 2011) and 6.6% (May 2011) of mean sample DOC concentration (July 2011 mean: 2.48 mg/L and May 2011 mean: 4.08 mg/L).

Beginning with the June 15, 2011 sampling event, samples for DOC analysis were additionally filtered through 0.2 µm "Supor" polyethersulfone filters (Pall Corporation, Port Washington, NY) to remove turbidity found in some wells (addressed in Section V below). Following filtration, samples were decanted into 250 mL precombusted glass

bottles, 20 mL TOC vials, and/or 1-dram vials with Teflon-lined lids for absorbance/fluorescence, total organic carbon, and molecular weight analyses, respectively.

Samples for absorbance and fluorescence analysis were acidified to pH = 2 (± 0.05 pH units) with approximately 1 M H_2SO_4 in sampling events prior to Aug 17, 2011. This acidification was intended to remove pH-related variation in DOC fluorescence (Pullin & Cabaniss, 1995; Mobed et al., 1996). In the July 2011 sampling event, all samples were analyzed both acidified and unacidified. On average, acidification increased the samples' fluorescence index (FI) by 0.05, and decreased UV absorbance by 0.038 absorbance units, although the magnitude of change in these metrics due to acidification varied from sample to sample. All DOC concentration measurements were made in unacidified sample fractions, so the effect of acidification on DOC concentration was not determined. Samples collected after July 2011 were not acidified so as to alter the sample as little as possible from its natural state.

To investigate the amount of DOC associated with sediments, 2 kg of sediment collected from installation of well 32 was sieved to remove grains with a diameter > 2 mm, dried at 150°C overnight and autoclaved at 151°C for 15 minutes to kill biofilm biota while preserving organic material coating sediment grains. 30 mL of 0.1 M $NaClO_4$ (Pullin et al., 2004) was mixed with 10 mg of sediment in six replicate vials and shaken at 60 rpm for 48 hours. Vials were then centrifuged, and the supernatant decanted for DOC analysis.

When not in use, samples were kept in dark refrigeration (4°C) and were discarded when all analyses were complete, typically within less than one week of sample collection. Approximately 2 mL of each sample were frozen in case of any future analytical needs.

IV. Analytical Methodology

Absorbance was measured on a double-beam, scanning spectrophotometer with a premonochromator to reduce stray light and allow collection of accurate absorbance values up to 3.5 absorbance units (Shimadzu UV-2550). Spectra were collected from 200 to 700 nm with a step size of 1 nm at medium speed and 1 nm slit width using 1 cm quartz cuvettes. MilliQ water was used as a reference. The cuvettes were triple-rinsed with both MilliQ water and sample water between each sample analysis and acid washed between sampling dates. These data were used to calculate ε280 values and inner filter effect corrections in fluorescence data.

Most samples were analyzed for total organic carbon on an OI 9210E total carbon analyzer by reagentless electrochemical oxidation and nondispersive infrared (NDIR) CO_2 detection. Samples from the August and September 2011 sampling events were analyzed on a Shimadzu TOC-VCSH total organic carbon analyzer by Pt catalyzed combustion at 680°C and NDIR CO_2 detection after acidification and sparging to remove inorganic carbon. The OI instrument analyzed for both total organic carbon (TOC) and total inorganic carbon (TIC), with the final reported value an average of at least three replicate measurements. The Shimadzu instrument reported both TOC and total nitrogen (TN), with the final reported value an average of five replicates. Mean relative standard deviation for replicate TOC measurements on the OI 9210E was 8.5%.

Fluorescent excitation and emission matrices (EEMs) were collected on a dual monochromator, scanning, PTI fluorometer with a 75 W xenon arc lamp source and a photon-counting photomultiplier tube detector. EEM scans were collected over an excitation range of 230 to 450 nm with a step size 5 nm, and an emission range of 250-600 nm with a step size 5 nm and integration time of 0.5 sec. A spectrum of the water Raman scattering signal was collected at excitation wavelength 350 nm and emission wavelengths 370 – 450 nm using MilliQ water, and the area under the Raman scattering peak was used to correct the sample EEMs for variation in lamp output over time (Stedmon et al., 2003). A 1 cm quartz cuvette was used throughout. The cuvettes were triple-rinsed with both MilliQ water and sample water between each sample analysis, and acid washed between sampling dates. Following instrument checks and a Raman scan, a MilliQ blank EEM was collected, followed by each of the samples. All EEMs were collected at room temperature.

EEM data correction was performed using MATLAB™ (The MathWorks), using a code written by Dr. Diane McKnight's group at the University of Colorado-Boulder and modified for the PTI instrument at New Mexico Tech. The code removes first and second order Rayleigh scattering, performs Raman correction, corrects for the inner-filter effect and subtracts the MilliQ blank. It also calculates the sample's fluorescence index (McKnight et al., 2001).

Analysis of inorganic cations was carried out by inductively coupled plasma-optical emission spectroscopy (ICP) using a Perkin Elmer 3500 XL instrument, analyzing for aluminum, barium, calcium, iron, potassium, lithium, magnesium, manganese, sodium, phosphorus, sulfur, silicon, and strontium. Inorganic anion analysis was carried out on a

Metrohm Personal Ion Chromatograph 790 with a Dionex IonPac AS9 – HC 4x250 mm column, and using 9 mM Na_2CO_3 as eluent and 20 mM H_2SO_4 for conductivity suppression. Ion chromatography analyzed for fluoride, chloride, nitrite, bromide, nitrate, phosphate, and sulfate.

A three component parallel factor (PARAFAC) model was fitted to 310 sample EEMs using the DOMFluor MATLAB toolbox (Stedmon & Bro, 2008). The model was validated with split-half analysis and random initialization. PARAFAC is a multi-way data decomposition method, similar to principal component analysis (although performed with three-dimensional data). PARAFAC determines the number and spectral properties of components that explain the spectral variability in the dataset and determines the "loadings," or fluorescent intensities, of these components present in each sample. Measured EEMs can be modeled by recombining the PARAFAC components according to these loadings (ibid.). PARAFAC modeling identifies consistent fluorophores in DOC EEM data, some of which have been identified as humic-like or protein-like (Coble, 1996; Fellman et al., 2010). Some components remain unidentified (Cory & McKnight, 2005). PARAFAC analysis has been used to trace sources of DOC through a hydrologic system (Stedmon & Markager, 2005; Mladenov et al., 2007), through manmade systems (Baghoth et al., 2011), and to assess redox conditions of a DOC sample (Cory & McKnight, 2005).

High pressure size exclusion chromatography (HP-SEC) was performed on an Agilent 1200 Series (Santa Clara, CA) high pressure liquid chromatograph (HPLC) according to the method of Zhou et al. (2000). Number-average (M_n) and weight-average (M_w) molecular weight was calculated according to the following equations (Chin et al., 1994).

$$M_n = \sum_{i=1}^{N} h_i \,/\, \sum_{i=1}^{N} \frac{h_i}{M_i}$$

$$M_w = \sum_{i=1}^{N} (h_i * M_i) \,/\, \sum_{i=1}^{N} h_i$$

where h_i is the amount of absorbance at eluted time *i* and M_i is the calibrated molecular weight, also at time *i*. These metrics have been used to discern seasonal variation in DOC sources in natural systems (Maurice et al., 2002; Kothawala et al., 2006), and to investigate the dynamics of DOC sorption onto mineral surfaces and photodegradation (Zhou et al., 2001; Pullin et al., 2004).

Due to spatial variability in sampling sites, sample data in wells exhibit a high standard deviation. Statistical tests were employed to quantify the variation between well and stream samples. Given the variation in sample size and variance between stream and well samples, Welch's t-test was used to generate a *t* statistic to compare the significance of differences of means. The null hypothesis for each comparison was $\mu_1 = \mu_2$ (i.e. no significant difference between stream and well samples), with the alternative hypothesis $\mu_1 \neq \mu_2$. Statistical tests were evaluated at the 95% confidence level.

V. Results

Hydrology

Interpolated water levels at the Jemez River meander are displayed in Figure 5. During the 2011 snowmelt and 2011 monsoon water levels rise northeast of the meander bend, creating higher hydrologic gradients and suggesting that larger-scale hydrologic processes interact with meander-scale hydrology. As water levels decrease with the onset

of summer 2011, these gradients decrease and the stream itself appears to become the primary driver of groundwater flow (Gomez & Wilson, 2011). Measurements of streambed water flux from in-stream piezometers show downwelling water fluxes, suggesting that the East Fork Jemez River streambed is a losing reach for most of the year (ibid.).

As shown in Figure 5, the groundwater hydraulic gradient continues through the stream channel to the other stream bank. This trend is also seen in groundwater well levels. Examining groundwater elevations in a transect perpendicular to the stream (wells 28, 26, 20, 14, 9, 3, 23, H3, 32, and 33; see Figure 3) reveals that groundwater elevations generally decline along this transect, even when crossing the stream (Gomez, pers. comm.).

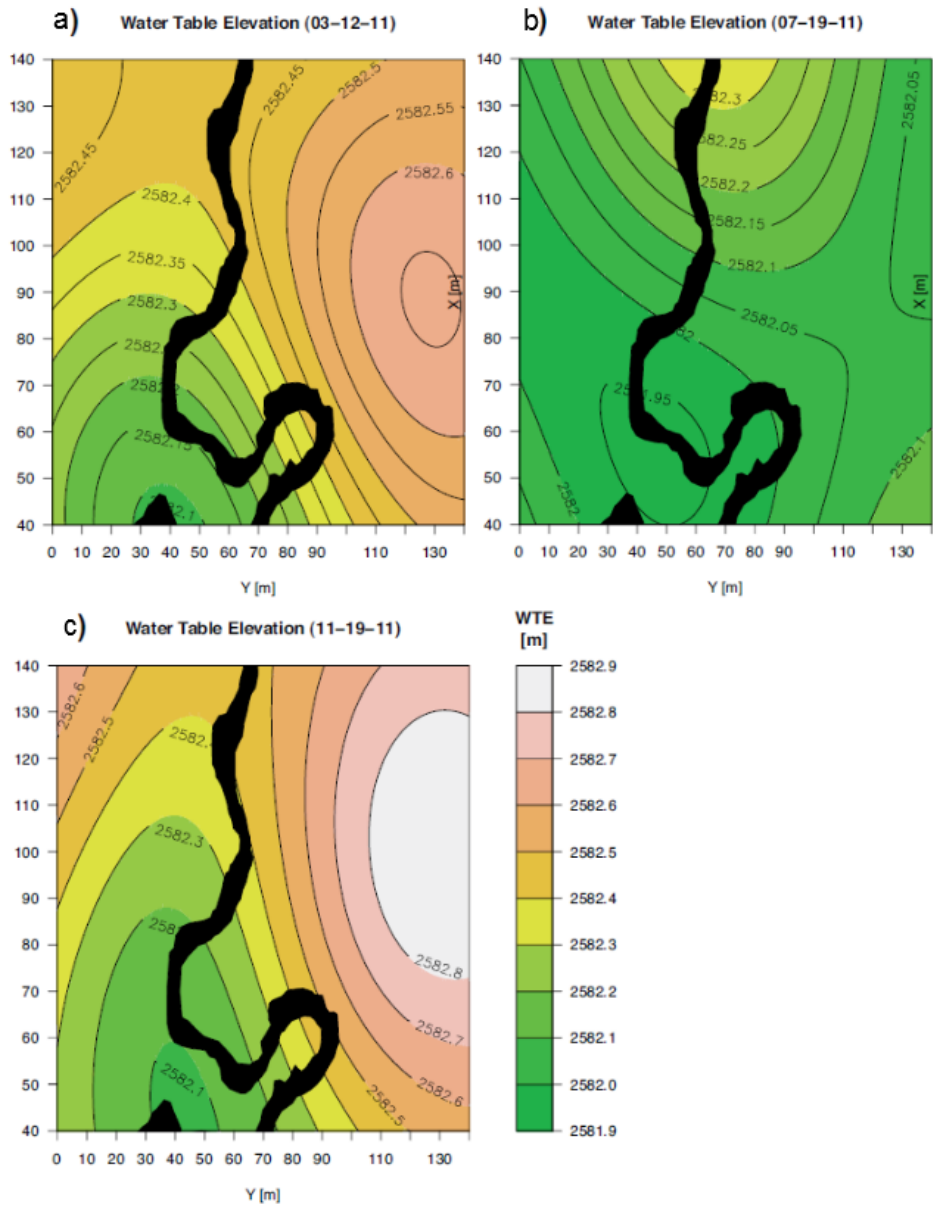

Figure 5. Interpolated maps of water level elevations at the Jemez River meander site, interpolated by kriging. a) shows water levels from March 12, 2011, during snowmelt. b) shows water levels from July 19, 2011, prior to the monsoon season. c) shows water levels from Nov 19, 2011, after monsoon season. From Gomez & Wilson, 2011.

Within meander bend sediments, horizontal flow velocities are extremely low. Based on slug tests conducted in July 2010, aquifer hydraulic conductivity was estimated to be on the order of 10^{-4} m/s (Gomez, unpublished), at the low end of the typical range of a

gravel lithology (Fetter, 2001). However, water level measurements revealed general differences in head on the order of 0.1 cm between wells, within the error of the water level meters. Figure 5c displays the steepest gradients in interpolated water levels, in which the gradient (northeast to southwest) is 0.01 m/m (although a gradient of 0.001 is also possible; Gomez, pers. comm.). By the following equation (Fetter, 2001),

$$V_x = -\frac{Kdh}{n_e dl}$$

where V_x represents seepage velocity (m/s), K the hydraulic conductivity, n_e the effective porosity (assumed to be 0.3, within the typical range for mixed sand and gravel, ibid.), and dh/dl the hydraulic head gradient, an upper bound seepage velocity may be as high as 3×10^{-6} m/s, while a lower bound may be one third of that, or 10^{-6} m/s.

Figures 6 and 7 display groundwater elevations and stream discharge data, respectively, for the latter half of 2011, which includes the monsoon season. Groundwater elevations are from wells 10, 14, and 8. The magnitude of groundwater fluctuation, from dry conditions in July 2011 to monsoonal events in August and September, is on the order of 0.5 m. Fluctuating water levels can have an impact on DOC mobility and may be in part a result of local recharge, which may mobilize and transport soil DOC. Stream discharge (Figure 7) is from a USGS stream gauge below the confluence of the East Fork Jemez River and San Antonio Creek. These data show that strong hydrologic responses to monsoonal precipitation events commenced in late August 2011 and continued into fall months, although local precipitation events at the Jemez River meander site began in late July 2011 (see Figure 8 for local precipitation data).

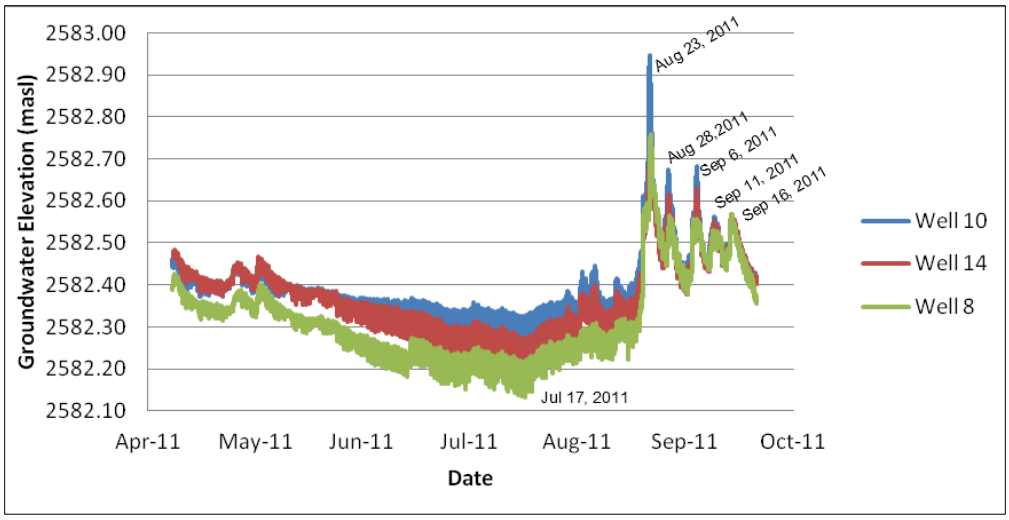

Figure 6. Groundwater elevations (in meters above sea level, masl) between Apr. and Sept. 2011 in wells 10, 14, and 8. Data courtesy of Jesus Gomez. Diel fluctuations in water level are reflected in the amplitude of the signal in each well.

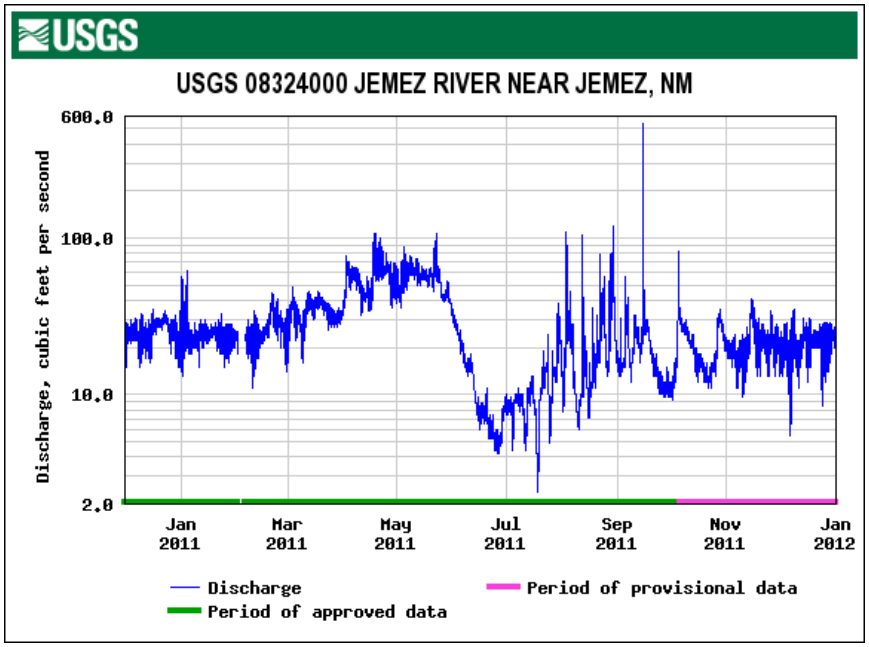

Figure 7. Discharge of the Jemez River below the confluence with San Antonio Creek during 2011. Note the commencement of snowmelt in Feb. 2011, the dry conditions in June and July 2011, and the high discharge events of the monsoon season in late summer and early fall 2011. Data and figure from the US Geological Survey National Water Information System (accessed 3/26/2012).

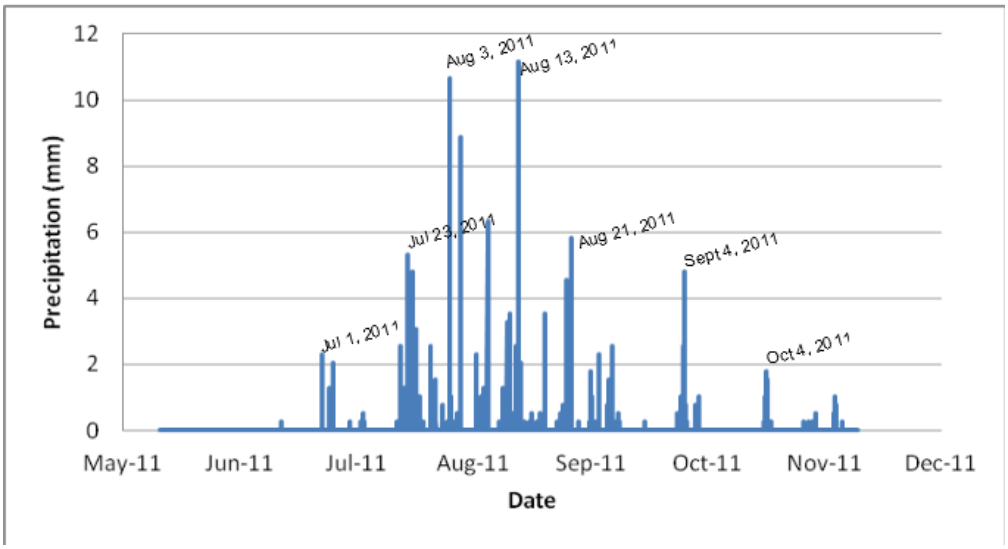

Figure 8. Precipitation totals at the Jemez River meander site. Major precipitation events by date are noted. Note that groundwater levels rise in wells (Figure 6) following Aug. 21, 2011 and Sept. 4, 2011 precipitation events. Data courtesy of Jesus Gomez.

Figure 6 shows that changes in groundwater elevations are highly temporally correlated. Observations at this site have shown that flood-like hydrological events (noted in Figure 6 with dates beginning August 23, 2011) are first seen in far-field wells, such as wells 28 and 31. Responses in wells nearer the stream occur approximately two days later and are nearly simultaneous with each other and with the stream (stream data not shown; Gomez & Wilson, 2011).

Figure 8 shows precipitation events measured locally at the Jemez River meander site. Comparing Figure 8 with Figure 6, it is apparent that not all monsoonal groundwater events are derived from local precipitation. Increases in groundwater elevations on August 23, 2011 and September 6, 2011 are likely in response to precipitation events that occurred two days previously. Groundwater events on August 28, September 11 and September 16 do not have corresponding precipitation events, suggesting that these events are driven by precipitation events elsewhere in the watershed.

Along with groundwater elevations, groundwater temperature was also monitored. Stream temperatures varied from 5 to 19°C during the sampling period (between fall 2010 and fall 2011). Well temperatures ranged from 4 to 13°C during the same period and were consistently distinct from stream temperatures with one exception: temperatures in well S3 (situated close to the stream, see Figure 3) exhibited the strongest positive correlation with stream temperatures ($r^2 = 0.71$).

Water Chemistry

As monitored by the Valles Caldera National Preserve, stream pH varies between approximately 4 and 11 with pH variations occurring on hourly time scales. Diel variation in in-stream autotrophic production, mediated by sunlight, affects CO_2 concentration and carbonate chemistry in the stream, which may be driving pH variation (Langmuir, 1997). pH in groundwater samples generally varied between 7 and 9 with August 2011 samples displaying an overall high pH among well samples (average 8.50).

Three independent assessments of dissolved oxygen (DO) in groundwater were undertaken between October 2010 and October 2011. On October 30, 2010, water from well 14 was pumped through an improvised flow-thru cell on a YSI 600 XL slim sonde using a membrane-based DO probe. After five minutes of pumping, the sonde recorded DO concentrations of 0.8 ppm.

YSI 650 XLM slim sondes installed in-situ in wells 3 and S2 by the University of New Mexico continuously recorded DO concentrations during the study period with a membrane-based DO probe. DO in well 3 is close to zero for most of the recorded period, but shows increased DO concentrations in March 2011, during snowmelt, and in

November 2011, following the monsoon season (see Figure 9). DO levels reached 4 ppm in March and 6 ppm in November. Well S2 is closer to the stream than well 3 (see Figure 3) and displays non-zero DO concentrations year-round (see Figure 10) with spikes up to 3 ppm from August 2011 to September 2011 during the monsoon.

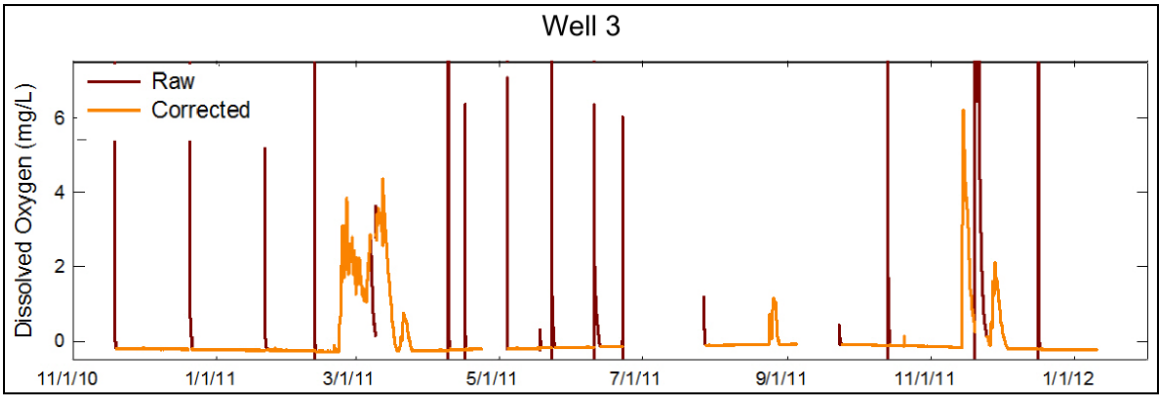

Figure 9. Dissolved oxygen concentrations as measured in well 3, Nov. 2010 through Jan. 2012. Adapted from a figure by Lauren Sherson (unpublished).

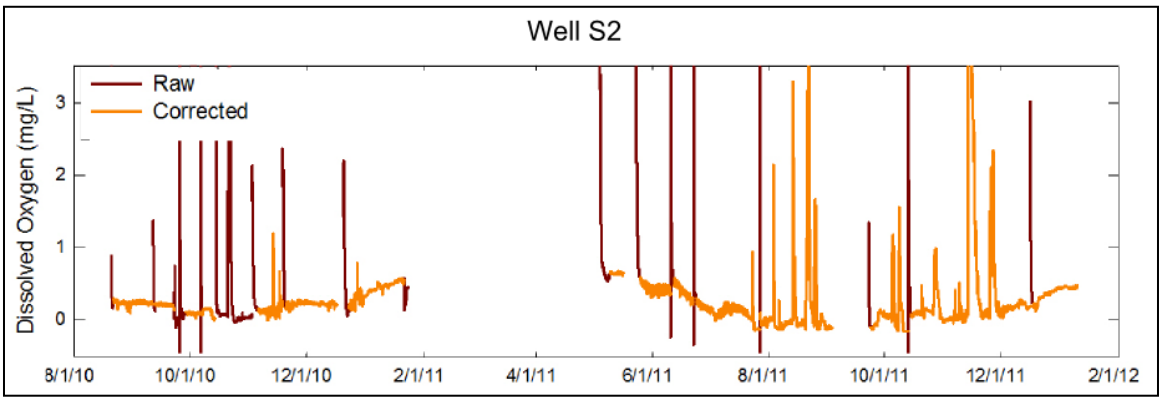

Figure 10. Dissolved oxygen concentrations in well S2, Aug. 2010 through Feb. 2012. Adapted from a figure by Lauren Sherson (unpublished).

Finally, groundwater was pumped from ten groundwater wells through a flow cell attached to a YSI Professional Plus hand-held multiparameter probe utilizing a membrane-based DO probe on October 20, 2011. DO levels in these ten wells (7, 8, 9,

10, 12, 13, 14, 15, 16, 31) averaged 0.32 ppm, compared to a mean of 11.2 ppm in three surface water readings (adjacent to wells S3, 12, and 16) taken the same day.

According to manufacturer specifications, each of these DO probes has a range down to 0 ppm with ± 2% or 0.2 ppm accuracy, whichever is greater. DO tests in October 2010 and October 2011 recorded DO concentrations that are very low compared to stream DO, but are still above zero, taking into account instrument accuracy. Measurements of 0.8 ppm and 0.32 ppm (October 2010 and October 2011, respectively) fall within suboxic levels (defined as an O_2 concentration between 1 µM and 30 µM, or 0.032 ppm and 0.96 ppm, respectively; Langmuir, 1997) but are not low enough to be considered anoxic (< 0.032 ppm; ibid.).

DOC Concentration

Stream sample DOC concentrations rise from a low of 1.3 – 1.5 mg/L in April and May 2011 to a high of 4.3 mg/L in September 2011. This rise during the summer months appears to be steady with no peaks in concentration. Mean stream DOC concentration in July 2010 is within 10% of the July 2011 concentration, providing a measure of interannual variability (although by July 2011 the Valles Caldera National Preserve was affected by the Las Conchas fire).

DOC concentration peaks twice in well samples, once in April 2011 and once in September 2011, as seen in Figure 11, which presents the mean of stream sample DOC and well sample DOC, respectively. Error bars in this and in following figures represent one standard deviation from the mean and are reflective of spatial variability in well and stream samples. DOC analysis replicates are typically <2% RSD, indicating that errors

calculated here are the result of intersample variability, not instrument error. Error bars on stream samples represent the homogeneity of stream DOC and the relatively lower number of samples. Three stream sites were sampled at each event; the number of wells sampled (for all metrics presented here) varies from event to event and is noted in Figure 11. The April peak occurs just after snowmelt (see Figure 7 for timing of peak stream flows related to snowmelt).

The difference in mean stream DOC and mean well DOC concentration is not statistically significant in June and July 2011. DOC concentrations in wells decreased by 63% between April and June 2011. The September peak coincides with the 2011 monsoon season, which started unusually late in July 2011. Figure 8 shows that precipitation events began in late July 2011, but significant monsoonal water level changes were recorded in the wells beginning in late August, after the August 17, 2011 sampling event.

Well sample DOC concentrations are higher than those in the stream in all events except for August 2011, where mean stream DOC concentrations were almost 2 mg/L higher than in wells. The difference in means between stream and well DOC concentration is statistically significant in August 2011.

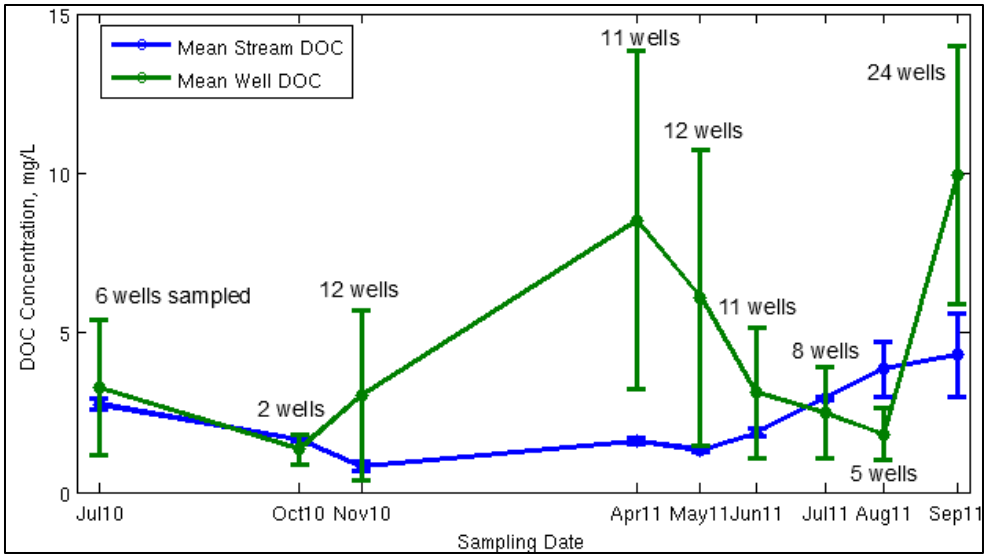

Figure 11. Mean DOC concentrations for stream and well samples, July 2010 through Sept. 2011. Error bars in this figure and in following figures represent one standard deviation from the mean. Error reflects spatial variation, and not sampling error. The number of wells sampled at each event is noted.

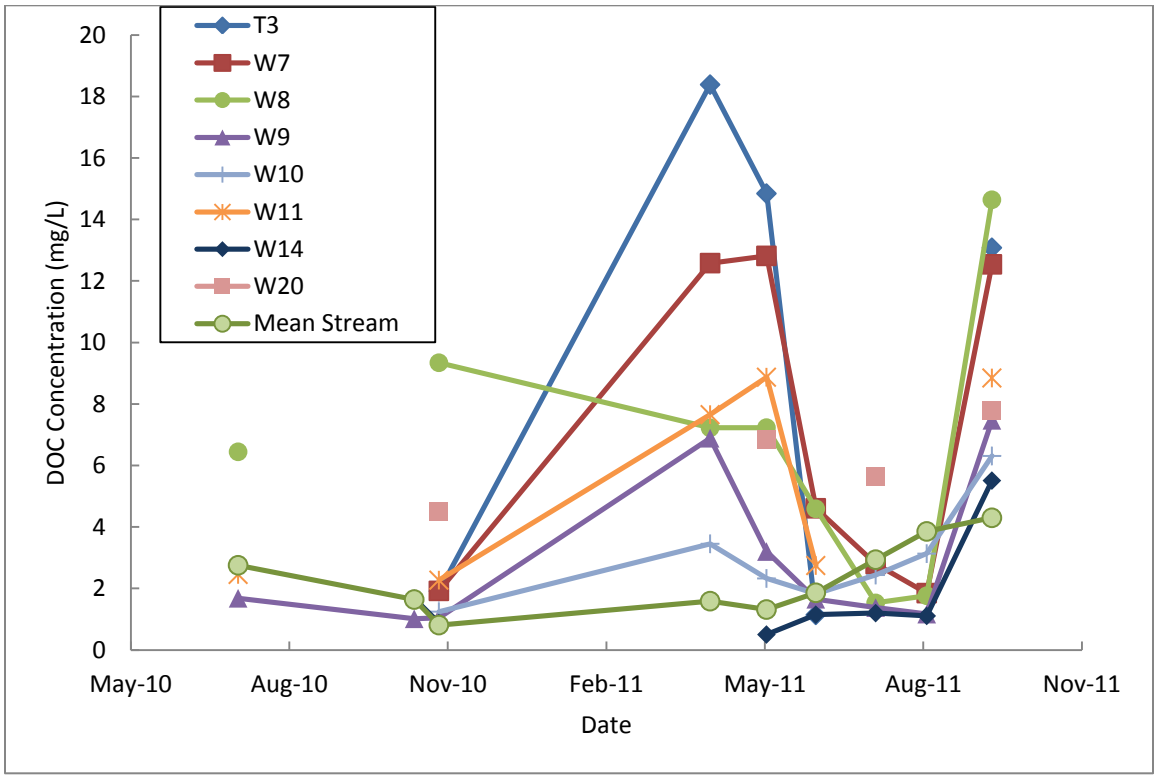

Figure 12. DOC concentration trends in "focus wells," wells sampled frequently. Unconnected points represent non-consecutive samples.

DOC concentrations in wells T3, 7, and 11 over all sampling events (Figure 12) are positively linearly correlated (r^2= 0.85). Wells 7 and 11 are both situated near to and north of the stream bank, albeit at different locations in the meander bend (Figure 3). DOC concentrations in wells 9, 10, 14, and 20, situated within the meander well field, are also well correlated linearly ($r^2 > 0.85$) to wells T3, 7, and 11, except in April and May 2011 sampling events when DOC in wells T3, 7, and 11 averaged 12.5 mg/L, compared to an average of 3.9 mg/L in wells 9, 10, 14, and 20. DOC concentration in well 8 was not correlated to any other surrounding well prior to the June 2011 sampling event.

Wells T3 and 8 (neither situated on a stream bank) exhibit no correlation to stream DOC. Wells 20 and 10 exhibit moderate correlation (r^2 = 0.55 and 0.47, respectively). While well 10 is situated near the stream, well 20 is located within the interior of the well field.

Turbidity

Stream water samples collected for this study exhibited relatively little turbidity. In-stream data collected by Valles Caldera National Preserve scientists shows turbidity in the East Fork Jemez River averaged 22 nephelometric turbidity units between 2005 and 2009 (unpublished). Some well samples were highly turbid, as seen in Figure 13. This occurrence was not spatially or temporally consistent. Turbidity was tracked qualitatively beginning with the April 2011 sampling event by photographing sample bottles. 83% of wells sampled on September 23, 2011 were turbid, with wells 19 – 22 exhibiting no turbidity. On other sampling dates one-third to half of samples were turbid, with the least turbidity (33% of samples) on August 17, 2011. Across all sampling dates, well 8 was consistently turbid, with nearby wells 9 and 10 also frequently turbid.

Figure 13. An example of turbidity observed in samples from the Sept. 23, 2011 sampling event. Samples displayed, from left to right, are from wells 27, 3, and 15.

Combustion analysis of the turbid material (see Appendix E for method) revealed that 22% of the material by weight consisted of organic matter. In the sample from well 8 on August 17, 2011, turbid material retained on 0.7 µm filter papers amounted to 150 mg per liter of sample. Given the organic carbon percentage determined from combustion analysis, approximately 31 mg/L of organic carbon in turbid samples may be associated with particulate (retained on a 0.7 µm filter) material. On average, turbid samples in all sampling events had a DOC concentration 2.6 times higher than non-turbid samples. Even turbid samples filtered to 0.2 µm (which removed all visible turbidity) had higher DOC concentrations than non-turbid samples (see Table 3).

Table 3. Comparison between DOC concentrations in non-turbid vs. turbid samples. Samples filtered through a 0.7 µm filter were collected prior to June 15, 2011, and those filtered through a 0.2 µm filter were collected on and after June 15. Higher DOC concentrations persist in turbid samples even after filtration through a 0.2 µm filter.

	Filter Size	
	0.7 µm	0.2 µm
Turbid	9.5 mg/L	8.3 mg/L
Non-turbid	2.8 mg/L	3.6 mg/L

This turbidity may be comprised of iron oxyhydroxides (FeOOH). FeOOHs are formed by the oxidation of soluble, reduced ferrous iron to insoluble ferric iron by dissolved oxygen at circumneutral pH (Groffman & Crossey, 1999). Ferrous iron can accumulate in reducing systems, especially when iron-reducing organisms are present (Chappelle, 1993). DOC adsorbs to FeOOHs by ligand exchange, and DOC can coprecipitate with iron oxides (Boyle et al., 1977; Pullin et al., 2004). Acidification of samples to pH 2 caused the suspended particles to settle. At this pH iron is soluble and humic acid is insoluble (Thurman, 1985). Acidification would cause Fe(III) to dissolve, dissociating the ferric-organic complex (Langmuir, 1997). To assess metals present in turbid material, samples of suspended particles that had previously been combusted were dissolved in HNO_3 (reactive with metals) to dissolve metal oxides. Dissolution was not complete. One sample had been acidified to pH = 2 prior to combustion, the other had not. Inductively-coupled plasma (ICP) analysis revealed that iron and aluminum comprised, together, 10% of the dissolved mass in the acidified sample, and 3% of the dissolved mass in the unacidified sample.

Fluorescence Index

The Fluorescence Index (FI) is a proxy measurement for the source of a DOC sample. Lower FIs (~1.3) are associated with allochthonous, terrestrial, aromatic plant-derived DOC sources, while higher FIs (~1.9) are associated with autochthonous algal sources and/or microbially generated DOC (McKnight et al., 2001).

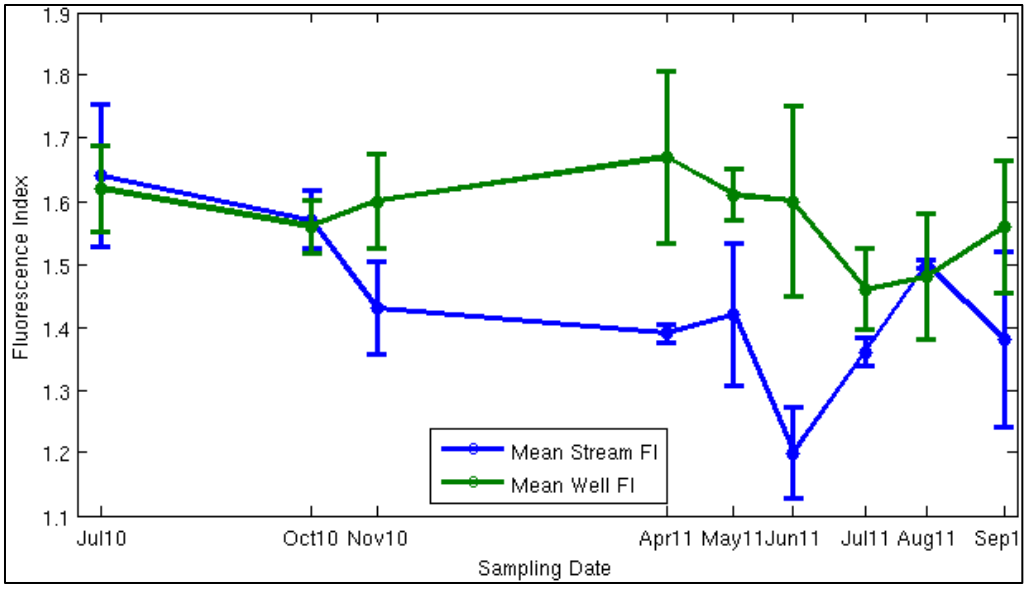

Figure 14. Trends in fluorescence index (FI) over the sampling period. A higher fluorescence index implies a more microbial source of DOC, while a lower FI suggests a more terrestrial source.

Mean FI of stream and well samples (as seen in Figure 14) differ by no more than 1% in July and October 2010. Stream DOC exhibited a lower FI (more allochthonous) than well DOC between November 2010 and August 2011. Stream FI reached a minimum (1.20) in June 2011. Unlike DOC concentration, FI does not show consistency between July 2010 and 2011 samples. July 2010 stream FI was 1.64, higher than the July 2011 FI (1.36). Stream discharge was extremely low in 2011 compared to 2010 (see Figure 2).

FI in well DOC (see Figure 14) decreased from a high during April 2011 to a minimum in July 2011. DOC concentration in wells (Figure 11) followed a similar trend, decreasing after snowmelt and through pre-monsoonal months. The magnitude of decrease is not as dramatic in FI; between April and June 2011 mean FI in well DOC decreased by 4%. DOC concentrations over the same period decreased by 63%.

Mean FI in wells did not significantly differ from mean stream FI in the May, August, and September sampling events.

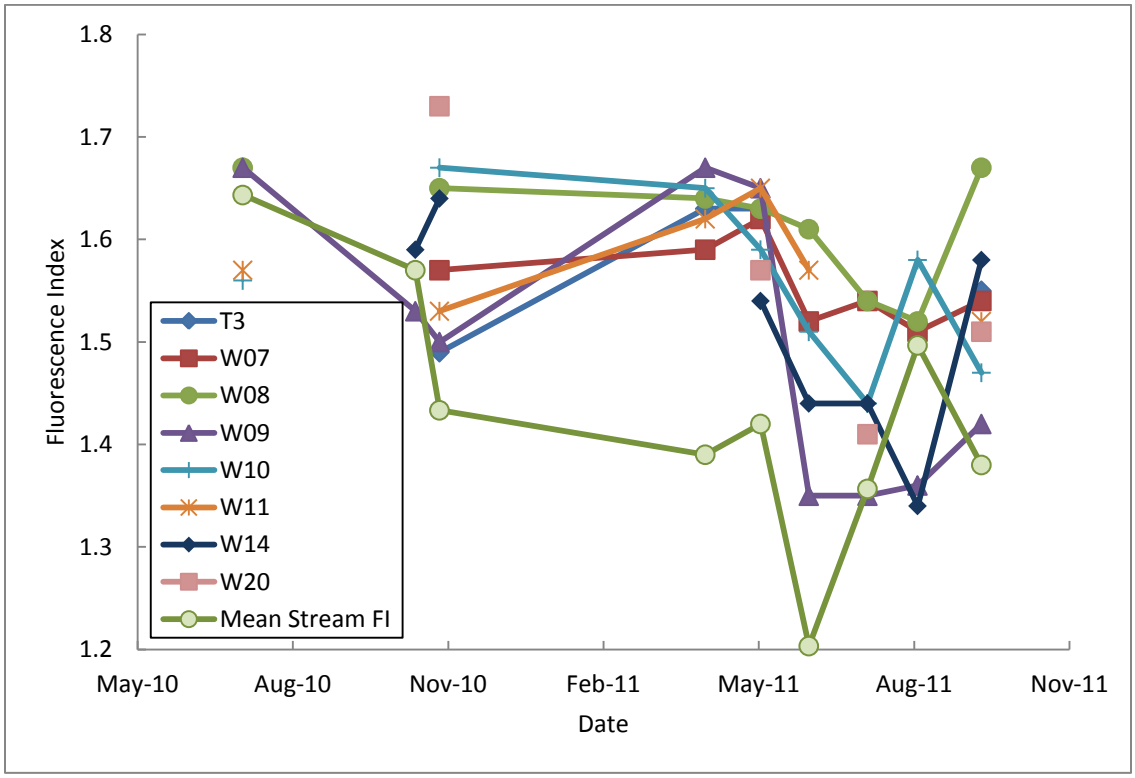

Figure 15. Focus well fluorescence indicies.

FIs in wells 14, 8, 20, and 7 are well correlated with each other (Figure 15, $r^2 > 0.79$), peaking in May 2011 and reaching a low in August 2011. Well 9 correlatea with these wells in April and May 2011, but displays a lower FI in June, July, August, and September 2011. FI in well 10 and in stream samples peaks in August and decreases in September, while other well FIs increase in September.

Between May and June 2011, stream FI decreases from 1.42 to 1.20. During that same interval, FI in focus wells 7, 9, 10, 11, and 14 also experience sharp decreases. Well 9 experiences the greatest drop (1.65 to 1.35) and well 7 the least (1.65 to 1.57). Wells 7 and 11 are situated on north streambanks, and yielded high DOC concentrations during

hydrologic events. Well 10 is situated on a south streambank and wells 9 and 14 are situated in the interior of the well field.

PARAFAC Model Components

The three-component PARAFAC model displayed in Figure 16 was fitted to 310 sample EEMs from the Jemez River Meander site and throughout the East Fork Jemez watershed. Excitation and emission maxima for components 1 and 3 correspond to the C and M peaks, respectively, of Coble (1996). Coble (1996) identified peak C as humic-like and peak M as marine-like humic, since her study involved marine DOC samples. Fellman et al. (2010) identified Coble's C peak as high-molecular-weight humic with a terrestrial origin and Coble's M peak as low-molecular-weight and associated with in-situ biological DOC production. Originally observed in marine DOC, the M peak has also been observed in terrestrial and fresh water environments. Component 2 corresponds to Component 2 in Ishii & Boyer (2012) who identify it as a humic peak likely to be photodegraded (due to ultraviolet absorbance) and consisting of high-molecular-weight humic substances.

Although this model has been validated by split-half analysis (Stedmon & Bro, 2008) it does not necessarily represent all the variation present in EEMs collected from the Jemez River meander site. Residual plots (not shown) indicate that fluorescence in the low excitation – low emission region is not represented in this three-component model. This region corresponds to protein-like fluorescence (Coble, 1996; Fellman et al., 2010). As more EEMs are collected at the Jemez River meander site, more refined PARAFAC models can be developed.

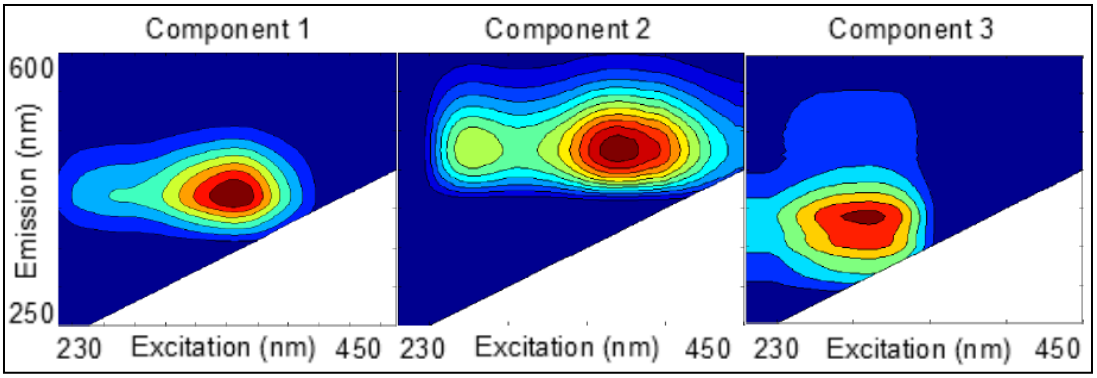

Figure 16. A three-component PARAFAC model of EEMs collected from Valles Caldera National Preserve samples. Model generated and validated using the DOMFluor toolbox (Stedmon & Bro, 1998).

EEMs modeled using PARAFAC are comprised of the model components added together, with each component multiplied by a coefficient to represent that component's intensity in the sample. This coefficient is the "loading" of the component in the sample, and the sum of components is not unity, but rather a representation of total fluorescence intensity in a sample. Figures 17 and 18 show the loadings of components 1 and 3, respectively, in stream water and well water samples, divided by DOC concentration. This normalization is done to remove variation in component loading due to total DOC concentration in a sample (since DOC concentration and sum of all three loadings are positively correlated) and reveal each sample's relative component loadings. For comparison, raw loadings of components 1 and 3 appear in Figure 19. Component 2 is not plotted, as loadings of components 1 and 2 are highly positively correlated (r^2 = 0.95), which is not surprising, given the similar description of these two components in the literature. Loadings of components 1 and 3 are weakly positively correlated (r^2= 0.25), as are components 2 and 3 (r^2= 0.21).

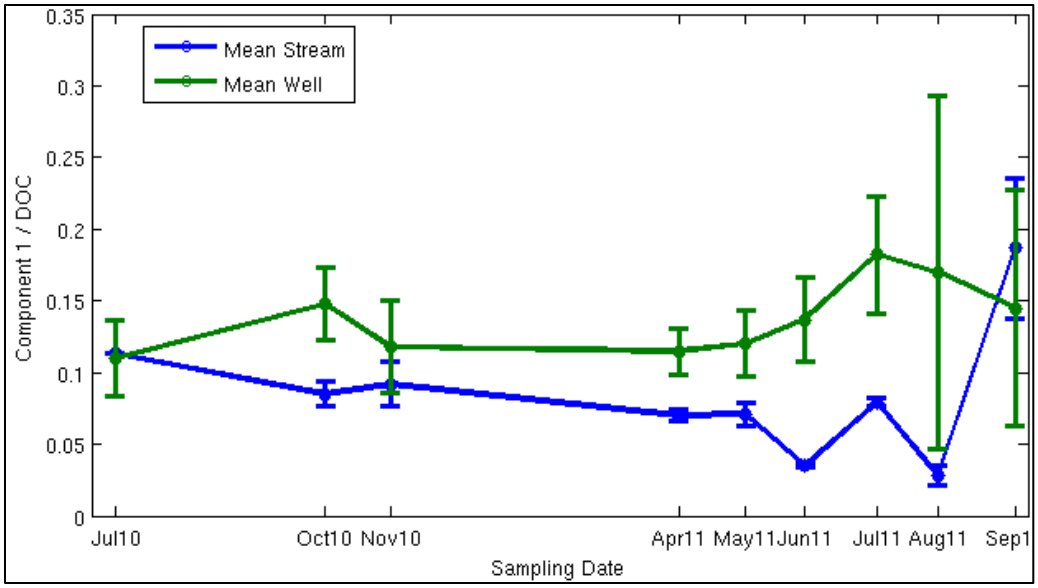

Figure 17. Trends in component 1, normalized to DOC, contributing to EEM fluorescence. Peak fluorescence of component 1 is similar to previously identified peak C (Coble, 1996).

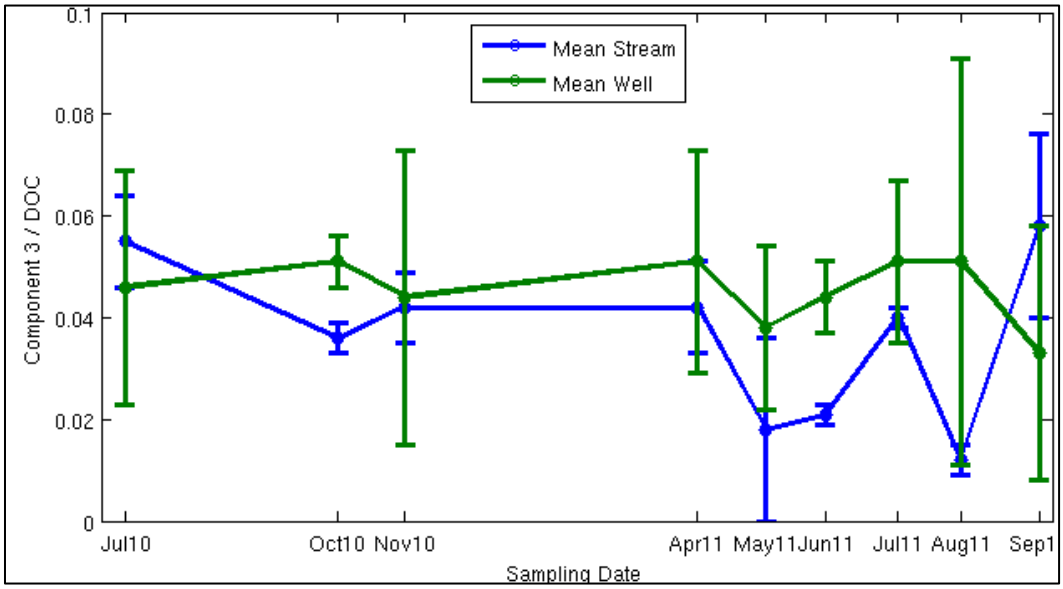

Figure 18. Trends in component 3, normalized to DOC. Peak fluorescence of component 3 is similar to previously identified peak M (Coble, 1996).

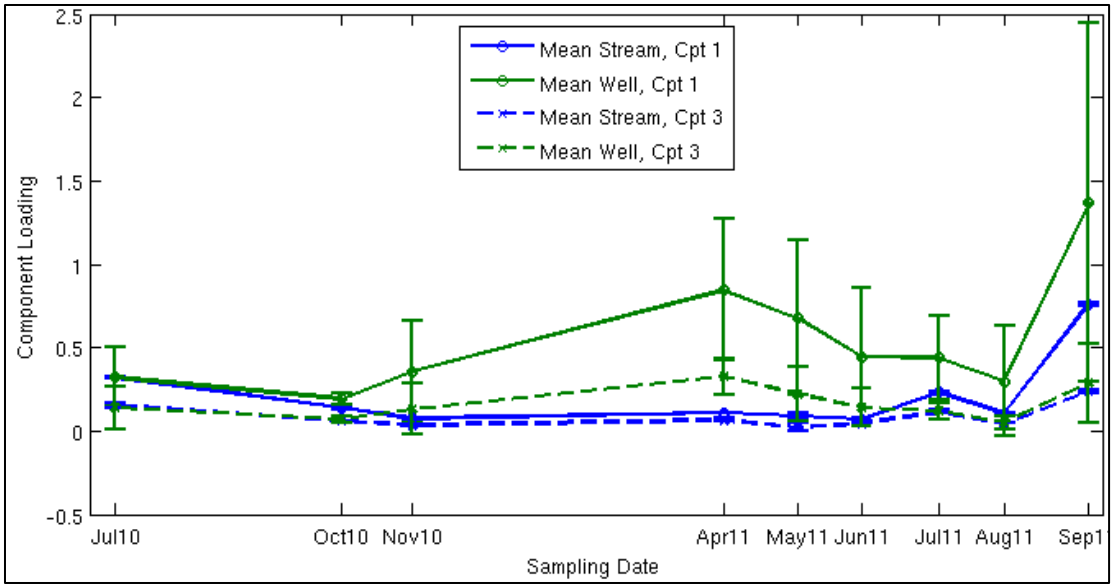

Figure 19. Raw (not normalized to DOC concentration) loadings for PARAFAC components 1 and 3. Compare with Figure 11 for correlation between component loadings and DOC concentration. Component 2 is not plotted, as it correlates positively very well with component 1 loadings (r2 = 0.95).

Beginning in April 2011, normalized component 1 values (Figure 17) rise in wells and drop in streams. Component 1 peaks in wells in July 2011 and declines afterwards. This trend is opposite to the trend observed in DOC concentration and FI. Mean well loadings of component 1 are well correlated, negatively (r^2 = 0.88), to mean well FIs (Figure 14). This relationship is due to the terrestrial nature of component 1. Terrestrial DOC produces a lower FI, resulting in a negative correlation. In-stream mean values of component 1 do not display the same correlation to stream FIs.

Unfortunately variation in normalized sample values of component 3 (Figure 18) are such that mean stream and mean well values do not significantly differ except at the June 2011 sampling event, when component 3 values in wells are higher than those in the stream. Based on previous interpretations (Fellman et al., 2010; Ishii & Boyer, 2012), this component represents autochthonous DOC production, but these results display high

variation, complicating interpretation and application to DOC dynamics at the Jemez River meander.

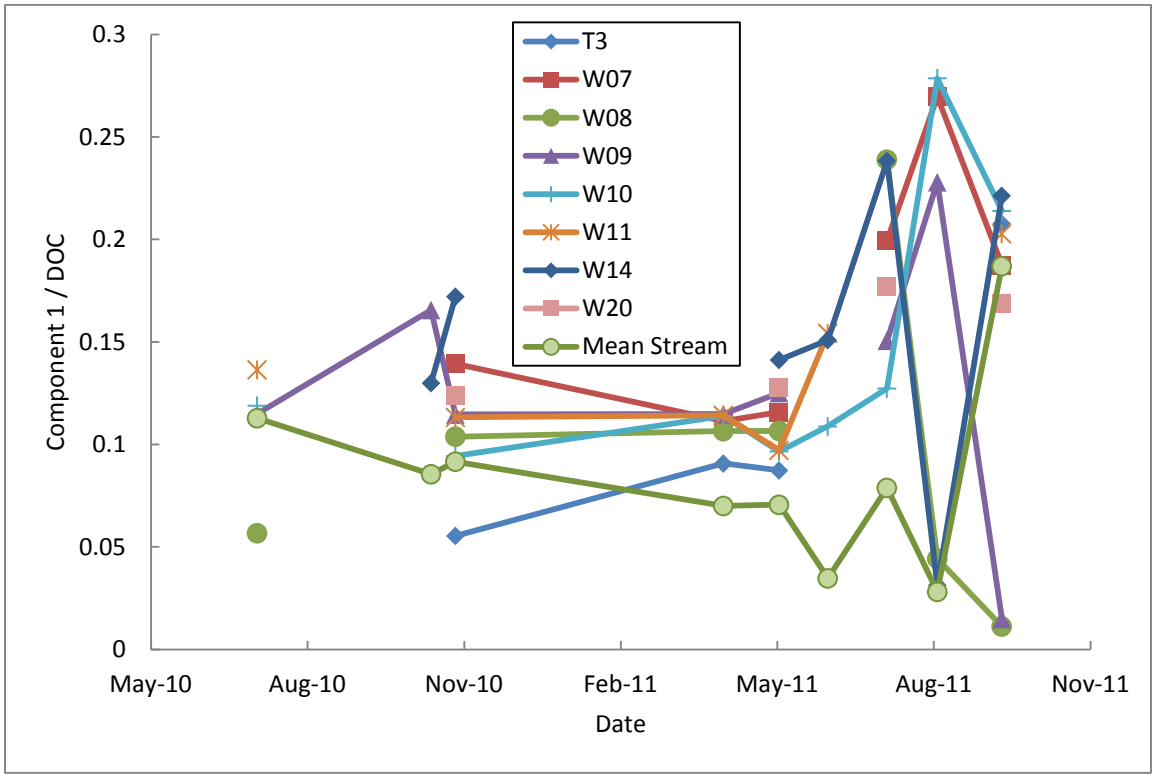

Figure 20. Focus well trends in PARAFAC component 1 loading normalized to DOC concentration.

Component 1 loading in well 14 peaks in July, as seen in Figure 20, after which its trend closely follows the stream trend. Loadings in wells 10, 7, and 9 peak in August 2011. In September 2011 stream and well values are well correlated. Only well 9 and well 8 experience sharp drops.

Stream component 3 values (figure not shown) follow a similar trend to component 1 values. As in component 1, well 14 peaks in July 2011 while wells 10, 7, and 9 peak in August 2011. Well 9 displays a similar steep drop in September 2011, but in this case well 8 values also drop in September.

Aromaticity

DOC aromaticity typically ranges from 10 – 30% (Chin et al., 1994; McKnight et al., 2001). Lignin-derived DOC contains a higher percentage aromatic carbon than microbially-derived material (McKnight et al., 2001). The ε280 value used here to estimate aromaticity is based on light absorbance in a sample. Inorganic, light-absorbing or light-scattering colloidal material in a sample may yield an over-estimation of aromaticity (Pullin et al., 2007). Also, the relationship between DOC aromaticity and ε280 for Jemez River meander site data may not be the same as for the DOC used to develop the relationship in Chin et al. (1994).

As seen in Figure 21, average aromaticities range from approximately 20% to 60%, with stream values consistently below well values. Means significantly differ only in July 2011 and August 2011 when well aromaticity rises. July and October 2010 sampling dates also show higher well sample aromaticity. Variability in aromaticity measurements also increases in July and August 2011. The mean aromaticities in July 2010 and July 2011 differ by no more than 1%, although July 2011 data shows more spatial variation.

Mean stream and well values differ by only 10% in April 2011, during snowmelt, at the same sampling event where mean well DOC concentration was 400% higher than the mean stream concentration. In contrast to DOC concentration and FI metrics, in which mean stream and mean well values are well-correlated with each other in June, July and August 2011, mean stream and well aromaticity values differ most in these months.

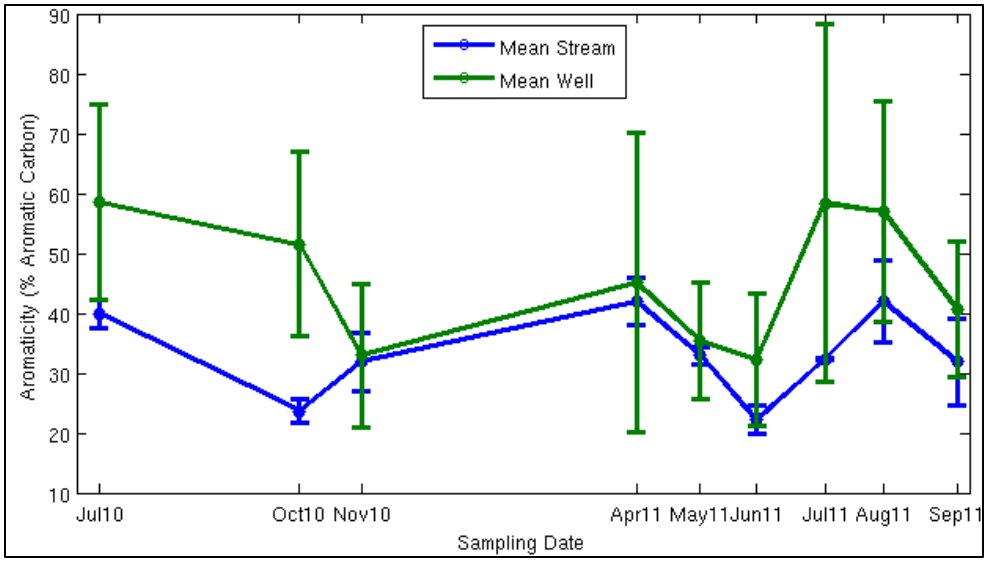

Figure 21. Aromaticity, or percent aromatic carbon, as estimated from ε280.

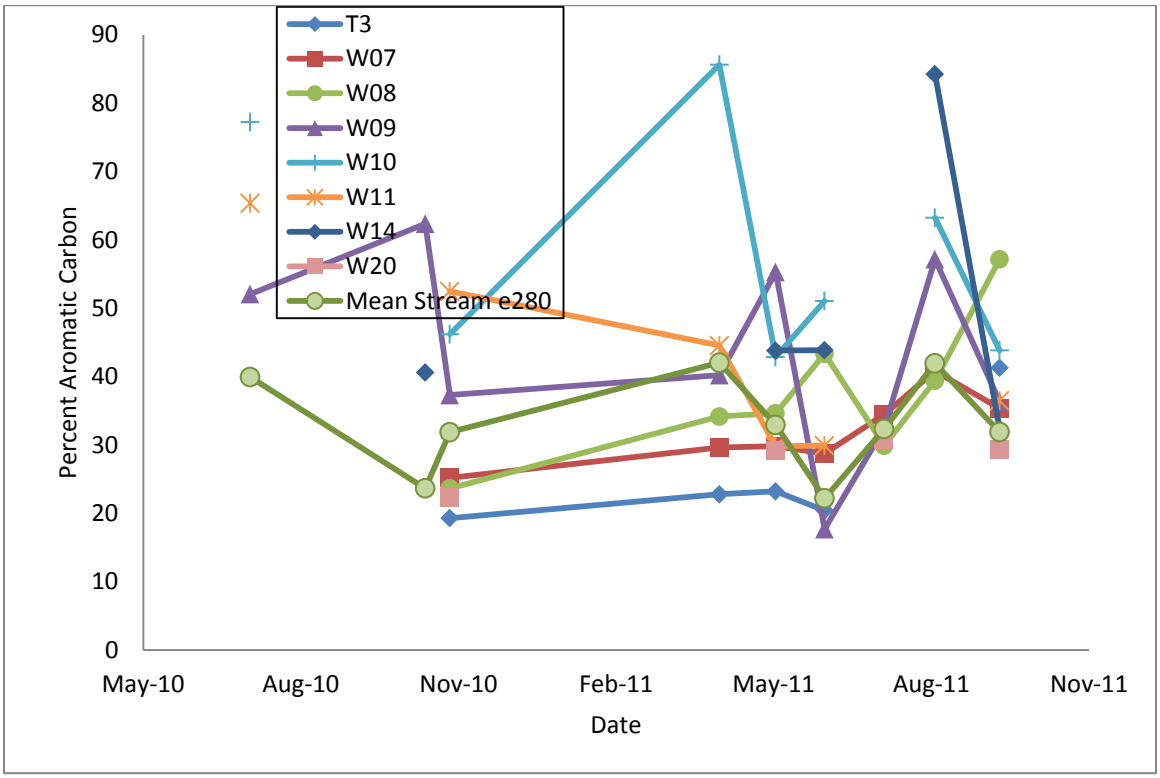

Figure 22. Aromaticity trends in focus wells, as estimated from ε280.

Wells 20, 7, 9 and 11 follow an aromaticity trend similar to the stream trend, particularly after June 2011, as seen in Figure 22. Well 14 exhibits the highest aromaticity in July and August 2011, with well 10 following a similar trend. Well 10 accounts for the highest aromaticity variation in April 2011, while well 14 accounts for high variation in July and August 2011. If these highly aromatic well samples are neglected, then mean stream and well aromaticity in July 2011 differs by only 3%, following the pattern of DOC and FI values mentioned above. Well T3, situated northwest of the majority of the wells, displays a consistently low aromaticity, despite consistently high DOC concentration and turbidity.

Average Molecular Weight

Reported log molecular weight values (Chin et al. 1994) can range from the very low end, measured in Lake Michigan sedimentary pore waters (log M_w 2.93, log M_n 2.73) to high values, measured in Suwannee River fulvic acid (log M_w 3.36, log M_n 3.13). Molecular weight (MW) measurements at the Jemez River meander site only exist for sampling date June 15, 2011 and after. In the June 2011 sample, log M_w values (Figure 23) are relatively high in streams and wells. Stream and well values are most similar in the July 2011 sampling event, following which mean stream log M_w rises while mean well log M_w falls. Mean stream and well MW averages do not significantly differ in the July and August 2011 samples. Log M_n values co-vary with log M_w values (Figure 24).

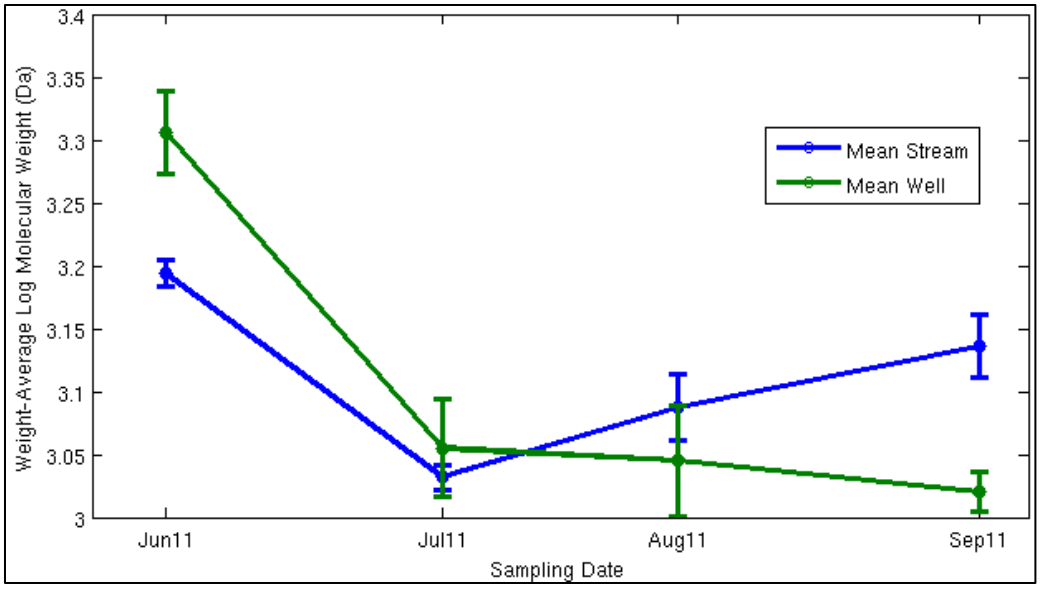

Figure 23. Weight-average log molecular weight trends. The weight average is the weight of the molecule to which the average atom belongs.

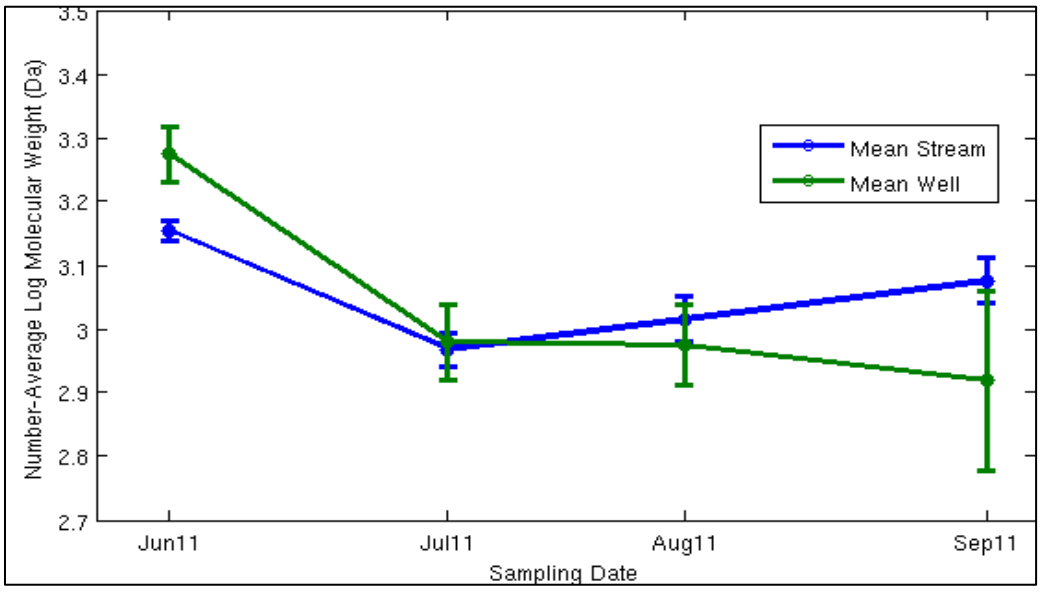

Figure 24. Number-average log molecular weight trends. The number average is the weight of the mean molecule in the sample.

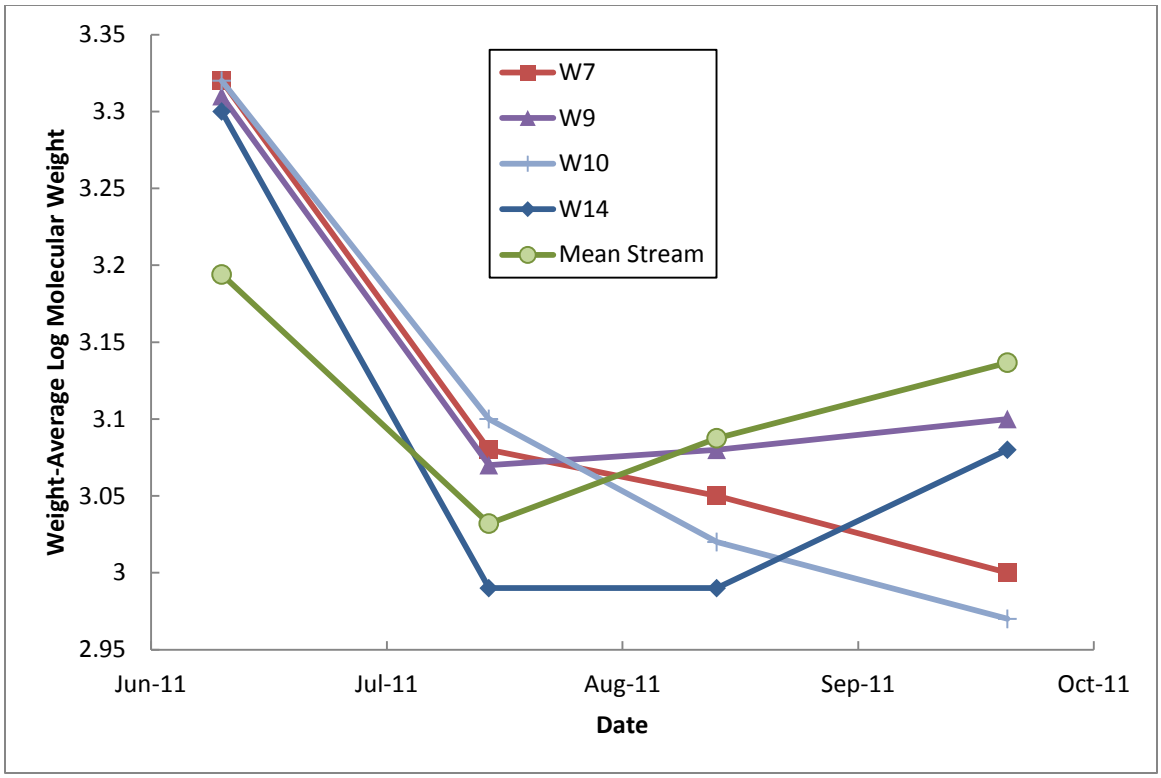

Figure 25. Log M_w trends in focus well samples analyzed for molecular weight.

Focus well M_n trends are not plotted since well trends are nearly identical to M_w trends. In July 2011 samples, all focus well samples have a log M_w of approximately 3.1, while only well 14 has a lower log M_w of 2.99 (Figure 25). Between August and September 2011, M_w in wells 7 and 10 continue to decline while averages in well 14 and stream samples rise.

Polydispersities (figure not shown, ratio of M_w to M_n, a measure of the symmetry of the distribution) in focus well samples steadily increase between June and September 2011, with well 14 the only sample to show a clear decrease in polydispersity between August and September 2011. This decline in polydispersity (trend toward higher symmetry) was also seen in stream samples.

There are no clear correlations between metrics when individual samples are compared. ε280 and polydispersity show the best correlation between independent metrics (r^2 = 0.271), suggesting a weakly positive relationship between asymmetrical molecular weight distributions and aromaticity. There are no other correlations between any of the metrics presented here, except for M_w and M_n, which are positively correlated (r^2 = 0.92).

Inorganic Chemistry

Because DOC is a non-conservative tracer, inorganic chemistry was also analyzed. Chloride and iron concentrations are presented here; chloride is traditionally used as a conservative tracer, while iron may be reactive and bioavailable.

Stream chloride concentrations (see Figure 26) averaged 1.7 mg/L, increasing by 100% between August and September 2011. Well chloride concentrations in May 2011 and July 2011 displayed strong spatial variation due to two wells in May 2011 with chloride concentrations above 15 mg/L (wells 19 and 21) and one well in July 2011 with chloride concentration of 13 mg/L (well 9). August and September 2011 sampling data also contain anomalously high chloride. Well 14 displays high chloride levels (> 10 mg/L) in August and September 2011 due to a test conducted at that well that involved chloride (see Activites Required to Answer Remaining Questions). Neglecting these high concentration wells, well and stream chloride concentrations are positively correlated (r^2 = 0.9569). Considering all chloride data, including high chloride concentration wells, stream and well mean concentrations do not significantly differ on any of the sampling dates reported here.

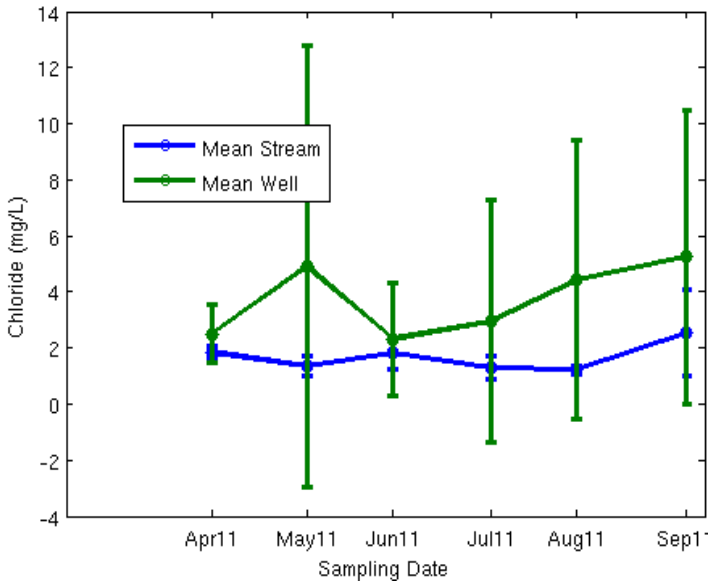

Figure 26. Chloride concentrations in well and stream samples between April 2011 and September 2011.

Iron concentrations (Figure 27) are elevated in well samples in July 2010 and in April 2011. Both of these concentrations could be the result of iron percolating into the hyporheic zone from overlying sediments during snowmelt and monsoon events. In July 2010 and April, May, and June 2011 stream iron concentration was at or near zero mg/L, suggesting that the iron in groundwater samples was not transported to the stream, possibly due to different redox conditions between groundwater and streams. In August 2011 mean iron concentration was ~100% higher in stream samples than in well samples, which indicates an increase in iron inputs into the stream, possibly from groundwater contributions to the stream or ash and debris from the Las Conchas fire.

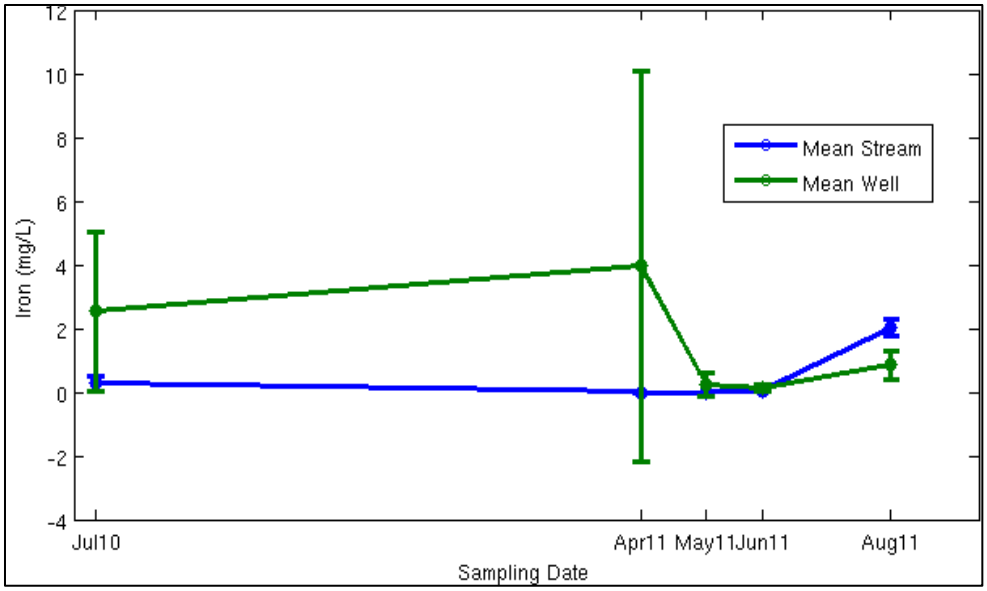

Figure 27. Iron concentrations in well and stream samples for five sampling events.

Desorption

After 48 hours of shaking in a 0.1 $NaClO_4$ solution, aquifer sediments yielded 30 mg/L of DOC, with a fluorescence index of 1.61. Molecular weight distributions were improperly calibrated and are not reported here.

VI. Discussion

Seasonal Hydrology

During snowmelt and monsoon seasons, regional groundwater levels rise, creating stronger lateral hydrologic gradients that could suppress meander bend hyporheic exchange (Cardenas, 2009). During the same wet seasons, high stream stage and flood events could also drive hyporheic exchange. During drier seasons, however, regional lateral gradients are low, creating better conditions for possible sinuosity-driven hyporheic exchange. The extent and seasonality of actual groundwater exchange with the stream is still unclear. Six hypotheses for surface water-groundwater connection are

possible and will be evaluated in context of the DOC quality data presented here. These hypotheses are in part based on developing conceptual models of site hydrology (Gomez, pers. comm.).

1. The stream is gaining water year-round.
2. The stream is losing water year-round.
3. Groundwater flows into the stream during wet seasons, and hyporheic flow develops during dry seasons.
4. Flood events during wet seasons drive hyporheic exchange, and baseflow (groundwater-supported) dominates streamflow during dry seasons.
5. Groundwater flows through the stream from one bank to the other (throughflow).
6. There is no local lateral exchange between surface water and groundwater.

Groundwater dynamics on the scale depicted in Figure 5 clearly show seasonality in groundwater elevations, discounting hypotheses 1 and 2. In-stream piezometer data show almost year-round flux of water from the stream-bed to groundwater (Gomez, unpublished), supporting hypothesis 2. Hypothesis 5 is based on the observation that a hydraulic head gradient in a well transect perpendicular to the stream continues on the other side of the stream, suggesting groundwater flow through and under the streambed. Modeling of lateral hyporheic zones similar to the one studied here showed an increased hyporheic zone area during dry seasons (Wroblicky et al., 1998), supporting hypothesis 3. Since hydraulic conductivity of meander sediments is within the range of a gravel lithology (Fetter, 2001) and wells near the stream respond to peak hydrological events almost simultaneously (see Figure 6), it may be that wells are either reasonably well

connected to each other horizontally, or isolated from each other and simply responding to the same vertical hydrologic fluxes. Further, low lateral gradients raise the question of whether lateral or vertical (recharge-driven) flow dominates this system. Lateral flow may generate exchange with stream water, as in Hypotheses 1, 3, 4, and 5, whereas strictly vertical flow would primarily support Hypotheses 2 or 6. Vertical hydraulic conductivity in aquifer materials is uncharacterized.

Several strong groundwater responses to hydrologic events are depicted in Figure 6. Since not all of these events correspond to local precipitation events, groundwater elevations may be responding to precipitation events elsewhere in the watershed. Heightened stream stage due to these events could generate flood events, which could generate hyporheic exchange and would support hypothesis 4. Flood events could also deliver oxygenated water to the system, as observed in Figures 9 and 10.

Sources and Pools of DOC

Investigating the hypotheses above requires defining possible sources of water at the Jemez River meander site. For the purpose of discussion, it is assumed that stream water, local recharge (precipitation), and regional groundwater flow are the three possible sources.

DOC at this site may have several sources. Local sources may include grass litter and in-stream production by algae and aquatic macrophytes. Unfortunately the field study did not include collection of these possible sources. Previous studies have determined DOC quality of end member plants by leaching samples in MilliQ water (Mladenov et al., 2007), but this approach is limited in its representation of field conditions. Desorption

experiments showed up to 30 mg/L of DOC associated with aquifer sediments, with a fluorescence index of 1.61, comparable to the mean FI in groundwater across all sampling dates (1.60). This sample better represents field DOC under environmental conditions.

Between May 2011 and June 2011, mean DOC concentration in groundwater wells decreased by 48%. In similar snowmelt flushing events, Hornberger et al. (1994) and Baker et al. (2000) attributed the logarithmic decrease in DOC concentration to increased heterotrophic activity, driven by an influx of labile carbon into a carbon-limited subsurface ecosystem.

In the Jemez River meander system, mean subsurface DOC concentrations exceed concentrations in the stream in all sampling events except for August 2011. Sobczak and Findlay (2002) observed that hyporheic DOC concentrations in vertical hyporheic zones never exceeded surface water DOC concentrations. Baker et al. (2000) showed that in a lateral hyporheic system subsurface DOC concentration exceeded concentration in the stream through most of the year (except during snowmelt). If the source of DOC in a vertical hyporheic zone is solely stream DOC then it is not surprising that hyporheic DOC concentration is consistently below stream DOC. But in lateral hyporheic zones where DOC is seasonally derived from overlying sediments (Baker et al., 2000; Brooks et al., 1999) groundwater DOC concentration may (and does at the Jemez River meander site) exceed stream concentration during flushing events. In August 2011, mean DOC concentration in wells is 2 mg/L lower than mean stream concentration. In a carbon-limited system, as hyporheic zones have been shown to be (Baker et al., 1999, 2000), groundwater DOC decreases with time through heterotrophic activity. In the case of

Hypothesis 3, hyporheic exchange in August 2011 may deliver labile stream DOC into the hyporheic zone where it is rapidly utilized by microbes.

As noted above, the contribution of vertical hydrologic recharge to the hyporheic zone has not yet been fully assessed at this site. Vertical recharge would leach soil DOC derived from grass litter into aquifer sediments. In a similar experiment to the leaching experiments above, soil DOC could be leached in MilliQ water (Kothawala et al., 2009) and characterized as a contributing source that is more directly connected to aquifer sediments than fresh grass litter. Although sediment samples have been collected from the meander site as part of well installation, and aquifer samples subjected to desorption experiments, soil layers have not been leached and analyzed. Fresh samples will need to be collected to accurately ascertain soil organic matter properties. Seasonal contributions of soil DOC can be assessed by collecting and analyzing several samples throughout the year. The impact of collecting numerous soil samples on the field site will need to be addressed and minimized while balancing the need to collect a sufficient volume of soil to obtain a useful amount of DOC.

Another source of organic matter at this site may be soil DOC transported horizontally along shallow groundwater flowpaths. This DOC would have leached vertically into the soil elsewhere in the watershed. Currently, groundwater sampling wells only exist within the elk exclosure fence, within approximately 100 m of the stream. Consistent sampling of these farther wells (installed in June 2011 and sparsely sampled throughout the remainder of the field season) can contribute to understanding of this DOC source.

The April 2011 DOC concentration spike is likely due to flushing of overwinter soil DOC during snowmelt (Hornberger et al., 1994) and the September 2011 spike is likely due to monsoonal flushing, also from soil DOC, and may be vertically and/or horizontally transported, with possible local and regional DOC sources. Resolving the source of water in meander bend sediments will help resolve the source of seasonally flushed DOC. In this high mountain system, snowmelt and monsoon precipitation are the two dominant hydrologic drivers. Infiltration of snowmelt and monsoon precipitation can mobilize pools of DOC that have built up in soils during low-flow periods (Hornberger et al., 1994; Boyer et al., 1996; Brooks et al., 1999). The areal extent of DOC source will not be examined here, but previous studies have suggested that a significant fraction of the watershed may contribute to spring DOC flushing (Boyer et al., 1996). DOC concentration spikes are not observed in stream water grab samples. Given the intermittent nature of grab samples, it is possible that any stream DOC pulse was missed in sampling. The highest concentrations of DOC are found in wells T3, 7, and 11, especially in April and May 2011. As mentioned above, wells 7 and 11 are near to and north of the stream, whereas well T3 is a relatively farther distance northwest of the stream. Wells in the interior of the meander bend sediments display lower DOC concentrations. The high concentrations could be zones of DOC accumulation on south stream banks, horizontally transported (see Figure 28) or could be due to variation in amount of DOC leached vertically from overlying soil and plant litter. Desorption of DOC from aquifer sediments could also produce these high DOC concentrations.

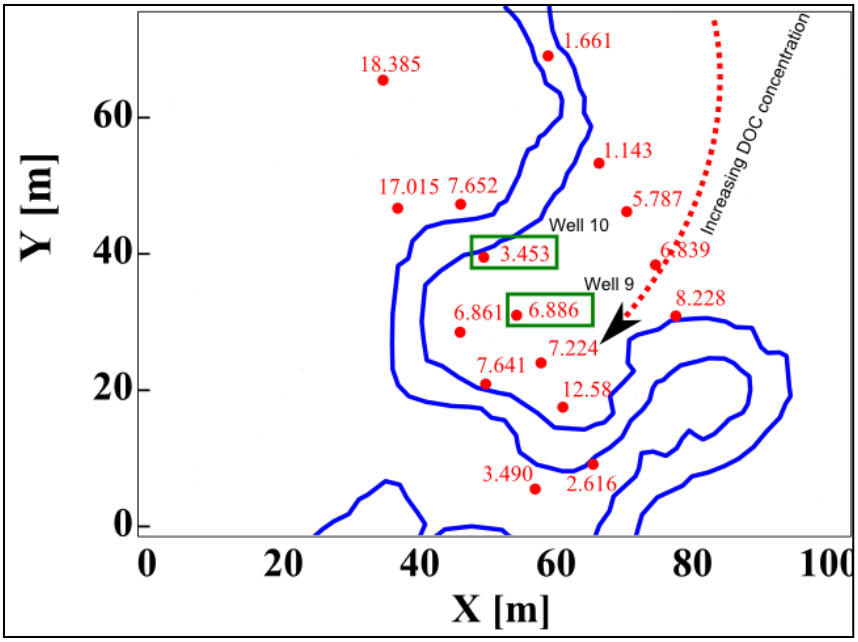

Figure 28. Map showing DOC concentrations in groundwater wells in April 2011 (with some results for May 2011 for wells not sampled in April) showing southward trends of increasing DOC concentration within meander bend sediments. A dotted line depicts the trend of increasing DOC concentration. Wells 9 and 10 are noted with green boxes.

Well fluorescence indices (FIs) in April and May 2011 are well correlated with each other and very distinct from those in the stream (mean 1.67 versus 1.39, respectively). From June 2011 onward, focus well FI patterns diverge, with wells 7, 8, and 11 retaining a relatively high FI while the FI of well 9 decreases to stream-like levels. Thus, wells 7, 8, and 11 have a persistent hyporheic zone groundwater-like FI signal, while wells 9 and 10 show stronger influence from the stream. From July onward, FI in well 10 is very well correlated with the stream.

Higher FI in ground waters, suggesting a microbial origin, has been observed by McKnight et al. (2001) in groundwater entering a Minnesota lake, by Wong & Williams (2009) in a streambed hyporheic zone, and by Johnson et al. (2011) in longer flowpaths of a tropical forested watershed. A measure of microbial respiration such as pCO_2

formation (Baker et al., 1999), not conducted during this study, would discern whether this high ground water FI is due to microbial processing or to a less lignaceous DOC source.

In contrast, FI in stream water is consistently low, especially in the June sampling event. During the summer season, significant in-stream plant and algal growth occurs, which should increase FI and lessen the terrestrial nature of the DOC. However, Lutz et al. (2012) have shown that in the presence of a more bioavailable form of DOC, such as that produced autochthonously, heterotrophs will preferentially consume the autochthonous DOC and allow the allochthonous, terrestrial, refractory DOC to flow downstream, increasing the terrestrial nature of in-stream DOC (decreasing FI).

Between May and June 2011, FI in stream samples decreased by 14%, from 1.42 to 1.20. In this same interval, FIs in focus wells also decreased. The magnitude of decrease was not uniform in all focus wells. Well 9 FI decreased 18%, from 1.65 to 1.35. Well 7, 10, and 11 FIs decreased ~6%. Well 8 FI only decreased 1%. Because a low FI indicates the presence of aromatic, lignaceous and terrestrial material and a high FI indicates its absence (McKnight et al., 2001) it is unlikely that this decrease in FI is due to groundwater influence on stream water, as groundwater consistently displays a higher FI than stream water. This FI decrease is strong evidence for stream water influence on groundwater DOC quality. The spatial variation in FI decrease in focus wells may result from both conservative mixing and non-conservative DOC processing. Streamwater influence on groundwater in dry seasons supports Hypothesis 3.

Mean hyporheic zone aromaticity, as estimated from ε280, significantly differed from mean stream aromaticity only during July and August 2011. This challenges Hypothesis 3, in which streamwater DOC influences groundwater DOC during dry periods (neglecting a time lag of several months between stream and groundwater chemical responses), and supports Hypothesis 4, in which hyporheic exchange develops during wet periods due to flood pulses and the stream is gaining groundwater during dry periods.

Following July 2011, groundwater molecular weight averages decreased while stream molecular weight averages increased. Ågren et al. (2008) observed seasonal trends of molecular weight and aromaticity in boreal streams, comparing forest-derived and wetland-derived DOC. Wetland-derived DOC had a higher molecular weight average and higher aromaticity than forest-derived DOC. During snowmelt, forest-derived DOC contributed more to stream DOC quantity and quality, and during low flow periods wetland-derived DOC dominated if wetland coverage exceeded 10% of the catchment area.

As mentioned above, the broad, flat grasslands of the Valle Grande can develop into ponds and saturated grasslands during periods of high water table, such as snowmelt and monsoon events. Increased "wetland" area during the early monsoon period of 2011, beginning in late July, could be the source of increased molecular weight averages in the stream in August and September 2011 samples. If this is the case, then it lends evidence to hypotheses 3 or 5; that the stream is gaining during wet seasons or that groundwater flows through the stream, respectively. In either case, high molecular weight DOC from upstream wetlands would produce the increasing molecular weight trend, and decreased

hyporheic exchange due to strong lateral hydrologic gradients could explain why molecular weight averages in groundwater do not rise with streamwater.

PARAFAC component1 loadings, normalized to DOC concentration, represent loading of a terrestrial humic signal, possibly derived from grasses and derivative soil DOC. These loadings are highest in well samples in July 2011. Stream loadings do not follow this trend. As discussed above, microbial consumption of labile DOC can cause an apparent trend toward a more terrestrial quality. If that is the case here, then this is another challenge to Hypothesis 3, since the same result would occur if groundwater DOC were being microbially processed in isolation from replenishment from the stream.

The effect of the Las Conchas fire on this system is not readily discernible, partly due to a lack of interannual DOC data, but also due to the intermittent nature of sampling events. Because the fire occurred in the dry pre-monsoonal months and was fully extinguished during the monsoon, it is difficult to separate fire-related effects from seasonal effects. The rise in aromaticity in well and stream samples in July 2011 occurred at the same time as the Las Conchas fire. If this increase in aromaticity is due to fire effects, it sheds light on the magnitude of the time lag between stream and groundwater chemical responses. DOC and FI do not exhibit dramatic changes between June and July 2011, but MW averages, as has been noted, dropped between June and July. This is inconsistent with an influx of black carbon, though, as combustion depletes low MW compounds and produces high MW compounds (Kiersch et al., 2012).

Chloride concentrations in well and stream samples illustrate the connectivity between stream water and groundwater, but they do not indicate seasonal variation in flow

patterns. Iron data indicate that iron concentrations in stream samples were at or near zero in summer 2010 and in late spring/early summer 2011. Iron concentrations in August 2011, though, were non-zero and suggest groundwater as the source of in-stream iron, supporting hypothesis 4.

Suspended particles in the well waters appear to hold a large amount of particulate organic matter and inorganic colloids, comparable to the quantity of DOC adsorbed to sediments, making turbidity dynamics a critical component of DOC dynamics in this system. Observed pulses of turbidity follow snowmelt and monsoonal rains, suggesting that they respond to an influx of water and dissolved oxygen. A sudden inflow of oxygenated water would cause FeOOHs to form and precipitate, adsorbing DOC. Pulses of dissolved oxygen recorded in wells 3 and S2 during snowmelt and monsoon seasons reinforce this hypothesis, as do elevated concentrations of iron in groundwater in April 2011.

As noted above, acidification of samples to pH = 2 caused suspended particles to settle and, at this pH, would cause metal oxides to dissolve. The humic materials associated with these iron oxides would then be released into solution. However, humic acids are insoluble at pH = 2, and would precipitate and settle. DOC can act as an electron donor in the reduction of Fe (III) to soluble Fe (II) either abiotically or as part of a biological process (Lovely & Phillips, 1988; Deng & Stumm, 1994). In the case of Hypothesis 6, the iron chemistry of the hyporheic zone could be a controlling factor on DOC mobility and transport along with recharge.

Hypothesis 5, postulating throughflow, is not currently able to be investigated with DOC quality data because the majority of samples were collected from wells east of the stream. Wells do exist west of the stream, and future efforts to characterize the Jemez River meander system should examine DOC quality dynamics in west wells to more fully develop this throughflow hypothesis.

VII. Conclusions

Evidence for Working Hypotheses

DOC quality is used here to address the question of groundwater-surface water connectivity in a meander bend of the East Fork Jemez River, which may follow one of the six hypotheses stated above.

Figure 5b offers evidence of seasonal periods in which the stream is losing water to streambank sediments in contrast to groundwater elevation patterns in Figures 5a and 5c, which show a hydrologic gradient towards the stream. This seasonality eliminates Hypotheses 1 and 2.

The correlation between stream DOC quality metrics and groundwater DOC metrics in the pre-monsoon season is plausible evidence for stream-groundwater connectivity during dry seasons, supporting Hypothesis 3. This hypothesis is also supported by low regional groundwater elevations in pre-monsoon months and by the high temporal correlation between stream and well hydrologic responses. However, not all metrics support this hypothesis. Well 10 (situated on the stream bank) does not follow stream trends in aromaticity or molecular weight averages during pre-monsoon months. If any hyporheic exchange is occurring in streambank sediments, wells closest to the stream are

the most likely to retain a streamlike DOC quality. Hyporheic zone processing and alteration of DOC quality may mask the true extent of hyporheic exchange. Processing of DOC within the hyporheic zone is explored further in Chapter 3. A significant drop in fluorescence index between May and June 2011 in both stream and well samples provides the best evidence for stream water influence on groundwater DOC dynamics during dry seasons.

Hypothesis 4 is supported by iron chemistry data, suggesting a groundwater source of in-stream iron, and by groundwater elevation data that indicate hydrologic responses to precipitation events occurring elsewhere in the watershed. These responses can generate hyporheic exchange during wet seasons.

Hypothesis 6 retains merit, especially in light of low horizontal hydraulic gradients in groundwater wells. If vertical recharge is a source of DOC to groundwater then it is plausible that DOC processing occurs in isolation from streamwaters and any correlation between stream and groundwater DOC quality is coincidental.

Activities Required to Answer Remaining Questions

A key question is whether vertical or lateral flow is dominant in the meander system. Vertically nested wells and vadose zone samplers at the Jemez River meander would provide an estimation of vertical hydrological flux versus lateral flux. Data from these nested wells can be coupled with data from soil moisture sensors already in place at the Jemez River meander to evaluate vadose zone hydrology at this site. Several sets of nested wells within meander bend sediments would need to be compared with far-field nested wells to compare regional and near-stream flow.

A conservative tracer test would shed light on hydrologic flow paths at a scale on the order of meters. Because site hydrology changes seasonally, multiple tracer tests throughout the year may be necessary. Tracers may be introduced either in the stream channel, to trace stream water in hyporheic sediments, or directly into wells to measure interwell flow. Both of these approaches have been attempted at this site, with neither providing meaningful results. In the stream channel injection, tracer concentration was not constant, possibly due to incomplete mixing of the injection solution. In the well injection, periodic sampling and maintenance at injection wells disrupted continuous tracer monitoring. Further tracer tests at the site are planned for the 2012 field season.

Understanding of site chemistry is still developing. In-situ sondes in wells 3 and S2 (Figures 9 and 10) are providing valuable water chemistry information, including dissolved oxygen concentrations. Chemical responses to hydrologic events, such as the oxygen detected during snowmelt and monoon events, illuminate the system's chemical response to perturbations. Grab samples are useful for first-order characterization of the system, but continuous in-situ monitoring is necessary to capture responses to strong hydrologic events. Baseline dissolved oxygen concentration varies with time in well S2 (Figure 10) but the same magnitude of baseline variation is absent in well 3 (Figure 9) indicating spatial variation in groundwater dissolved oxygen. Measurements of groundwater chemistry in far-field wells will help assess the relative influence of vertical infiltration on groundwater chemistry, essentially independent of streamwater influence. Wells that would provide valuable data from in-situ water chemistry measurements are wells 8 (in the center of the well field and displays trends independent from surrounding

wells), 12 (situated on the stream bank on a smaller meander bend), and 27 (well situated farthest from the stream to investigate vertical chemical effects as mentioned above).

An assessment of biological activity in groundwater, key to attributing changes in FI and DOC concentration to biological processes, could be undertaken by assessing the CO_2 produced in the groundwater system over time (see Baker et al., 1999; Brooks et al., 1999). In most terminal electron acceptor processes (methanogenesis using CO_2 as an electron acceptor being the notable exception), heterotrophic microorganisms will produce CO_2 as the end product of respiration. A further assay of the microbial ecology at this site, which may be highly variable from well to well, would have to take into account the relative amount of bacteria present in surficial biofilms, as opposed to just free-living bacteria. Assessment of microbial substrate utilization, hydrolysis rates, or substrate preferences might also help address the question of the importance of microbial processes in the hyporheic zone for determining DOC quality and mobility.

The dynamics of turbidity in the meander wells pose questions related to DOC mobility and subsurface geochemistry. In-situ turbidity and dissolved oxygen meters provide a way to correlate groundwater oxidation state with the presence of this turbid material, and monitoring of groundwater and stream water iron chemistry would provide further insight into the source and fate of the iron possibly producing this turbid material. The nested well sets would be ideal locations to place this equipment to identify how iron and oxygen flow through this system in three dimensions.

A lignin phenol or $\delta^{13}C$ analysis (Onstad et al., 2000) may be able to identify the contributions of grasslands and conifer forests to the DOC observed at the Jemez River

meander. Since conifers contain a higher lignin and hemicellulose content (Aerts & Chapin, 2000), and grasslands contain C4 photosynthetic species, estimating the contribution of each major plant type may resolve FI dynamics.

Implications for Climate Change in Mountain Headwater Streams

The transient and seasonal nature of a possible hyporheic zone in the Jemez River meander system has implications for forecasting climate change scenarios. Since a larger hyporheic zone may develop under low water table conditions, a drier climate in the Valles Caldera would result in a longer dry season in which a hyporheic zone could exist. Also, the monsoonal input pulse of DOC into meander sediments shows that the annual pool of labile soil organic carbon is not fully depleted during snowmelt. Subsurface DOC leaching during hydrological events would still occur under climate change scenarios in which precipitation type shifts from snow to rain. DOC flushing would likely be proportional to the timing and magnitude of these events (Brooks et al., 2007) and the duration since the last flushing event (Dahm et al., 2003).

REFERENCES

Aerts, R., and F.S. Chapin III, 2000. The mineral nutrition of wild plants revisited: A re-evaluation of processes and patterns. In Advances in Ecological Research, Vol. 30, A.H. Fitter & D.G. Raffaelli, eds. Academic Press.

Ågren, A., I. Buffam, M. Berggren, K. Bishop, M. Jansson, H. Laudon, 2008. Dissolved organic carbon characteristics in boreal streams in a forest-wetland gradient during the transition between winter and summer. Journal of Geophysical Research 113, G03031.

Baghoth, S.A., S.K. Sharma, G.L. Amy, 2011. Tracking natural organic matter (NOM) in a drinking water treatment plant using fluorescence excitation-emission matrices and PARAFAC. Water Research 45,797-809.

Baker, M.A., C.N. Dahm, H.M. Valett, 1999. Acetate retention and metabolism in the hyporheic zone of a mountain stream. Limnology and Oceanography 44, 1530-1539.

Baker, M.A., H.M. Valett, C.N. Dahm, 2000. Organic carbon supply and metabolism in a shallow groundwater ecosystem. Ecology 81, 3133-3148.

Bowen, B., 1996. Rainfall and climate variation over a sloping New Mexico plateau during the North American monsoon. Journal of Climate 9, 3432-3442.

Boyer, E.W, G.M. Hornberger, K.E. Bencala, D.M. McKnight, 1996. Overview of a simple model describing variation of dissolved organic carbon in an upland catchment. Ecological Modeling 86, 183 – 188.

Boyle, E.A., J.M. Edmond, E.R. Sholkovitz, 1977. The mechanism of iron removal in estuaries. Geochimica et Cosmochimica Acta, 41, 1313–1324.

Brooks, P.D., D.M. McKnight, K.E. Bencala, 1999. The relationship between soil heterotrophic activity, soil dissolved organic carbon (DOC) leachate, and catchment-scale DOC export in headwater catchments. Water Resources Research 35, 1895-1902.

Brooks, P.D., P.A. Haas, A.K. Huth, 2007. Seasonal variability in the concentration and flux of organic matter and inorganic nitrogen in a semiarid catchment, San Pedro River, Arizona. Journal of Geophysical Research 112, G03S04.

Cardenas, M.B., 2009. Stream-aquifer interactions and hyporheic exchange in gaining and losing sinuous streams. Water Resources Research 45, W06429.

Chappelle, F.H. 1993. Ground-water Microbiology and Geochemistry. John Wiley & Sons, New York, NY. 424 pp.

Chin, Y-P., G. Aiken, E. O'Loughlin, 1994. Molecular weight, polydispersity, and spectroscopic properties of aquatic humic substances. Environmental Science & Technology 28, 1853-1858.

Coble, P.G., 1996. Characterization of marine and terrestrial DOM in seawater using excitation-emission matrix spectroscopy. Marine Chemistry 51, 325-346.

Cory, R.M., D.M. McKnight, 2005. Fluorescence spectroscopy reveals ubiquitous presence of oxidized and reduced quinones in dissolved organic matter. Environmental Science & Technology 39, 8142-8149.

Dahm, C.N., M.A. Baker, D.I. Moore, J.R. Thibault, 2003. Coupled biogeochemical and hydrological responses of streams and rivers to drought. Freshwater Biology 48, 1219-1231.

Deng, Y.W., and W. Stumm, 1994. Reactivity of aquatic iron(III) oxyhydroxides: Implications for redox cycling of iron in natural waters. Applied Geochemistry 9, 23 – 36.

Fellman, J.B., E. Hood, R.G.M. Spencer, 2010. Fluorescence spectroscopy opens new windows into dissolved organic matter dynamics in freshwater ecosystems: A review. Limnology and Oceanography 55, 2452-2462.

Fetter, C.W. 2001. Applied Hydrogeology. Prentice-Hall, Upper Saddle River, NJ. 598 pp.

Goff F, Gardner J.N., 1994. Evolution of a mineralized geothermal system, Valles Caldera, New Mexico. Economic Geology 89: 1803–1832.

Goff, F., Gardner, J.N., Reneau, S.L., Goff, C.J., 2005. Preliminary geologic map of the Redondo Peak quadrangle, Sandoval County, New Mexico. N.M. Bureau Geology & Mineral Res, Open-file Geol. Map OF-GM-111, scale 1:24,000.

Gomez, J.D. and J.L. Wilson, 2011 "Flow dynamics and connectivity of meandering streams and shallow aquifers: an observational study in northern New Mexico." Poster, AGU Fall Meeting, Dec 2011.

Groffman, A.R., L.J. Crossey, 1999. Transient redox regimes in a shallow alluvial aquifer. Chemical Geology 161, 415 – 442.

Hedin, L.O., J.C. von Fischer, N.E. Ostrom, B.P. Kennedy, M.G. Brown, G.P. Robertson, 1998. Thermodynamic constraints on nitrogen transformations and other biogeochemical processes at soil-stream interfaces. Ecology 79, 684-703.

Helms, J.R., A. Stubbins, J.D. Richie, E.C. Minor, D.J. Kieber, K. Mopper, 2008. Absorption spectral slopes and slope ratios as indicators of molecular weight, source, and photobleaching of chromophoric dissolved organic matter. Limnology and Oceanography 53, 955-969.

Hornberger, G.M., K.E. Bencala, D.M. McKnight, 1994. Hydrological controls on dissolved organic carbon during snowmelt in the Snake River near Montezuma, Colorado. Biogeochemistry 25, 147 – 165.

InciWeb Incident Information System, http://inciweb.org/incident/2385/ , updated 8/3/2011, accessed 1/5/2012.

Ishii, S.K.L., T.H. Boyer, 2012. Behavior of reoccurring PARAFAC components in fluorescent dissolved organic matter in natural and engineered systems: A critical review. Environmental Science & Technology 46, 2006 – 2017.

Johnson, M.S., E.G. Couto, M. Abdo, J. Lehmann, 2011. Fluorescence index as an indicator of dissolved organic carbon quality in hydrologic flowpaths of forested tropical watersheds. Biogeochemistry 105, 149-157.

Kiersch, K., J. Kruse, K-U. Eckhardt, A. Fendt, T. Streibel, R. Zimmerman, G. Broll, P. Leinweber. 2012. Impact of grassland burning on soil organic matter as revealed by a synchrotron- and pyrolysis-mass spectrometry-based multi-methodological approach. Organic Geochemistry 44, 8 – 20.

Kostrzeski J.M., P.D. Brooks, 2005. Quantifying the effects of vegetation and water source on water quality in three watersheds in Valles Caldera National Preserve, New Mexico. EOS Trans. AGU, 86(52), Fall Meet. Suppl., Abstract H31B-1312.

Kothawala, D.N., R.D. Evans, P.J. Dillon, 2006. Changes in the molecular weight distribution of dissolved organic carbon within a Precambrian shield stream. Water Resources Research 42, W05401.

Kothawala, D.N., T.R. Moore, W.H. Hendershot, 2009. Soil properties controlling the adsorption of dissolved organic carbon to mineral soils. Soil Science Society of America Journal 73, 1831 – 1842.

Langmuir, D. 1997. Aqueous Environmental Geochemistry. Prentice-Hall, Upper Saddle River, NJ. 600 pp.

Liu, F., R. Parmenter, P.D. Brooks, M.H. Conklin, R.C. Bales, 2008. Seasonal and interannual variation of streamflow pathways and biogeochemical implications in semiarid, forested catchments in Valles Caldera, New Mexico. Ecohydrology 1, 239-252.

Lovely, D.R., E.J.P. Phillips, 1988. Novel mode of microbial energy metabolism: Organic carbon oxidation coupled to dissimilatory reduction of iron or manganese. Applied and Environmental Microbiology 54, 1472-1480.

Lutz, B.D., E.S. Bernhardt, B.J. Roberts, R.M. Cory, P.J. Mulholland, 2012. Distinguishing dynamics of dissolved organic matter components in a forested stream using kinetic enrichments. Limnology and Oceanography 57, 76-89.

Maurice, P.A., S.E. Cabaniss, J. Drummond, E. Ito, 2002. Hydrogeochemical controls on the variations in chemical characteristics of natural organic matter at a small freshwater wetland. Chemical Geology 187, 59-77.

McKnight, D.M., E.W. Boyer, P.K. Westerhoff, P.T. Doran, T. Kulbe, D.T. Anderson, 2001. Spectrofluorometric characterization of dissolved organic matter for indication of precursor organic material and aromaticity. Limnology and Oceanography 46, 38-48.

Mladenov, N., D.M. McKnight, S.A. Macko, M. Norris, R.M. Cory, L. Ramberg, 2007. Chemical characterization of DOM in channels of a seasonal wetland. Aquatic Sciences 69, 456-471.

Mobed, J.J., S.L. Hemmingsen, J.L. Autry, L.B. McGown, 1996. Fluorescence characterization of IHSS humic substances: Total luminescence spectra with absorbance correction. Environmental Science & Technology 30, 3061-3065.

Morales, V.L., W. Zhang, B. Gao, L.W. Lion, J.J. Bisogni, Jr., B.A. McDonough, T.S. Steenhuis, 2011. Impact of dissolved organic matter on colloid transport in the vadose zone: Deterministic approximation of transport deposition coefficients from polymeric coating characteristics. Water Research 45, 1691-1701.

New Mexico Environment Department, 2006. Final approved total maximum daily load for the Jemez River watershed, Valles Caldera National Preserve, boundaries to headwaters. 207 pp.

Onstad, G.D., D.E. Canfield, P.D. Quay, J.I. Hedges, 2000. Sources of particulate organic matter in rivers from the continental USA: Lignin phenol and stable carbon isotope compositions. Geochimica et Cosmochimica Acta 64, 3539 – 3546.

Phillips, E.H., 2004. Collapse and resurgence of the Valles caldera, Jemez Mountains, New Mexico: 40Ar/39Ar age constraints on the timing and duration of resurgence and ages of megabreccia blocks. M.S. thesis, N.M. Inst. Mining Technol., Socorro, N.M. 200 pp.

Pullin, M.J., C. Anthony, P.A. Maurice, 2007. Effects of iron on the molecular weight distribution, light absorption, and fluorescence properties of natural organic matter. Environmental Engineering Science 24, 987 – 997.

Pullin, M.J., C.A. Progress, P.A. Maurice, 2004. Effects of photoirradiation on the adsorption of dissolved organic matter to goethite. Geochimica et Cosmochimica Acta 68, 3643-3656.

Pullin, M.J., S.E. Cabaniss, 1995. Rank analysis of the pH dependent synchronous fluorescence spectra of six standard humic substances. Environmental Science and Technology, 29, 1460-1467.

Puls, R.W., M.J. Barcelona, 1996. Low-flow (minimal drawdown) ground-water sampling procedures. USEPA Office of Research and Development. 12 pp.

Rodriguez, M., and E. Moser, 2010. Hydrology – Existing Condition Report. Valles Caldera Trust, 21 pp.

Smith, R.L., R.A. Bailey, C.S. Ross, 1970. Geologic map of the Jemez Mountains, New Mexico. Misc. Geol. Invest. Map. I-571.

Sobczak, W.V., S. Findlay, 2002. Variation in bioavailability of dissolved organic carbon among stream hyporheic flowpaths. Ecology 83, 3194 – 3209.

Stedmon, C. A., S. Markager, and R. Bro, 2003. Tracing dissolved organic matter in aquatic environments using a new approach to fluorescence spectroscopy. Mar. Chem., 82, 239 – 254.

Stedmon, C.A., S. Markager, 2005. Resolving the variability in dissolved organic matter fluorescence in a temperate estuary and its catchment using PARAFAC analysis. Limnology and Oceanography 50, 686-697.

Thurman, E.M. 1985. Amount of Organic Carbon in Natural Waters, in Organic Geochemistry of Natural Waters, Nijhoff/Junk, p. 7-65.

vallescaldera.com, "85% of Las Conchas Fire now contained; smoldering blaze dampened by moisture, causing flash flood threat." July 22, 2011. http://vallescaldera.com/archives/date/2011/07, accessed 1/5/2012.

Wong, J.C.Y., D.D. Williams, 2009. Sources and seasonal patterns of dissolved organic matter (DOM) in the hyporheic zone. Hydrobiologia, 647, 99-111.

Wroblicky, G.J., M.E. Campana, H.M. Valett, C.N. Dahm, 1998. Seasonal variation in surface-subsurface water exchange and lateral hyporheic area of two stream-aquifer systems. Water Resources Research 34, 317 – 328.

Zhou, Q., S.E. Cabaniss, P.A. Maurice, 2000. Considerations in the use of high-pressure size exclusion chromatography (HPSEC) for determining molecular weights of aquatic humic substances. Water Research 34, 3505-3514.

Zhou, Q.H., P.A. Maurice, S.E. Cabaniss, 2001. Size fractionation upon adsorption of fulvic acid on goethite: Equilibrium and kinetic studies. Geochimica et Cosmochimica Acta 65, 803-812.

CHAPTER 3: MODELING ENVIRONMENTAL AND CHEMICAL EFFECTS ON SUBSURFACE DISSOLVED ORGANIC CARBON TRANSFORMATION

I. Introduction

The field results presented in Chapter 2 raise questions about the mechanism of DOC quality evolution in the Jemez River meander system, specifically whether the variation in DOC quality in meander bend sediments is due to stream influences or is coincidentally seasonally correlated to stream DOC quality. A model of DOC transformation in a natural environment is employed here to address controls on variation in DOC quality.

To model the various attributes of DOC quality, a multistate model is necessary. Conventional reactive transport continuum models are unable to model the practically infinite range of possible organic carbon molecules in a sample (Cabaniss et al., 2005). Individual DOC compounds can be modeled with another approach-- agent-based modeling. In this approach each molecule is modeled as an individual with unique properties that define its quality and determine its probability of chemical transformation. This approach can model numerous classes of DOC and even generate new classes

through biotic and abiotic processes. A review of previous DOC modeling efforts provides the context and framework for the model developed for this study.

II. Modeling DOC

Previous Modeling Efforts

Experiments involving metal complexation (Hering & Morel, 1988) led to the development of models of DOC effects on metal binding (Bartschat et al., 1992; Robertson & Leckie, 1999). These have developed into current speciation and binding models such as the Windemere Humic Aqueous Model (WHAM) which models ion binding with humic substances, metals, and clays.

Currently, modeling of DOC transport is carried out at soil profile scales (Michalzik et al., 2003; Tosiani et al., 2006) and scales of riverine export to oceans (Manizza et al., 2009). Michalzik et al. (2003) divide the soil DOC pool into three classes: immobile, hydrophilic, and hydrophobic. The latter two classes are transported through soil horizons, and adsorbed onto surfaces via an equilibrium partition coefficient model. Temperature-dependant rate constants determine mass flux between the three soil classes. Manizza et al. (2009), modeling export of DOC into the Arctic Ocean, estimated DOC export from river discharge and treated DOC concentration decay as a simple linear decay rate.

These and other DOC modeling approaches have modeled changes in average DOC properties, but at the trade-off of assuming DOC pools to be homogenous systems, or at least composed of a minimum number of reactive component classes. While useful for

large-scale applications, these approaches cannot capture the molecular-scale dynamics that contribute to large-scale effects.

Agent-Based Modeling

Agent-based modeling (ABM) is a Monte Carlo modeling approach in which individual agents' behavior is determined by both the agents' properties and probabilistic rules (see Figure 29).

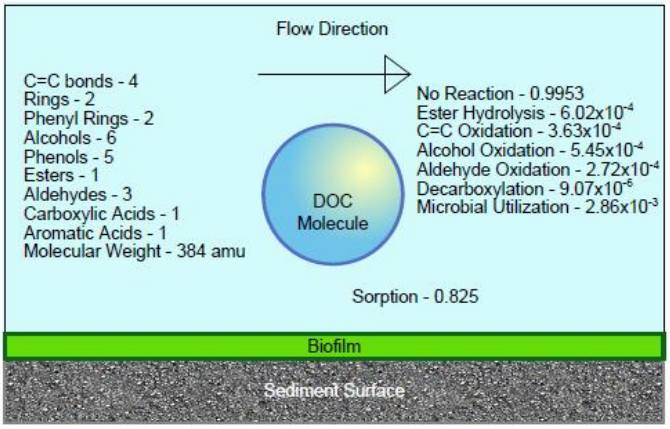

Figure 29. Representation of an agent-based approach for modeling DOC transformation. This hypothetical DOC molecule's functional groups are listed on the left. Its probabilities for transformation, as determined by AlphaStep (Cabaniss et al., 2005) are listed on the right. A biofilm and sediment surface illustrate the molecule's potential to diffuse into the biofilm or sorb onto the sediment surface. Particulate organic matter is not considered in this model.

As DOC is a heterogeneous mixture with individual molecules possessing individual properties, ABM is an ideal approach to modeling DOC evolution in which emergent properties and new molecular structures (agent classes, limited only by chemical structural plausibility) arise from the interactions and transformations of individual DOC molecules (agents). Other applications of agent-based modeling include sorption kinetics (Mishra, 1997), ecological modeling (Grimm et al., 2005), software system design

(Jennings, 2001), and human systems such as business processes and market behavior (Bonabeau, 2002).

Cabaniss et al. (2005) developed the model AlphaStep, the first agent-based forward model of DOC evolution from precursor materials. These precursors are defined molecules that possess chemically plausible functional groups and elemental ratios. These properties in turn determine the molecule's probability of undergoing one of several reactions, which alters the molecule's properties to create a new and unique molecular structure. AlphaStep was designed as a well-mixed reactor with no inputs, outputs, or transport.

To introduce a transport component, Arthurs et al. (2004) developed NOMAdSim, which advected DOC molecules and included algorithms for surface adsorption and desorption, but did not include the chemical transformation algorithms of AlphaStep.

The model presented here is the next step in developing agent-based models of DOC transformation in natural systems. It incorporates the transformation algorithms of AlphaStep with the surface reactions of NOMAdSim. It also employs a Lattice Boltzmann fluid dynamics model to simulate fluid flow through a porous medium, critical for modeling DOC transport in subsurface systems. Using an agent-based model, DOC need not be divided into several lumped classes; rather each molecule can act as its own "class."

Pore-Scale Modeling

In this study, DOC dynamics are modeled at a pore scale. Since an agent-based approach considers individual molecules as agents, modeling at an aquifer or meander scale is

impractical. Pore-scale dynamics contribute to meander-scale DOC behavior, and the groundwork lain in this model will be directly applicable to upscaled modeling efforts. This scale of modeling addresses questions of reaction rates and environmental controls on reactions.

III. Methods

Model Architecture

This model is developed in the NetLogo modeling environment (Wilensky, 1999), using NetLogo 4.1.3, a Java-based program. Agents exist within a global environment, consisting of the entire simulation space. The global environment is divided into "patches" arranged in a lattice grid. Agents act according to probabilistic rules that depend on agent-specific properties, patch-specific properties, and/or properties of the global environment. Full code of this model appears in Appendix D.

Transformation of DOC molecules is governed by algorithms developed for the AlphaStep model (Cabaniss et al., 2005). These transformations fall under the following categories:

- Splitting – Hydrolysis reactions, cleaving either an amide or ester
- Modifying—In which one or more functional groups are changed or removed
- Removing—Microbial utilization, in which a molecule is removed from the simulation
- Bimolecular—Condensation of two molecules through an ester or aldol link

Reactions are described in Table 4 in terms of what environmental parameters affect their probability of occurrence.

Table 4. Types of chemical reactions possible within the AlphaStep algorithm and the environmental factors determining their probability of occurrence.

Reaction Name	Type	Probability Proportional to
Ester Hydrolysis	Splitting	$([OH^-] + [H^+])\ * e^{1/T}$
Amide Hydrolysis	Splitting	$(([OH^-] + [H^+]) + E) * e^{1/T}$
Alkene Hydration	Modifying	$[H^+]\ * e^{1/T}$
Alcohol Dehydration	Modifying	$[H^+]\ * e^{1/T}$
C=C Oxidation	Modifying and Splitting	$O_2 * E * e^{1/T}$
Alcohol Oxidation	Modifying	$O_2 * E * e^{1/T}$
Aldehyde Oxidation	Modifying	$O_2 * E * e^{1/T}$
Decarboxylation	Modifying	$[H^+] * E * e^{1/T}$
Microbial Utilization	Removing	B * (O/C + N) * MW
Ester Condensation	Bimolecular	$Conc * [H^+]\ * e^{1/T}$
Aldol Condensation	Bimolecular	$Conc * ([OH^-] + [H^+]) * e^{1/T}$

E = Enzyme Activity
B = Bacterial Density
T = Temperature
MW = Molecular Weight
O = Number of Oxygen Atoms
C = Number of Carbon Atoms
N = Number of Nitrogen Atoms
Conc = DOC Concentration

All reactions except for microbial uptake are temperature dependent. Hydrolysis splitting reactions are base and acid catalyzed. Alkene hydration and alcohol dehydration are strongly pH dependent. Oxidation and decarboxylation reactions are enzyme-mediated, with oxidation reactions depending on dissolved oxygen concentration. Microbial utilization depends on bacterial density, the molecular weight of the molecule, and the ration of oxygen to carbon. Bimolecular reactions are the only processes in which molecules interact with each other, and occur when two molecules with specified functional groups are in close proximity to each other; hence those reactions are noted as being dependent on DOC concentration. In all other processes, molecules act independently.

DOC molecules begin as one of six precursor structures, thoroughly described in Cabaniss et al. (2005).

- Lignin- Comprised of coniferyl alcohol units.
- Cellulose- Soluble cellulose fragment, comprised of D-glucose units.
- Protein- Comprised of residues of Glutamine, Lysine, Serine, Threonine, Glycine, Alanine, Valine, Leucine, and Phenylalanine.
- Terpenoid- Represented by abietic acid, a diterpenoid.
- Tannin- Represented by meta-digallic acid.
- Flavonoid- Represented by fustin, a pigment.

Four other precursor structures were defined for this model. They represent compounds used in the push-pull experiments described in Appendix A. The structure of these molecules as well as the rationale for selecting them are described in that Appendix. The four additional compounds are acetate, benzoic acid, 2-naphthoic acid, and chloride (as a conservative tracer). While these compounds were added to the code of this model (Appendix D), they were not used in the simulations reported in this chapter. Properties of the original six AlphaStep precursors appear in Table 5. Additional elemental compositions (such as phosphorus) and functional groups can be added; the molecular properties listed here are those that pertain to the original AlphaStep precursors.

Table 5. Properties of DOC precursor molecules. From Cabaniss et al. (2005).

	Protein	Cellulose	Lignin	Tannin	Terpenoid	Flavonoid
Carbon (# atoms)	240	360	400	14	20	15
Hydrogen (# atoms)	382	602	402	10	30	12
Nitrogen (# atoms)	60	0	0	0	0	0
Oxygen (# atoms)	76	301	81	9	2	6
C=C bonds	15	0	160	6	2	6
Rings	5	60	40	2	3	3
Phenyl rings	5	0	40	2	0	2
Alcohols	10	182	2	5	0	4
Phenols	0	0	1	5	0	3
Ethers	0	119	79	0	0	1
Esters	0	0	0	1	0	0
Ketones	0	0	0	0	0	1
Aldehydes	0	0	0	0	0	0
Acids	6	0	0	1	1	0
Aromatic Acids	0	0	0	1	0	0
Amines	6	0	0	0	0	0
Amides	54	0	0	0	0	0

For the simulation runs presented here, a two-dimensional simulation space of 21x45 lattice units was used, with the space scaled to represent an area of 1 mm x 2 mm. Three-dimensional modes of both the NetLogo modeling environment and Lattice Boltzmann fluid dynamic modeling are available; however, for the purposes of this work the benefits of adding a third dimension are not commensurate with the cost in programming complexity and computational resources. Sediment geometry consists of offset, roughly spherical, evenly spaced sediment grains with a minimum pore width of 3 lattice units (see Figure 30). As opposed to a random sediment field, this geometry ensures interconnectedness of pores. The offset of sediment grains leads to a four lattice unit pore width on the right side of the domain, as seen in Figure 30. Given the scaling of the simulation space, the sediment grains are approximately the size of medium sand grains (diameter = 7 lu, or 0.35 mm). This is a realistic sediment size, as medium sand

comprised 22% of aquifer sediment mass (excluding cobbles) at the Jemez River meander. Porosity of this simulation space, defined as the percentage of void space, is 53%.

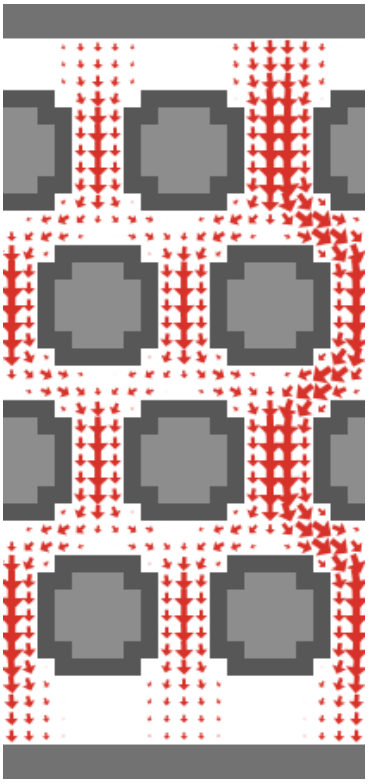

Figure 30. Simulation space, displaying sediment geometry and Lattice Boltzmann-generated velocity field, indicated by red arrows with larger arrows indicating a larger velocity.

Lattice Boltzmann Computational Fluid Dynamics

The fluid velocity field is determined with a Lattice Boltzmann (LB) model (Sukop & Thorne, 2005), a computational fluid dynamics approach that determines fluid properties from stochastic molecular interactions on a lattice grid or, in the case of the NetLogo environment, a "patch" grid. LB methods solve a modified form of the Boltzmann equation for particle movement within a fluid, preserving conservation of fluid mass and momentum. LB methods can simulate the Navier-Stokes equations for laminar flow and

are thus comparable to other computational fluid dynamics methods. A comprehensive explanation of the structure of the LB code presented here is found in Sukop & Thorne (2005). This computational approach is particularly suited to this application since the lattice structure and pattern of probability propagation is easily transferable to the patch-based NetLogo environment.

In this simulation, flow is driven by a pressure gradient on the north and south boundaries of the simulation space, with a periodic boundary on the east and west boundaries. Fluid density is specified at north and south boundaries, which density is related to pressure by an equation of state (Sukop & Thorne, 2005):

$$P = \frac{\rho}{3}$$

where P = pressure and ρ = density.

Fluid density is 1.5 times higher at the north boundary, generating a maximum fluid velocity of 0.048 lattice units per time step (lu/ts) and average fluid velocity (within pore space only) of 0.021 lu/ts. The Reynolds number for this simulation was 1.95×10^{-5}, using a length scale of 3 lattice units (one pore width) and a kinematic viscosity of 357 lu^2/ts (8.92×10^{-7} m^2/s, approximately the kinematic viscosity of water at 25°C; Young et al., 2004). The sediment geometry and velocity field is computed a priori and fixed from simulation to simulation. The velocity field is shown in Figure 30. A continuous density gradient exists between north and south boundaries, reflecting the constant density (pressure) boundaries used.

By using a density gradient as a proxy for a pressure gradient, many LB methods introduce a "compressibility error" (Sukop & Thorne, 2005). This model addresses that error by utilizing the incompressible LB model of Zou & He (1997) which compensates for the compressibility error and is able to reproduce the incompressible steady-state Navier-Stokes equations while still utilizing density boundary conditions as a proxy for pressure boundaries.

DOC molecules move through the simulation space by both advection and diffusion. Their advective velocity and direction is determined by the Lattice Boltzmann flow field, and diffusive velocity and direction is determined by a Brownian motion random walk in which diffusivity is related to molecule volume, which is in turn related to elemental composition in the following equation (Schwarzenbach & Gschwend, 1993).

$$D = \frac{13.26 \times 10^{-5}}{\mu^{1.14} \cdot V^{0.589}} \ (cm^2\ s^{-1})$$

D represents diffusivity (1 cm^2/s = 4000 lu^2/ts), μ the dynamic viscosity of water (variable with temperature; Young, 2004) and *V* represents molecular volume. V is determined by the following equation (ibid.).

$$V = C * 16.5 + H * 2 + O * 5.5 + N * 5.7 + S * 17 - (Rings * 20.2)$$

C, *H*, *O*, *N*, and *S* represent atoms of carbon, hydrogen, oxygen, nitrogen and sulfur, respectively, in a molecule.

The maximum allowable diffusivity was 1 lu^2/ts, since a diffusive movement of greater than one patch would involve inertial effects that are not considered here. Setting one time step equivalent to one second, and one lattice unit equal to 0.05 mm, the maximum

allowable diffusivity was 2.5 x 10^{-5} cm^2/s. Maximum diffusivities generated in simulation runs were on the order of 1 x 10^{-5} cm^2/s within the allowable limits.

Under base case conditions, molecular diffusivities ranged from 0.01 to 0.4 lu^2/ts, compared to a mean fluid velocity of 0.021 lu/ts. Peclet numbers of individual molecules (ratio of advective patch velocity to molecular diffusivity) ranged from 7 x 10^{-4} to 1.54. These values include those for molecules in areas of very low patch velocity, resulting in very low Peclet numbers. 10% of molecules had a Peclet number greater than 1. These numbers indicate that, in light of low advective velocities, diffusion is the dominant transport mechanism for most molecules.

Although methods for solute transport have been determined within a Lattice Boltzmann context (Sukop & Thorne, 2005), they would not be appropriate in this simulation since the Lattice Boltzmann model produces a velocity field only, then halts to allow particle transport and chemical transformation. Thus, a molecular advection-diffusion model based on Brownian motion is an appropriate approach at this stage of model development where the fluid velocity field is assumed to be in steady-state.

Time Scales

Determining appropriate spatial and temporal scales for this simulation required reconciling three time scales. Advective velocity, as generated by the Lattice Boltzmann method, has units of lu/ts. Each lattice unit corresponds to one patch. Diffusivity, as calculated according to the method above, has units of cm^2/s, and chemical kinetics, as determined in AlphaStep, operate optimally with a time step of 0.1 hr. As noted in

Cabaniss et al. (2005), modifying the default reaction time step of 0.1 hr may invalidate assumptions used to calculate reaction rate constants.

To accommodate the time scale of chemical kinetics, chemical transformation of molecules occurred every 360 time steps, or 0.1 hr. Advection, diffusion, sorption and desorption operated on the 1 s time scale, while chemical transformation operated on the 0.1 hr time scale.

Advective velocity, as with diffusivity, could not exceed 1 lu/ts. A minimum molecule residence time within the simulation space of 360 time steps (seconds) ensures that each molecule has at least one opportunity for chemical transformation. A maximum advective velocity of 0.048 lu/ts and mean velocity of 0.021 lu/ts led to a mean minimum residence time of 311 time steps (100 runs, $\sigma = 57$). Following a standard simulation length of 9000 time steps, under base case conditions, mean residence time of particles within the simulation space was 2008 time steps, or approximately 0.6 hr.

Model Assumptions

This model assumes that the velocity field and initial DOC composition do not change with time. Given the short duration of simulation runs, this is a fair assumption. For surface interactions, we assume that all surfaces are equally likely sites of microbial uptake, assuming that biofilms coat all surfaces, and that the free-floating microbial population is much less metabolically active compared to the biofilm population (Lyons & Dobbs, 2012). Hence, microbial utilization only occurs at surfaces. No processes involving electron acceptors other than oxygen are modeled in this version of the model. The oxygen concentration is not transient, as it would be in a biologically active system.

Additional model development is needed to address the low oxygen concentrations at the Jemez River meander site (see Chapter 2). All biotic interaction is contained in the microbial utilization process (which removes molecules from the simulation) and in enzyme activities (which mediate splitting and oxidation reactions). Environmental parameters pH, O_2 concentration, temperature, and enzyme activity are user-defined and are fixed throughout the simulation. Ionic strength is assumed to be low, making the model suitable for non-marine environments.

Beginning the Simulation

Following generation of the velocity field, users define the set of precursor molecules. Precursors are fixed in space at the north boundary and periodically emit DOC molecules into the simulation space. One molecule is emitted into the simulation space per time step, with random selection of the starter molecule that emits the dissolved molecule. These dissolved molecules are generated by, and are initially identical to, starter molecules. Starter molecules classified as large precursors are cellulose, lignin, and protein. Small precursors are tannins, terpenoids, and flavonoids.

Aqueous Chemical Transformation

Throughout the simulation, hundreds of unique structures may develop. At each reaction time step (every 360 time steps, or every 0.1 hr) the structure of the molecule determines the probability of undergoing a reaction. A pseudo-random number, unique to each molecule, is generated and the sum of probabilities is compared against this number to determine if a reaction occurs. If so, the number is then used to determine which reaction occurs. The sum of all reaction probabilities for a molecule on a 0.1 hr time scale should

remain below 0.01 (Cabaniss et al., 2005). The average probability of a reaction occurring among all molecules is on the order of 1×10^{-3}.

Surface Transformations

At sediment surfaces, molecules may adsorb or be taken up by microbes, depending on molecular properties. Sorption sites are exclusive; there is only one molecule sorbed at each site. Sorption and desorption probabilities are dependent on molecular weight (Arthurs, et al, 2004; Zhou, et al, 2001; see Figure 31), which is correlated to molecular hydrophobicity (Cabaniss et al., 2007).

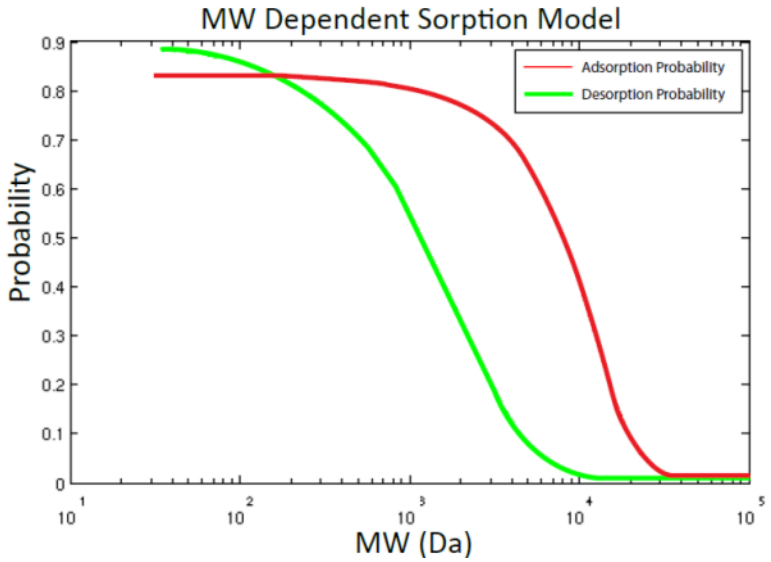

Figure 31. Probabilities of sorption and desorption are determined by molecular weight.

Microbial uptake probability is determined by molecular weight and the ratio of oxygen to carbon atoms (Cabaniss et al., 2005). Microbial uptake is the only process in this model in which molecules are removed from the simulation space and which ignores the products of the reaction.

When molecules reach the southern end of the simulation space, their transport and transformation is halted and they are classified as "dormant" to allow for later inspection of their final state. A diagram of the simulation space, as it appears during a simulation run, appears in Figure 32.

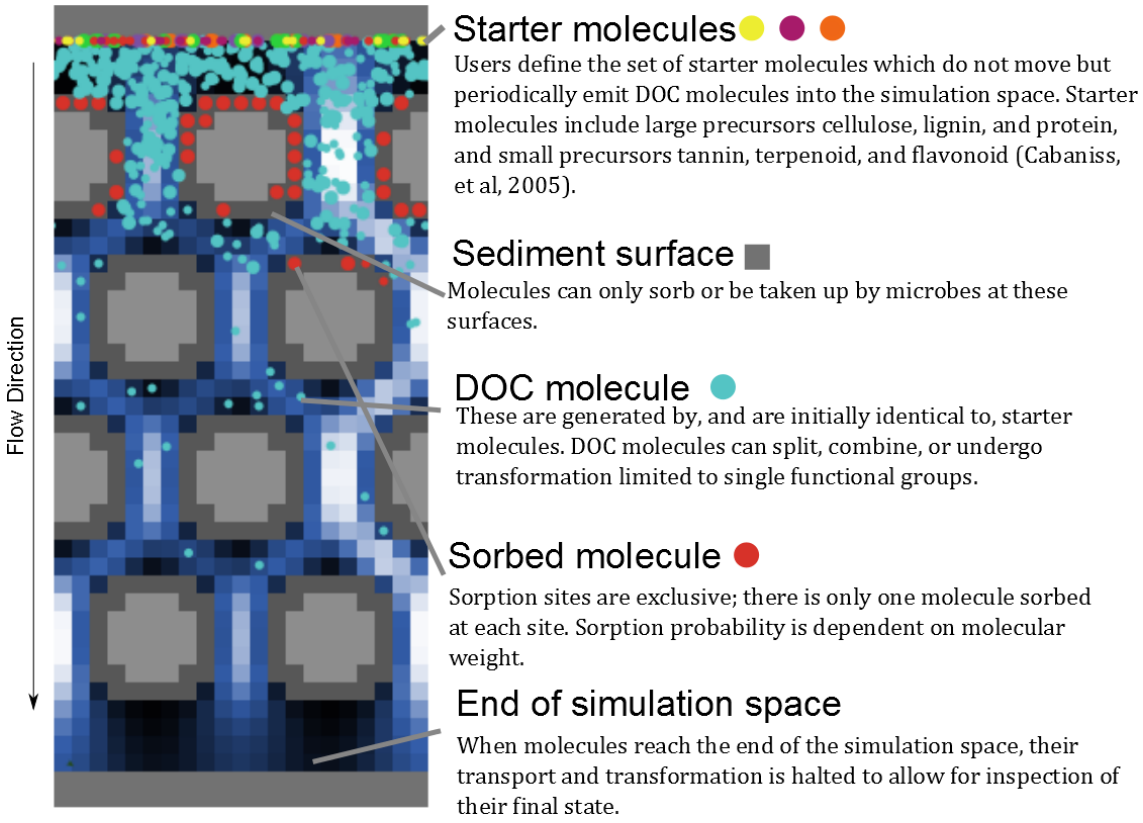

Figure 32. Simulation space for the agent-based model of DOC transformation. The space is 21 x 45 lattice units. Brighter blue patches indicate areas of higher fluid velocity.

Modeling Approach

To investigate the effect of changing conditions on DOC quality, model runs were executed, varying one parameter at a time, and recording output metrics at both the north and south ends of the simulation space. Temperature, pH, O_2 concentration, enzyme activity, bacterial density, percentage of large precursors, and initial number of starters

were independently varied in this sensitivity analysis. For each parameter, five settings were applied, ranging from the minimum to the maximum values of that parameter. The value reported for each combination of parameters is the average of five runs with identical conditions. Runs were conducted for 9000 time steps, with each step representing 1 s, for an approximate simulation time of 2.5 hr. The first 4000 time steps of each run were considered a spin-up period (to allow DOC "inflow" and "outflow" rates to stabilize) and were not included in average values. Intermediate conditions for all parameters were labeled as base case conditions. The settings of each parameter are summarized in Table 6.

Table 6. Settings for parameters examined in model runs. Enzyme Activity and Bacterial Density are dimensionless numbers and are not correlated to field metrics.

	Minimum	Low	Base Case	High	Maximum
Temperature (°C)	0	15	25	35	50
pH	0	3.5	7	10.5	14
O_2 Concentration (mM)	0	0.05	0.1	0.5	1
Enzyme Activity (dimensionless)	0	0.05	0.1	0.5	1
Bacterial Density (dimensionless)	0	0.05	0.1	0.5	1
Percentage Large Precursors	0	25	50	75	100
Number of Starters	6	50	100	150	200

These parameters are analogous to conditions that may exist in a natural system, although high temperatures and extreme pHs are outside natural ranges. Temperature variation represents seasonal climate variation. pH variation in a natural system may be controlled by a variety of factors including carbonate chemistry and sulfur oxidation. Oxygen concentration may vary due to inputs of oxygenated water and consumption of oxygen by biological processes. Enzyme activity may vary in response to the amount or quality of bioavailable substrate in the system, as may bacterial density. Percentage large precursors

represents a changing DOC source, with large precursors representing freshly derived DOC. Number of starters represents the concentration of the DOC source.

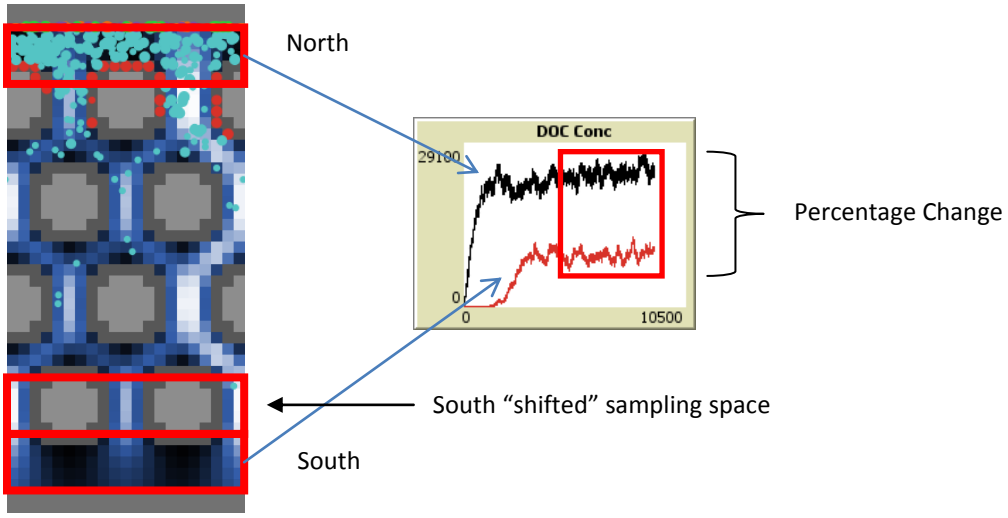

Figure 33. Areas of simulation space sampled. Results reported as a percent difference indicate the percentage change in the metric between the north and south sampling points. Sampling areas are 21 x 5 lattice units.

Some output metrics are presented as the percent difference between the north and south ends of the simulation space (see Figure 33) in order to highlight quality effects due to transport through the simulation space. Four output metrics, DOC concentration (measured as mass C / area of sampling point), aromaticity (measured as percent sp^2 hybridized carbon), number-average molecular weight (mean of the molecular weight distribution) and weight-average molecular weight (weight of molecule to which the average atom belongs, see Chapter 2 for equations used to calculate molecular weight metrics) are measured in simulations; all four are also measurable in field samples. Additional field metrics reported in Chapter 2 (fluorescence index and parallel-factor analysis loadings) are not yet measured with this model. The following non-field measureable metrics were tracked: amide hydrolysis rate, ester hydrolysis rate, C=C oxidation rate, number of molecules taken up by microbes, mean residence time of

dormant molecules, mean mass of sorbed molecules and mean mass of microbially utilized molecules. These microscopic metrics are useful in interpreting the macroscopic results found in the field-measurable metrics.

IV. Results

Macroscopic Properties

DOC concentration is reported in Daltons C per lattice unit (Da/lu). Under base case conditions, south DOC concentration was 59% lower than north concentration. Since molecules become dormant when they reach the south end of the simulation space, this south end serves as a sink of carbon and reduces the DOC concentration in the south sampling space. When the sampling space is shifted 5 lattice units north, to an area north of the current sampling space, DOC concentration at the shifted south sampling space is approximately equivalent to the concentration at the north sampling space. In subsequent references, "south sampling space" refers to the original, un-shifted sampling space. Sensitivity of north DOC concentrations varied strongly with variation in the percentage of large precursors; south DOC (Figure 34) exhibited a similar dramatic variation. This relationship is positive; a higher percentage of large precursors yielded a higher DOC concentration. Temperature variation produced the second strongest response in south DOC, but this response was negative. Higher temperature resulted in a lower DOC concentration. DOC concentration was relatively insensitive to other parameters.

Variation in DOC concentration can be attributed to size- and temperature-dependent diffusion. Smaller molecules have a higher diffusivity; likewise higher temperature increases diffusivity in all molecules. Molecules with higher diffusivity move through the simulation space faster and do not accumulate in sampling spaces, thus when diffusivity

is higher, DOC concentration is lower. This explains both the effect of percentage large precursor variation and temperature variation.

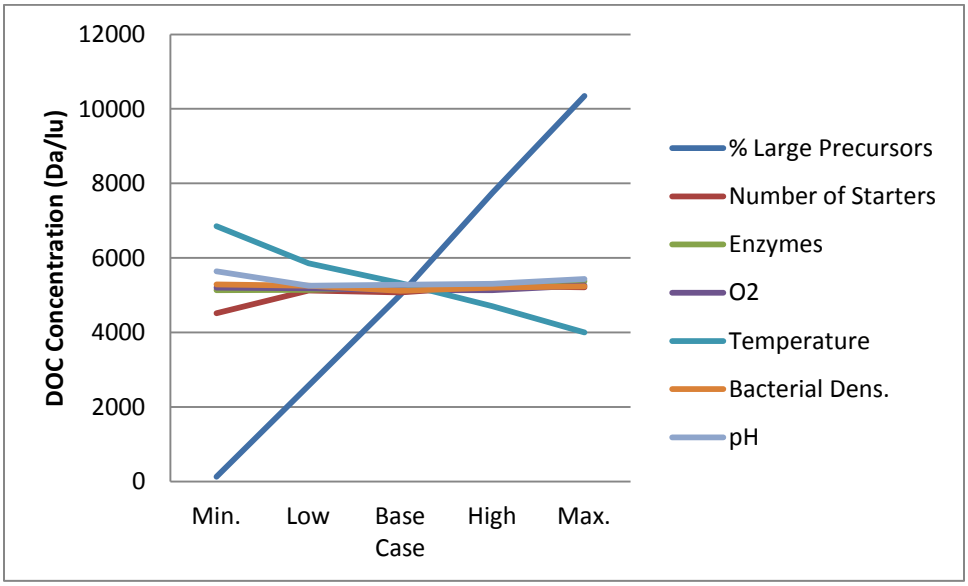

Figure 34. Variation in south DOC concentration due to variation in environmental and chemical parameters. The x-axis refers to the minimum, low, base case, high, and maximum conditions for each parameter defined in Table 6.

Under base case conditions, aromaticity essentially did not change over the sample space (no figure shown). In all cases except for pH extremes, the standard deviation of change (measuring deviation between five replicate runs for one set of environmental conditions) in aromaticity is greater than the mean change (~ 0.03%), suggesting that there was no statistically significant change in aromaticity between north and south sampling points. Under extreme pH conditions (pH = 0 and pH = 14, not typically found in natural waters) aromaticity increased by 13.3% and 9%, respectively, between north and south points.

Although the change in aromaticity over the sampling space appears to be statistically insignificant, the mean aromaticities at north and south sampling points varied in response to environmental parameters (Figure 35). Because aromaticity at north and

south sampling points is essentially equal, the north sampling point values will be reported here.

Aromaticity at base case conditions was 36%, which is high compared to the range of aromaticity in natural waters, which is between 10 – 30% (Chin et al., 1994). Cellulose, a large precursor, has 0% aromatic carbon, whereas tannins and terpenoids, with 14 and 15 carbons each, respectively, contain two aromatic rings, producing an aromaticity of 80-85%. A high aromaticity at base case conditions may suggest that the base case precursor molecule assemblage may not be representative of natural water DOC assemblages. The highest north aromaticity (57.4%) was found at 0% large precursors. High pH values resulted in higher north aromaticity (40% at pH = 14). With the exception of these two conditions, aromaticity was relatively insensitive to other parameters.

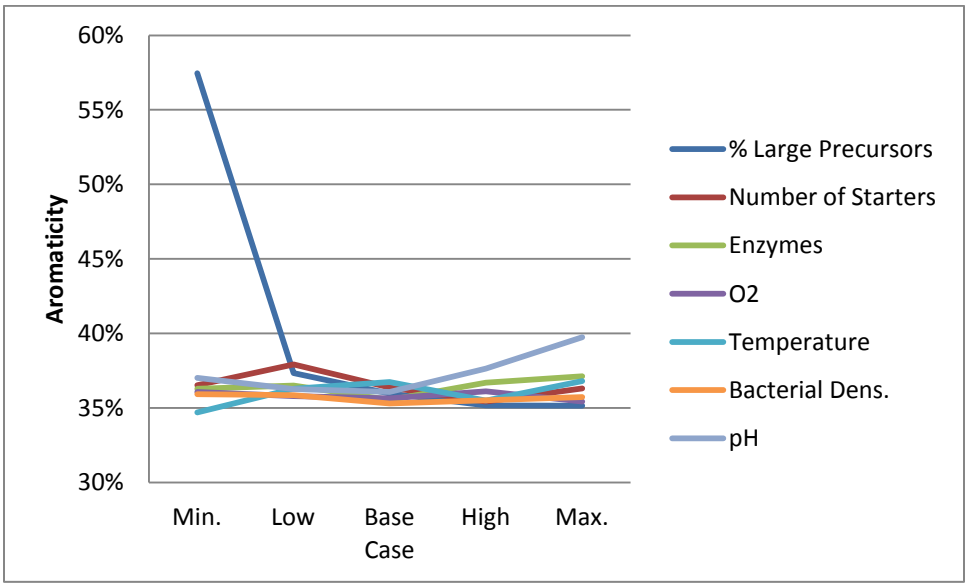

Figure 35. Variation in north aromaticity due to varying conditions.

Base case conditions saw an average increase in number-average molecular weight (M_n) of 43%, from 3700 Daltons (Da) to 5300 Da, an increase of 1600 Da between north and

south sampling spaces. Variation in M_n is an indication of a changing mean of the molecular weight distribution; an increasing M_n indicates a shift towards higher molecular weight molecules. As with DOC concentration, variation in large precursor percentage produced the strongest response, as seen in Figure 36, although this linear trend is interrupted at the 0% large precursors condition. A higher percentage of large precursors resulted in less M_n increase, except for 0% large precursors, which resulted in only a 0.01% increase in M_n. Higher enzyme activities (> 0.1) also reduced the magnitude of change in M_n. Extreme pH values (pH = 0 and pH = 14) resulted in less M_n increase. pH = 10.5 produced a higher increase in M_n between north and south points.

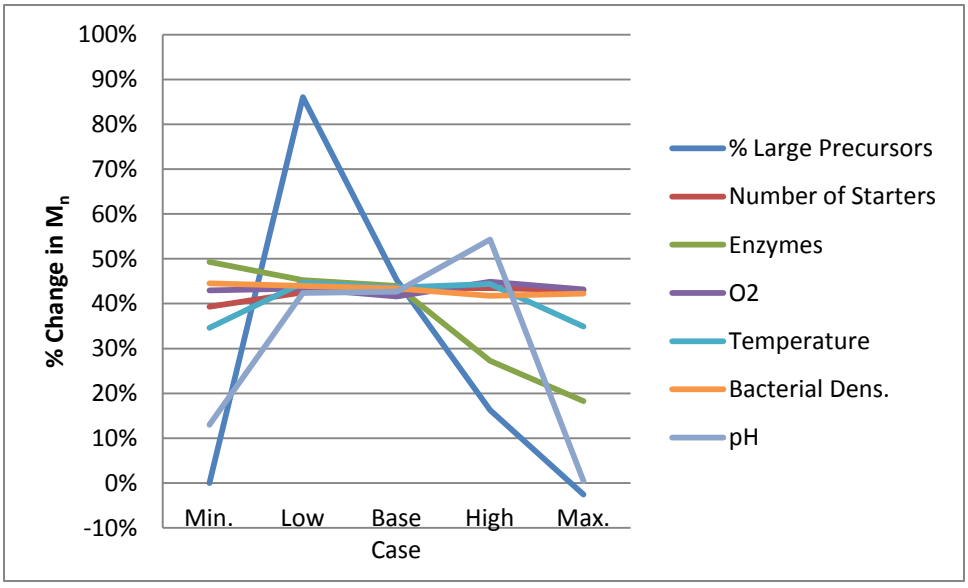

Figure 36. Variation in percentage M_n change between north and south sampling points due to varying conditions.

Conditions that produce high rates of splitting reactions produce less positive changes in M_n between north and south sampling points. Large precursor molecules are up to 30 times larger than small precursors. Even one large precursor can exert a strong control on M_n. If small precursors preferentially diffuse out of the simulation space or are taken up

by microbes, then the relative proportion of small molecules is decreased and large molecules exert an even stronger control over M_n. Splitting reactions, which usually affect large molecules, further increase the proportion of large molecules throughout the sample. At extreme pH values these reactions occur at rates 2 – 4 orders of magnitude higher than at intermediate pH.

At pH = 10.5 the rate of ester hydrolysis (which affects small precursors) increased by four orders of magnitude. This greatly increased the proportion of small precursors in the sample. As with the 25% large precursors condition, a higher proportion of small molecules results in a larger increase in M_n over the sampling space. As with the 100% large precursor condition and extreme pH conditions, a higher proportion of large molecules results in less of an increase in M_n.

Under base case conditions, weight-average molecular weight (M_w) increased, on average, 2.6% between north and south sampling spaces. M_w is a measurement of means based on atoms instead of molecules. For a given M_w, atoms in a sample will, on average, belong to a molecule of weight M_w. A changing M_w indicates a changing mode of the distribution. The most pronounced sensitivity in north M_w was to percentage large precursor and pH variations (no figure shown). At 0% large precursors, M_w was 300 Da, which reflects the absence of large molecules. M_w under all other conditions ranged from 6500 Da to 7600 Da with an average, under base case conditions, of 7350 Da. M_w increased with increasing percentage large precursors. Extreme pH values resulted in lower M_w values; 7000 Da at pH = 0 and 6500 Da at pH = 14. This result is due to splitting reactions which, as mentioned above, are prevalent at these extreme pHs. It does not contradict the behavior of M_n values at extreme pHs. M_n values were reported as the

percentage change over the sampling space, M_w values were discussed here as the weight-average molecular weight itself, which changed little over the sampling space.

Mean residence time was strongly sensitive to percent large precursor variation, with a mean residence time at 100% large precursors of 2200 s, compared to 1650 s at 0% large precursors. Mean residence time was high (2100 - 2200 s) at extreme pHs, but closer to the average (~ 2000 s) in intermediate pH ranges. Temperature increase produced a linear decrease in residence time, while enzyme activity variation produced a linear increase. Variations in oxygen concentration, bacterial density and number of starter molecules had comparatively little effect on mean residence times (see Figure 37).

These data confirm the above interpretation of DOC concentration variation; that higher molecular diffusivities due to temperature and molecular size determine molecular travel time through the simulation space. The positive sensitivity of mean residence time to percentage large precursors and the negative sensitivity to temperature are both reflected in DOC concentration variation as well (Figure 34).

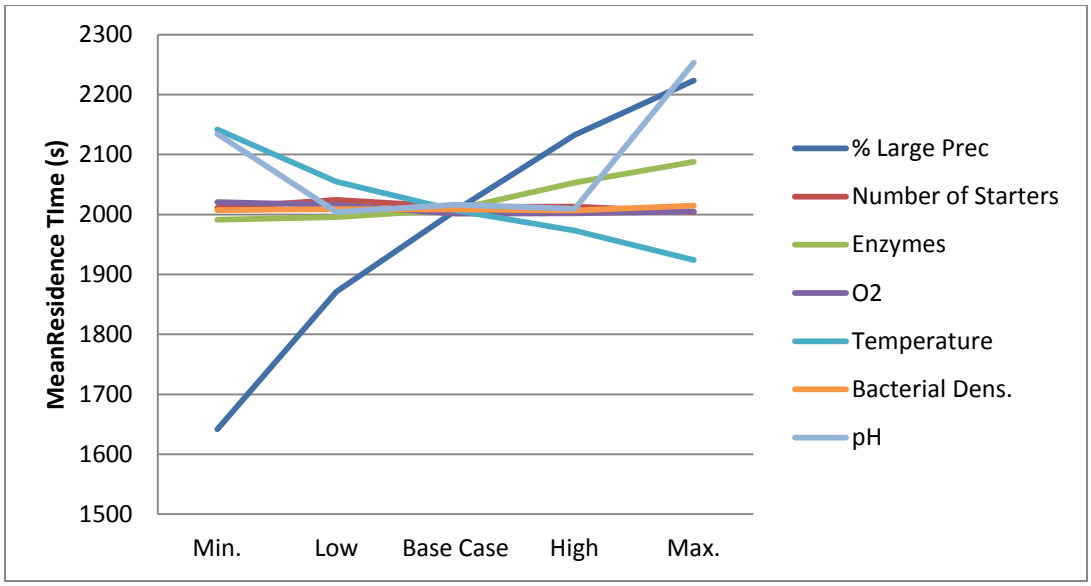

Figure 37. Mean residence time.

Microscopic Processes

Amide hydrolysis (AH), ester hydrolysis (EH), and strong C=C oxidation (SCC) are the three splitting reactions tracked in this simulation through the number of occurrences in a 9000 time step (second) run. These counts are considered a measure of the rate of reaction. AH and EH split a molecule at an amide and ester group, respectively. SCC oxidizes a C=C bond, decreasing molecular aromaticity. SCC may split a molecule as well. The rate of all three reactions increased exponentially in response to temperature (no figure shown). All AlphaStep reactions are temperature dependent, with probability of reaction partly dependent on the Arrhenius equation. AH and EH displayed very high rates at extreme pHs (0 and 14), on the order of 10^4-10^5 counts. SCC rates were very low at pH 0 (0.2 counts), and displayed counts on the order of 10^2 at higher pH values. SCC rates responded linearly and positively to oxygen concentration. AH and SCC responded linearly and positively to enzyme activity.

The processes of microbial uptake (MU) and sorption are almost exclusively size-dependant and do not preferentially take up or sorb one molecule over another, except on the bases of size. These metrics serve as a measure of the mean molecular weight of the small and large molecular weight fraction, respectively. Both the count of microbial utilizations (reported as MU rate) and the average mass of utilized molecules were tracked, as well as the average molecular weight of sorbed molecules.

Average mass of MU molecules reaches an all-time low at pH 10.5 (172 Da). At this same pH, EH rates increased by 4 orders of magnitude compared with rates at pH = 7 and since EH is a splitting reaction that affects small molecules the mean molecular weight of small molecules decreased, producing the minimum MU average mass observed. MU rates over the duration of a 9000 time step run linearly increased in response to enzyme activity, and average sorbate mass exponentially decreased. Higher enzyme activity increases rates of splitting reactions. As observed above, splitting reaction rates increased the ratio of large molecules to small molecules. As evidenced by the increase in MU rate, increased splitting reaction rates also increased the number of molecules eligible for microbial uptake. This result would also be observed in a carbon-limited system, such as a hyporheic zone (Baker et al., 1999, 2000), where microbes readily consume an increase in DOC supply.

MU rate linearly increased in response to increasing bacterial density. The average mass of MU molecules did not vary by more than 2% among non-zero bacterial densities, indicating that an increasing microbial population did not affect which molecules were eligible for uptake.

Enzyme-mediated reactions do not follow Michaelis-Menton kinetics because enzyme levels are expressed as enzyme activities; thus reaction rates continue to linearly increase with increases in substrate concentration, and enzyme binding to substrate does not reach a limit of saturation, as in Michaelis-Mention kinetics.

At 0% and 100% large precursors, the size-dependence of MU and sorption processes becomes apparent. At 0%, net sorption is essentially 0, and at 100% there is no microbial uptake. Low molecular weight molecules have a probability of desorption greater than that of sorption (Figure 31), and MU is constrained by a provision that a molecule must have a molecular weight of <1000 Da to be taken up. MU rate decreased linearly with percentage large precursors. Average sorption mass and mean MU mass remain essentially constant above 25% large precursors.

On average, across all runs conducted under base case conditions, only 3360 Da of mass were removed due to microbial uptake during a 9000 time step run and 1.2×10^6 Da of mass were retained as adsorbed molecules at any one time.

Model Validation

Several studies (Volk et al., 1997; Sobczak & Findlay, 2002, 2003; Parker et al., 2010) have utilized mesocosms (isolated chambers containing sediment and stream water) to study hyporheic DOC dynamics on a smaller scale and under less variable conditions, akin to the motivation behind DOC modeling. These mesocosm studies provide data that can be used to evaluate model performance.

Sobczak & Findlay (2002) constructed a 4 m long PVC mesocosm filled with washed crushed gravel. Stream water was pumped through the mesocosm for a month to allow

for microbial colonization of sediment surfaces. Stream water was pumped through the system at a rate of 10 cm/hr. DOC concentration decreased between 19% and 28% over the length of the mesocosm; this loss was attributed to microbial metabolism.

Mean model fluid velocity was adjusted to 0.54 lu/ts (corresponding to 10 cm/hr) by multiplying Lattice Boltzmann velocity vectors by a factor of 26. To upscale the length of the simulation space, north and south boundaries were set as periodic boundaries, allowing molecules to loop through the simulation space for 144,000 time steps, equivalent to 40 hours (10 cm/hr over 4 m). The model's "Tracer Mode" was employed, in which a set number of molecules are introduced and advected without a constant DOC source. DOC concentration, measured as mass of carbon atoms divided by pore area, was tracked throughout the simulation. Bacterial density was the variable in this experiment, and was adjusted to attempt to replicate DOC losses as described by Sobczak & Findlay (2002).

With 50% large precursors (base case condition) the maximum loss of DOC concentration (16%) occurred at a bacterial density of 100 (4 orders of magnitude higher than base case). Further increases in bacterial density (to 1000 and 10000) did not produce a greater DOC concentration loss, but rather a comparable loss (15% and 14%, respectively). With 0% large precursors a bacterial density of 0.1 (base case condition) produced a DOC concentration loss of 20%. At a bacterial density of 0.2, DOC concentration decreased by 28%. Sobczak & Findlay (2002) did not report on the quality of their source DOC, but it is not unreasonable to assume that the DOC introduced into their mesocosm system was closer in composition to the small precursors than the undegraded large precursors. Results from this validation suggest that base case bacterial

density may be producing valid rates of microbial uptake, given sufficient molecular residence time and proportion of small precursors.

Volk et al. (1997) employed a similar mesocosm experiment to examine changes in DOC quality in the mesocosm. Their mesocosms were filled with sintered glass beads and were continuously exposed to flowing 0.7 μm filtered stream water. Residence time of water in the microcosm was, on average, 1.8 hr, corresponding to 6500 model time steps. Volk et al. (1997) determined DOC in their study stream, White Clay Creek, PA, to be composed of 75% humic substances, 13% carbohydrates, and 2% amino acids, with 18% of DOC having a molecular weight greater than 100k Da. Biodegradable DOC, measured as the difference in DOC concentration between influent and effluent water of the bioreactor, comprised approximately 25% of DOC, a percentage similar to that reported by Sobczak and Findlay (2002). Volk et al. (1997) found that the biodegraded fraction of DOC was comprised of 75% humic substances, 30% carbohydrates, and 4% amino acids, with 39% of biodegraded DOC having a molecular weight greater than 100k Da. It is acknowledged that abiotic sorption may account for up to 10% of the estimated mass of biodegradable DOC, and may account for the high percentage of high-molecular weight molecules retained (Cabaniss et al., 2000).

As the model is currently constructed, there are no precursor molecules with molecular weights greater than 100k Da. Cellulose is the highest molecular weight precursor (9700 Da). Also, the fraction of humic substances is not currently determined, but can be estimated from aromaticity (Weishaar et al., 2003). Given the detailed chemical composition of the DOC assemblage described by Volk et al. (1997) future validation efforts can be directed toward constructing an equivalent DOC assemblage from

precursor materials and validating model algorithms with more of a focus on DOC quality fractions.

V. Discussion

Sources of Sensitivity

Diffusion is a hydrologic control on DOC quality. Since diffusivity is dependent on molecular size and diffusion dominates transport processes, smaller molecules traverse the simulation space faster than larger molecules. Any chemical transformation that reduces molecular size (i.e. a splitting reaction) will provide for more diffusion-driven transport of DOC. The effect of this control is most apparent in DOC concentration and in change in M_n, in which preferential removal of small molecules from the simulation space (through diffusion and molecular uptake) changes the relative proportions of large and small molecules, which ultimately affects the magnitude of change in M_n over the sampling space.

With increased fluid velocity (such as that used in model validation experiments), advection becomes the more dominant transport process and small molecules move no faster through the space than large molecules, even when taking into account sorption of large molecules. Exploration of effects of environmental parameters on DOC in an advection dominated system is a future direction of modeling efforts.

In diffusion-dominated simulation runs presented here, and with this physical control in mind, the condition that had the greatest effect on metric responses was variation in percentage large precursors. Large precursors affect north DOC concentration and molecular weight averages simply because more high molecular weight molecules enter the simulation space. DOC concentration and mean residence time were sensitive to

temperature variation, since diffusion is not only size-dependent but temperature-dependent as well.

Runs in which the percentage large precursors was 0% present an opportunity to investigate the dynamics of large precursors in the system through their absence. Of the splitting reactions, there were on average over five replicate runs, 0 amide hydrolyses and 3 strong C=C oxidations at 0% large precursors. Microbial utilization rates were high under these conditions, but since MU does not prefer one eligible molecule over another, microbial utilization did not alter molecular weight averages.

The 0% large precursor condition also presents an opportunity to examine which size classes of DOC exert the greatest control over quality. In cases where sensitivity to percentage large precursors is linear (i.e. DOC concentration and mean residence time) neither small nor large precursors exert a dominant control. However, sensitivity is non-linear in the case of aromaticity and M_n. Aromaticity is 57% at 0% large precursors, then drops to 37% at 25% large precursors. This shows that even a small number of large precursors can mediate aromaticity.

Sensitivity to percentage large precursors is also non-linear in M_n. At 0% large precursors there is essentially no change in M_n between north and south sampling points, indicating that splitting reactions do not affect small precursors at the same rates as they do large precursors. With large precursors present, microbial utilization of small molecules increases the relative number of large precursors and increases M_n. Both large and small precursors are present at the north sampling point. However, in addition to the microbial removal of small molecules, the relatively faster velocity of small molecules means that

by the south sampling point small molecules will have already diffused out of the simulation space while large molecules accumulate. This same principle applies to all simulations, since M_n almost consistently increases over the sampling space. While M_n decreases, however, M_w, or the mode of the distribution, changes by no more than 7% between north and south sampling spaces. If the removal of small molecules through microbial utilization and diffusion produces a large effect on the mean and not the mode of the distribution, then the larger molecules comprise and control the mode.

The metrics of mean sorbed mass and mean MU mass are essentially measures of the average masses of those size classes because there is no competition for small or large molecules for these processes.

Reaction rate responses to environmental parameters are unremarkable when considering that those responses can be directly inferred from the relationships in Table 4. The impetus of this modeling effort, however, was to determine the effects of these processes on DOC quality in a flowing porous medium, as measured by macroscopic properties. In light of this, the effect of a short residence time on this simulation must be addressed. Given the scale of the simulation space, results need to be upscaled to compare modeled results with real-world systems, as was done above in applying model results to mesocosm experiments. As mentioned earlier, mean residence time of molecules in the simulation space was less than 1 hr. This short residence time is the reason why variations in O_2 concentration produce such a small effect on DOC quality, whereas in a natural system variations in O_2 concentration would determine hetrotrophic metabolic pathways and rates (Sobczak & Findlay, 2002; Baker et al., 1999). The AH and EH splitting reactions do not depend on O_2 concentration, but SCC does. However, SCC rates

are, averaged over 5 runs, only 330 counts in 9000 time steps at maximum O_2 concentration. Under those same conditions, the AH rate was 900 counts. A longer residence time in the simulation space would increase SCC rates, which would in turn affect aromaticity and result in a stronger control on DOC quality. Increasing the length of the simulation space increases residence time, but also increases computing costs, as the number of agents to be accounted for increases with increased simulation space.

Upscalng can be addressed by adapting model initial conditions to changing environmental conditions in a larger system. Conditions could be altered to model several regions within a hyporheic zone with, for example, varying temperatures, oxygen concentrations, and biological activities. The model's "tracer mode," utilized in model validation runs, provides additional flowpath length when used in conjunction with periodic north and south boundaries. With this approach a single assemblage of molecules can be transported through the simulation space repeatedly, increasing residence time.

VI. Conclusions

This thesis asks how hyporheic zone processes interact with and control DOC quality. To answer that question, a hyporheic zone process (flow through a porous medium) was, for the first time, coupled with chemical transformation processes in a forward model.

The greatest effects on quality came from variation in source DOC composition. As observed in Chapter 2, hyporheic zones can undergo seasonal changes in hydrology and DOC source in which this control would come into play. pH and enzyme activity had significant effects on molecular weight and residence time metrics since they affect the

rates of molecular splitting reactions. These reactions highlight the role of biological influence on DOC quality, which splits large molecules, increasing the proportion of large molecules in the simulation. The controls on quality exerted by large molecules would be dominant in a hyporheic system, provided that breakdown of large molecules (mediated by enzymes such as cellulase and ligninase) is slow.

Future Model Development

As noted in Section III, oxygen concentration is held constant throughout the simulation, which does not account for terminal electron acceptor consumption in redox processes. Gradients of electron acceptor concentrations can be steep at the transition from surface waters to hyporheic zones (Morrice et al., 2000; Boano et al., 2010), necessitating consideration of these conditions and their effect on chemical reaction and microbial metabolism.

As executed here, the model environment is in steady state with regards to all conditions save for DOC chemistry. Implementation of transience in environmental parameters and in precursor DOC composition will allow for modeling of diel and seasonal variation. Environmental condition transience can be implemented by setting parameters equivalent to a value that changes with time step, either a set time series of values or a function that varies with time. DOC precursor composition can be varied through time by adding or deleting precursor molecules. The LB velocity field can be modified by multiplying velocity vectors by a coefficient; this will not change the original flow field, but will affect average velocity. Current time scales limit temporal variation to hourly and diel time scales.

Modeling these variations, however, will require re-scaling of the simulation space and rewriting the model as a parallel code, since model runs as presented here are time- and computational power-intensive. LB processes are independent of DOC modeling processes and can be handled efficiently on a parallel computer. Upscaling the simulation will also allow for modeling of complete hyporheic zones and coupled surface water-hyporheic systems at multiple scales, but may come at the cost of the individual molecule tracking aspect of agent-based modeling. The emergent properties generated by an agent-based model will be transferrable to a larger-scale model. A watershed-scale box model, for example, could utilize DOC transformation algorithms to model cellulose and lignin transformation between freshly derived organic matter and DOC delivered to streams. Developing this approach into a three-dimensional model is most beneficial at a meander scale where flow paths may be three-dimensional.

Biological responses to DOC could be modeled to increase bacterial density in response to abundant food supply and to adapt to changing source conditions by adjusting enzyme activities to more effectively utilize available carbon. As presented here, bacterial density and enzyme activity are presented as unitless numbers. To further connect DOC modeling with field studies of DOC interactions with aquatic microbiology, bacterial density and enzyme activity can be presented in terms of common units of these measures, i.e. cells per milliliter and enzyme units (μmol/ g C/ hr), respectively.

Field-measurable metrics fluorescence index (FI) and parallel-factor analysis (PARAFAC) component loadings are not yet measured by this model. Fluorescence index can be considered an additional proxy for aromaticity (McKnight et al., 2001), because of the contributions of aromatic carbon to sample fluorescence, and this

relationship can be incorporated into future models to investigate FI dynamics. Similarly, existing characterizations of known PARAFAC components (Cory & McKnight, 2005; Fellman et al., 2010; Ishii & Boyer, 2012) can be used to develop new metrics to model sources of sample fluorescence.

REFERENCES

Arthurs, L., P.A. Maurice, X. Xiang, R. Kennedy, G.R. Madey. 2004. "Agent-based stochastic simulation of natural organic matter adsorption and mobility in soils." Oral presentation, Eleventh International Symposium on Water-Rock Interaction. Saratoga Springs, New York. June 2004.

Baker, M.A., C.N. Dahm, H.M. Valett, 1999. Acetate retention and metabolism in the hyporheic zone of a mountain stream. Limnology and Oceanography 44, 1530-1539.

Baker, M.A., H.M. Valett, C.N. Dahm, 2000. Organic carbon supply and metabolism in a shallow groundwater ecosystem. Ecology 81, 3133-3148.

Bartschat, B.M., S.E. Cabaniss, F.M.M. Morel, 1992. Oligoelectrolyte model for cation binding by humic substances. Environmental Science & Technology, 26, 284-294.

Boano, F., A. Demaria, R. Revelli, L. Ridolfi. 2010. Biogeochemical zonation due to intrameander hyporheic flow. Water Resources Research 46, W02511.

Bonabeau, E., 2002. Agent-based modeling: Methods and techniques for simulating human systems. Proceedings of the National Academy of Sciences of the United States of America 99, 7280 – 7287.

Cabaniss, S.E., G. Madey, L. Leff, P.A. Maurice, R. Wetzel. 2005. A stochastic model for the synthesis and degradation of natural organic matter. Part I. Data structures and reaction kinetics. Biogeochemistry 76, 319-347.

Cabaniss, S.E., G. Madey, L. Leff, P.A. Maurice, R. Wetzel. 2007. A stochastic model for the synthesis and degradation of natural organic matter. Part II. Molecular property distributions. Biogeochemistry 86, 269-286.

Cory, R.M., D.M. McKnight, 2005. Fluorescence spectroscopy reveals ubiquitous presence of oxidized and reduced quinones in dissolved organic matter. Environmental Science & Technology 39, 8142-8149.

Fellman, J.B., E. Hood, R.G.M. Spencer, 2010. Fluorescence spectroscopy opens new windows into dissolved organic matter dynamics in freshwater ecosystems: A review. Limnology and Oceanography 55, 2452-2462.

Grimm, V., E. Revillia, U. Berger, F. Jeltsch, W.M.Mooij, S.F. Railsback, H.H.Thulke, J. Weiner, T. Weigand, D.L. DeAngelis, 2005. Pattern-oriented modeling of agent-based complex sustems: Lessons from ecology. Science 310, 987 – 991.

Hedin, L.O., J.C. von Fischer, N.E. Ostrom, B.P. Kennedy, M.G. Brown, G.P. Robertson, 1998. Thermodynamic constraints on nitrogen transformations and other biogeochemical processes at soil-stream interfaces. Ecology 79, 684-703.

Hering, J.G., F.M.M. Morel, 1988. Humic acid complexation of calcium and copper. Environmental Science & Technology, 22, 1234-1237.

Ishii, S.K.L., T.H. Boyer, 2012. Behavior of reoccurring PARAFAC components in fluorescent dissolved organic matter in natural and engineered systems: A critical review. Environmental Science & Technology 46, 2006 – 2017.

Jennings, N.R., 2001. An agent-based approach for building complex software systems. Communications of the ACM 44, 35 – 41.

Kaplan, L.A., J.D. Newbold. 2000. Surface and subsurface dissolved organic carbon. pp. 237-258 In: Streams and Ground Waters, J.B. Jones and P.J. Mulholland, eds. Academic Press.

Lyons, M.M., F.C. Dobbs. 2012. Differential utilization of carbon substrates by aggregate-associated and water-associated heterotrophic bacterial communities. Hydrobiologia 686, 181-193.

Manizza, M., M.J. Follows, S. Dutkiewicz, J.W. McClelland, D. Menemenlis, C. N. Hill, A. Townsend-Small, B.J. Peterson, 2009. Modeling transport and fate of riverine dissolved organic carbon in the Arctic Ocean. Global Biogeochemical Cycles, 23, GB4006.

McKnight, D.M., E.W. Boyer, P.K. Westerhoff, P.T. Doran, T. Kulbe, D.T. Anderson, 2001. Spectrofluorometric characterization of dissolved organic matter for indication of precursor organic material and aromaticity. Limnology and Oceanography 46, 38-48.

Michalzik, B., E. Tipping, J. Mulder, J.F. Gallardo Lancho, E. Matzner, C.L. Bryant, N. Clarke, S. Lofts, M.A. Vicente Esteban, 2003. Modelling the production and transport of dissolved organic carbon in forest soils. Biogeochemistry, 66, 241-264.

Mishra, A.K., 1997. Reactive Transport in Chemically and Physically Heterogeneous Porous Media: Effect of Non-Equilibrium Linear Sorption. PhD Dissertation, New Mexico Institute of Mining and Technology, 217 pp.

Morrice, J.A., C.N. Dahm, H.M. Valett, P.V. Unnikrishna, M.E. Campana, 2000. Terminal electron accepting processes in the alluvial sediments of a headwater stream. Journal of the North American Benthological Society 19, 593 – 608.

Parker, S.R., S.R. Poulson, M.G. Smith, C.L. Weyer, K.M. Bates, 2010. Temporal variability in the concentration and stable carbon isotope composition of dissolved inorganic and organic carbon in two Montana, USA rivers. Aquatic Geochemistry 16, 61 – 84.

Robertson, A.P., J.O. Leckie, 1999. Acid/Base, copper binding, and Cu^{2+}/H^{+} exchange properties of a soil humic acid, an experimental and modeling study. Environmental Science & Technology, 33, 786-795.

Schwarzenbach, R.P., P.M. Gschwend. 1993. Environmental Organic Chemistry. John Wiley & Sons, New York, NY.

Sobczak, W.V., S. Findlay, 2002. Variation in bioavailability of dissolved organic carbon among stream hyporheic flowpaths. Ecology 83, 3194 – 3209.

Sobczak, W.V., S. Findlay, S. Dye, 2003. Relationships between DOC bioavailability and nitrate removal in an upland stream: An experimental approach. Biogeochemistry 62, 309 – 327.

Sukop, M. C., D. T. Thorne, Jr, 2005. Lattice Boltzmann Modeling: An Introduction for Geoscientists and Engineers. (2^{nd} ed.) Springer, New York, NY. 172 pp.

Tosiani, T., W. Melendez, F. Vivas, 2006. Modeling humic acids transport in a bauxite profile: Los Pijiguaos, Venezuela. Journal of Geochemical Exploration, 88, 246-248.

Volk, C.J., C.B. Volk, L.A. Kaplan, 1997. Chemical composition of biodegradable dissolved organic matter in streamwater. Limnology & Oceanography 42, 39 – 44.

Weishaar, J.L., G.R. Aiken, B.A. Bergamaschi, M.S. Fram, R. Fujii, K. Mopper, 2003. Evaluation of specific ultraviolet absorbance as an indicator of the chemical composition and reactivity of dissolved organic carbon. Environmental Science & Technology 37, 4702-4708.

Wilensky, U. 1999. NetLogo. http://ccl.northwestern.edu/netlogo/. Center for Connected Learning and Computer-Based Modeling, Northwestern University. Evanston, IL. (Accessed 2 Mar 2012).

Young, D.F., B.R. Munson, T.H. Okiishi, 2004. A Brief Introduction to Fluid Mechanics (3rd ed.) John Wiley and Sons, Inc., Hoboken, NJ. 533 pp.

Zhou, Q.H., P.A. Maurice, S.E. Cabaniss. 2001. Size fractionation upon adsorption of fulvic acid on goethite: Equilibrium and kinetic studies. Geochimica et Cosmochimica Acta 65, 803-812.

Zou, Q, X. He, 1997. On pressure and velocity boundaries for the lattice Boltzmann BGK model. Physics of Fluids 9, 1591-1598.

CHAPTER 4: SYNTHESES AND CONCLUSIONS

I. Review of Research Question

As stated in the Introduction, the driving research question of this study was:

How do hyporheic zone physical, chemical, and biological processes interact with and control DOC quality (physical and chemical characteristics) in stream ecosystems?

Seasonal variation in hyporheic DOC quality was investigated in the context of seasonal variation in stream DOC quality. Hydrologic, chemical, and biogeochemical controls on DOC quality were investigated through field activities described in Chapter 2 and the modeling effort described in Chapter 3. While those chapters focus on their respective efforts, this chapter will integrate and synthesize the work of this thesis as a whole.

II. Contributions of Field Study to Modeling Approaches

Although elements of the agent-based model are conceptual, it is still rooted in physical processes and is an approximation of reality. Therefore, observations at the field site provide a reality check on metrics obtained in model runs.

Some modeled conditions, particularly temperature and pH, were modeled in Chapter 3 at values outside their conceivable environmental range. Water temperatures in Jemez River

meander wells never rose above 12°C between September 2010 and September 2011, and in-stream pH values, mediated by carbonate chemistry, ranged from 6.57 to 9.66 in data collected by Valles Caldera National Preserve scientists between 2005 and 2008. With this in mind, the extreme rates of splitting reactions observed in modeled simulations can be neglected, and enzyme activity becomes the strongest control on splitting reaction rate. Enzyme activities are currently being studied in benthic sediments at the Jemez River meander.

Under Base Case conditions, aromaticity in model runs averaged 36%. In field samples, estimated aromaticity ranged from 7 to 98% (aromaticity may be overestimated since the estimate relies on an optical measurement, see Chapter 2), with an average of 39%. Modeled M_n and M_w values under Base Case conditions were ~4500 Da and ~7500 Da, respectively, while field samples had mean values of ~1000 and ~1300 Da, respectively. Field sample MW averages were more typical of those for DOC in natural systems (Chin et al., 1994). The large precursors used in model runs represent unaltered DOC compounds, while DOC in the hyporheic zone at the Jemez River meander has likely been extensively altered from its precursor compounds, a possible explanation for the discrepancy in MW averages.

The limitations of the agent-based model are noted in Chapter 3. This includes suggestions for future model development. Field observations suggest that iron chemistry, a probable cause of turbidity dynamics, is a key process to model, taking into account redox conditions, iron speciation, and DOC-iron oxide sorption kinetics. While the model, as it stands, can report many field metrics, it currently does not predict fluorescence spectra and therefore PARAFAC component loadings, both important tools

in diagnosing DOC source and history. Fluorescence index can be estimated from aromaticity.

III. Contributions of Reactive Transport Modeling to Field Interpretation

Modeling results indicated that the greatest influence on DOC quality is from precursor chemical composition. Temperature, enzyme activity, and pH all exerted influence on DOC quality, but not to the same extent. This implies that changing seasonal inputs have a great impact on quality outputs in a natural system.

As discussed in Chapter 3, DOC concentration was in part controlled by size-dependent diffusion. It is hypothesized in Chapter 2 that high DOC concentrations in some wells during hydrologic events may be due to accumulation of DOC in low-velocity zones of the aquifer. Further characterization of flow fields within the well field will test this hypothesis. While not conducted on a meander scale, model runs of DOC transport show an inverse relationship between velocity and DOC concentration at a given lattice point.

As modeled, changes in aromaticity are due to either degradation of aromatic molecules through microbial utilization or through enzyme-mediated C=C oxidation. Temperature, oxygen concentration, and enzyme activity are the controlling parameters on C=C oxidation. All of these parameters vary in the natural environment; however, temperature varies on long (week to month) time scales and oxygen concentration ranges from zero to very low in ground water for most of the year. Enzyme activity, then, controlled by biological activity, could be a control on aromaticity variation in hyporheic systems.

Percentage large precursors had the strongest effect on molecular weight averages. pH, a controlling parameter in splitting reactions, had the second strongest effect, albeit at

extreme pH values.Extreme pH values are not observed in the field meander system, leaving variation in precursor molecular weight as the likely source of MW variation in modeled processes.

IV. Conclusions From This Work

Application of the results and implications of the modeling work depends on which of the hypotheses put forth in Chapter 2 is correct.

Hypotheses 1 and 2 were largely discounted by the hydrological observations at the meander.

Hypotheses 3 and 4, in which seasonal fluctuations in stream and groundwater hydrology lead to development of seasonal hyporheic zones, suggests variations in DOC quality influenced by hydrology and microbial metabolism. Model results imply that such seasonal variations could significantly control hyporheic DOC quality. Baker et al. (2000) observed seasonal variations in DOC at Rio Calaveras, a first-order stream also within the Jemez Mountains. Following a strong influx of DOC and DO during snowmelt in wells adjacent to the stream, DOC concentration and DO logarithmically declined. This influx of DOC was derived from the seasonally unsaturated zone or possibly, in the case of the Jemez River meander site, the overlying soil. During snowmelt, when DO and DOC were abundant, the microbial population did not respond to an addition of labile carbon. Carbon additions during base flow doubled microbial respiration rates, indicating that, under those conditions, the microbial population was carbon-limited. Baker et al. (2000) concluded that seasonal DOC dynamics controlled microbial activity through variations in DOC bioavailability.

Hypothesis 5 is supported by the observation that groundwater elevations gradients continue to decrease after crossing the stream channel.

Hypothesis 6 posits that there is no hydrologic connection between the stream and the groundwater. In this case the modeling work may not be applicable to meander DOC dynamics in its current time and spatial scale.

Resolving the hydrology of the Jemez River meander site is the single most important future step in assessing the role of the hyporheic zone in DOC processing. This thesis asks how the quality of DOC entering the hyporheic zone affects how it is transformed and to be able to observe these changes in a natural hyporheic system, the timing and extent of hyporheic exchange must be ascertained. Further exploration of hyporheic zone processes and their interaction with DOC will enhane the modeling effort. Experiments such as adsorption experiments involving DOC of varying quality, push-pull experimentation (see Appendix A), and studies of DOC bioavailability further answer the driving question behind this thesis: How do hyporheic zone physical, chemical, and biological processes interact with and control DOC quality (physical and chemical characteristics) in stream ecosystems?

V. Coupled Field and Modeling Studies of DOC in a Changing Environment

Developing connections between field studies and DOC modeling expands the scope of the studies being performed and transcends place. Future developments in modeling will enable simulations better tied to field conditions. Both efforts inform each other, with field studies providing measured parameters and acting as a check on model

performance, and modeled processes providing information on sources of DOC quality variation.

This coupled approach, in which field studies establish patterns of changing DOC quality and modeling explains the drivers of change, will benefit areas of study in which DOC quality is a key component, such as metal biogeochemistry and hyporheic zone microbial ecology (as described in the Introduction). As the intricately interrelated effects of climate change affect seasonal hydrology and DOC dynamics worldwide, well-developed predictive modeling will be critical in understanding how these changes will affect natural and human systems.

APPENDIX A: PUSH-PULL SINGLE-WELL TRACER TESTS

I. Introduction

Modeling of DOC dynamics in Chapter 3 introduced "model" molecules, well-defined and well-characterized DOC compounds, into a simulated natural system and observed the resultant changes in quality. This approach can be applied to a physical system to test hypotheses in a natural environment through a reactive tracer test. In the Jemez River meander, horizontal groundwater velocities are estimated to be very low with flow fields largely uncharacterized, complicating any effort to introduce a tracer at one well and recover it at another. A single well (push-pull) tracer test is an appropriate method to interrogate the aquifer with surety of tracer recovery.

Push-pull methods have been used to characterize bioremediation potential at contaminated groundwater sites (Istok et al., 2001) and to characterize groundwater hydraulics (Huang et al., 2010). Push-pull tests involve injecting a conservative tracer and one or more reactive tracers into a well. In some applications biological carbon substrates are also injected. The injection is followed with a tracer-free "chaser" to push the tracer solution into the formation. After a specified time, determined by the nature of the study being performed, the injection well is pumped until at least two injection

volumes of water have been extracted (Istok et al., 2001), which will ideally recover all of the conservative tracer. Samples taken during the recovery, or "pull" phase, produce a breakthrough curve (Huang et al., 2010, Cassiani et al., 2005) and reveal how reactive tracers were altered or removed by subsurface processes. While some push-pull investigations have utilized organic carbon as a reactive tracer (to assess methanogenic rates; Kleikemper et al., 2005), no other studies to our knowledge have conducted push-pull tests to investigate hyporheic DOC dynamics.

A push-pull test was employed to test the interaction of three reactive tracers with subsurface sediments. These reactive organic tracers (acetic acid, benzoic acid, and 2-naphthoic acid) are of differing quality (see Table 7), and were employed to interact with different subsurface processes.

Table 7. Physical properties of push-pull injection compounds. Values calculated by EPI Suite (EPA) based on molecular functional groups. K_{ow} refers to the compound's octanol-water coefficient.

Compound	Mol. Wt. (amu)	Log K_{ow}	Solubility (mg/L)	Probability of Anaerobic Degradation
Acetic Acid	60.05	-0.17	4.759×10^5	0.9433
Benzoic Acid	122.12	1.87	2493	0.8427
2-Naphthoic Acid	172.18	3.28	94.92	0.4336

Acetic acid, a highly bioavailable compound (Baker et al., 1999, Lutz et al., 2012), was used to assess the magnitude of the microbial community's response to a labile carbon addition. 2-naphthoic acid, comprised of two adjacent benzene rings and a carboxyl group on the 2 carbon, was included as a less bioavailable (EPI Suite, USEPA) and more hydrophobic compound (K_{ow} = 3.28; Hansch et al., 1995) likely to sorb rather than be taken up by microbes. Benzoic acid, consisting of one benzene ring with a carboxyl

group, was included as an intermediary between the two. See Figure 38 for tracer compound structures. Benzoic acid is bioavailable under anaerobic conditions (Elder & Kelly, 1994) as are assumed to exist in Jemez River meander groundwater, but is also somewhat hydrophobic (K_{ow} = 1.87, Hansch et al., 1995) and thereby may participate in both microbial uptake and sediment surface adsorption.

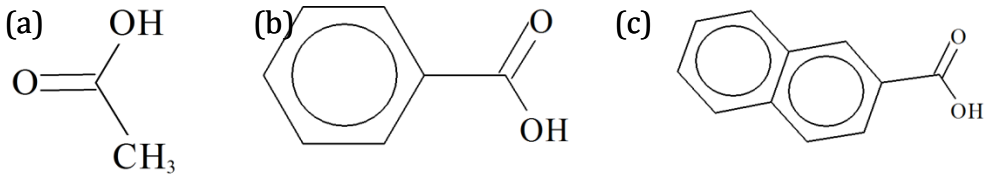

Figure 38. Chemical structures of injection compounds acetic acid (a), benzoic acid (b), and 2-naphthoic acid (c).

II. Methods

40 mg of each tracer were dissolved into 100 mL of MilliQ water. Dissolution of 2-naphthoic acid was accelerated by heating the solution.

At the Jemez River meander, 4 L of groundwater were extracted out of five wells (wells T3, 8, 12, 14, and 22). The 100 mL tracer solution was mixed with groundwater to a volume of 4 L which yielded a tracer concentration of approximately 10 mg/L. This pre-injection mixture was sampled to determine initial concentrations, then poured into the well. Tracers were injected between 6:45 pm and 7:45 pm on September 22, 2011. Injections were followed by 1 L of tracer-free "chaser", also comprised of extracted groundwater.

The pull phase of the experiment was conducted on September 23, 2011 (see Figure 39), between 1:00 pm and 3:15 pm. Injected tracers were in contact with subsurface sediments

for approximately 20 hours, with one exception: due to equipment limitations, the pull phase at well T3 was postponed until October 20, 2011. Since this experiment was the first of its kind performed at this site, an optimal contact time had not yet been established, so the contact time used here was arbitrarily determined. The pull phase was carried out using a Masterflex field sampling pump operating at its maximum pumping rate, 0.667 L/min. Samples of the pull solution were collected immediately at the commencement of pumping, at two minutes of pumping, and every minute thereafter. Samples were collected in precombusted 40 mL glass centrifuge tubes, capped with a Teflon-lined lid.

Figure 39. Paul Gabrielsen (left) and Jesus Gomez (right) conduct the pull phase of the push-pull experiment on Sep 23, 2011. Photo by John Wilson.

Water levels in Jemez River meander wells indicate that wellbores usually contain approximately 1 L of water. As the pull phase progressed, excessive drawdown in sample wells necessitated pausing pumping and resuming after a recovery period. Sample timing for each well is detailed in Section III.

Samples were preserved on ice during transport to the lab, at which point they were frozen for later analysis. Samples were filtered through a 0.2 µm polyethersulfone filter

on Oct 31, 2011. Samples from wells 12 and 22 were analyzed for chloride and acetate on Nov 4, 2011, after which all samples were again refrozen. Sample analysis resumed and was completed on Mar 14-15, 2012.

Samples were analyzed for chloride and acetate on a Metrohm Personal IC 790 with a Dionex IonPac AS9 – HC 4x250 mm column, using 9 mM Na_2CO_3 as eluent and 20 mM H_2SO_4 for conductivity suppression. Analysis for benzoic and 2-naphthoic acids was carried out on an Agilent 1100 Series HPLC at a flow rate of 1 mL per minute using an Eclipse XD8 column, and a mobile phase consisting of 50% methanol and 50% $NaPO_4$ buffered to pH = 7.0, with detection at 254 nm.

Samples are numbered in the order they were collected, with sample 0 for each well comprising the pre-injection solution as sampled immediately prior to the push phase. Sample 1 comprises the first water extracted during the pull phase. Sample 2 was collected after two minutes of pumping, with a sample taken every minute thereafter, pausing as necessary due to excessive drawdown. In well T3 pumping was paused after minute 4 and minute 6. In well 8, pumping was paused after minute 7 and minute 9. In well 12 no pause was necessary, but the sampling pump battery failed during pumping, and the pull phase at this well was not completed. In well 14, pumping was paused after minute 6. In well 22, no pause was necessary.

III. Results

Time series of tracer concentrations at each well appear in Figures 39 – 43 at the end of this Appendix.

Anomalous Chloride and Acetate Levels

Analysis of chloride and acetate yielded concentrations and total masses of tracers much larger than were introduced in the push phase. While 40 mg of each tracer were introduced, at a concentration of 10 mg/L, the average Cl^- concentration in pre-injection samples (sample 0) was 70 mg/L. Acetate concentrations averaged 17 mg/L with a concentration >40 mg/L in well T3 and 0.02 mg/L in well 14.

Sources of these anomalous readings were examined. Analysis of tracer solution (prepared in the lab prior to the push phase) verified correct tracer concentrations. Concentrations of benzoic acid and 2-naphthoic acid in pre-injection samples (sample 0) were analyzed and verified to be 8 – 11 mg/L, confirming that correct concentrations were introduced into wells. Finally, the calibration curve constructed for these analyses was re-evaluated with fresh standards and verified. Labware contamination was ruled out by analyzing for chloride in clean glass centrifuge tubes filled with MilliQ water. No chloride was detected. The source of high chloride and acetate levels may be in groundwater samples. Previous to the push-pull test, a conservative tracer test injected 1000 mg of chloride per well into wells 4, 7, 8, 9, 10, 14, and 23. These injections were made during the July 2011 and August 2011 sampling events.

Interpretation of analytical results may be a source of acetate variation. In the ion chromatography process described above, acetate elutes at approximately 1.5 minutes. However, acetate standards have also been observed to elute at 1.95 – 2.04 minutes. Fluoride elutes at 1.12 minutes, and additional peaks have been observed in that range, lessening confidence that the peak identified truly represents acetate concentration.

Background acetate levels in hyporheic systems on Rio Calaveras, also within the Jemez mountains, have been observed at around 2.34 mg/L (Baker et al., 1999). It was noted that acetate comprised up to 70% of measurable DOC. Although background levels need to be taken into consideration, it is unlikely that background levels approach measured levels of greater than 30 mg/L.

Benzoic Acid and 2-Naphthoic Acid Results

Tracer concentrations for benzoic acid and 2-naphthoic acid were within expected levels. Table 8 shows the percentage recovery of benzoic acid and 2-naphthoic acid during the pull phase of this experiment. Several sources of variation between wells need to be noted.

Table 8. Percent recovery for tracers benzoic acid and 2-naphthoic acid. Total Volume Injected includes "chaser" volume. Less volume was pumped from well 12 due to equipment failure, and recovery of sample from well T3 occurred on Oct 20, 2011, 27 days after initial injection.

Well	Benzoic Acid Recovered	Naphthoic Acid Recovered	Volume Extracted (L)	Tot.Volume Injected (L)	Contact Time
T3	17.8%	15.5%	9.71	5.0	27d
8	82.1%	62.0%	8.71	5.0	20 h
12	20.1%	24.9%	2.28	5.0	20 h
14	69.7%	69.0%	7.38	2.0	20 h
22	12.9%	14.2%	8.71	5.0	20 h

Only 1 liter of injection solution (plus 1 liter chaser) was introduced into well 14 to rectify an error in which an insufficient concentration of tracer solution was prepared in the lab. Well 14 was the only well affected by this error. Since less volume was injected, the extracted volume in this well is more than three injection volumes, enhancing tracer recovery.

Equipment failure led to the pull phase in well 12 being prematurely halted after less than half an injection volume had been extracted. The true extent of recoverable tracer from this well is not known.

As previously noted, the pull phase on well T3 was conducted 27 days after initial injection. The decrease in recovered tracer is likely due to this delay, although the fate of the lost mass is indeterminable without a reliable conservative tracer.

Wells 22 and 8 are the only two wells in which push and pull phase conditions are comparable. Again, a reliable conservative tracer is necessary to evaluate the fate of lost mass.

Table 9 shows the peak concentration times of benzoic acid and 2-naphthoic acid tracers.

Table 9. Time of peak concentration (min) of benzoic acid and 2-naphthoic acid tracers. A time of 0 indicates peak concentration was in sample 1, the first sample collected during the pull phase.

	Benzoic Acid	2-Naphthoic Acid
T3	3	3
8	0	2
12	5	0
14	2	2
22	4	4

Assuming that the first sample collected from the well is representative of tracer concentrations in wellbore storage water, the percentage of tracer mass that never left the wellbore is calculated in Table 10. Up to approximately 20% of tracer was retained in well 14 while only 1% was retained in well 22. Percentage retained mass correlates positively with mass recovery with one outlier: well 8 displayed a very high recovery rate with no more than 12% of tracer retained in the well bore.

Table 10. Estimation of tracer mass remaining in wellbore storage at time of pull phase commencement. This calculation assumes that tracer concentration at time 0 (sample 1) is representative of wellbore storage concentration.

	Wellbore Volume (L)	Mass benzoic acid at time 0 (mg)	Mass naphthoic acid at time 0 (mg)	Percentage original benzoic acid mass	Percentage original naphthoic acid mass
T3	1.16	1.5	2.1	3.6 %	4.4 %
8	1.32	1.3	4.7	6.8 %	11.6 %
12	0.98	3.1	6.70	6.8 %	15.1 %
14	1.63	1.6	1.6	18.0 %	19.2 %
22	0.99	0.4	0.5	1.2 %	1.3 %

IV. Discussion

It was expected that benzoic acid would participate in both microbial uptake and sorption processes while 2-naphthoic acid would primarily participate in sorption. Table 8 does not show consistent trends in relative recovery rates between the two tracers, i.e. one is not consistently better recovered than the other. Two hypotheses arise from this result, to be investigated in future experiments. First, it is possible that neither tracer participated in subsurface processes as expected and both were transported essentially conservatively. Second, it may be that the relative amount of mass lost to these processes is insufficient to distinguish process effects from tracer recovery rates.

Table 9 displayed times of peak tracer concentration during the pull phase. Taken in conjunction with the recovery breakthrough curve of a conservative tracer, these peak times could be used to evaluate the transport behavior of these tracers.

V. Future Work

Chloride is not an ideal conservative tracer for this site, where background levels are elevated (possibly due to chloride contamination) such that injecting a sufficiently large

concentration of tracer may introduce unwanted density effects. Bromide is a better choice, but was not used here so as to avoid contaminating the aquifer for other researchers.

Future experiments at this site will need to rectify the deficiencies of this experiment, i.e. introducing sufficient quantities of conservative tracer and labile carbon source to assess both microbial activity and subsurface hydrology at the injection well. 2-napthoic acid is, in theory, a good choice as a tracer to investigate adsorption with its high K_{ow} and low estimated bioavailability. More hydrophobic compounds (3-hydroxy 2-naphthoic acid, for example) would more strongly adsorb, but their hydrophobicity introduces solubility issues in solution preparation.

It was not anticipated that pumping would need to be paused to account for excessive drawdown in wells. This must be taken into account when designing future experiments. A pumping rate of 0.1 L/min has been successfully used at the Jemez River meander site for sustained pumping (up to 20 mins continuously).

To resolve the fate of mass not recovered, future push-pull experiments need to incorporate a laboratory sorption test (Baker et al., 1999; Zhou et al., 2000; Pullin et al., 2004) to assess the role of sorption in retaining tracer mass.

VI. Time Series of Tracer Concentrations

Figures 40 - 44 below display measured concentrations over time during the pull phase at each well.

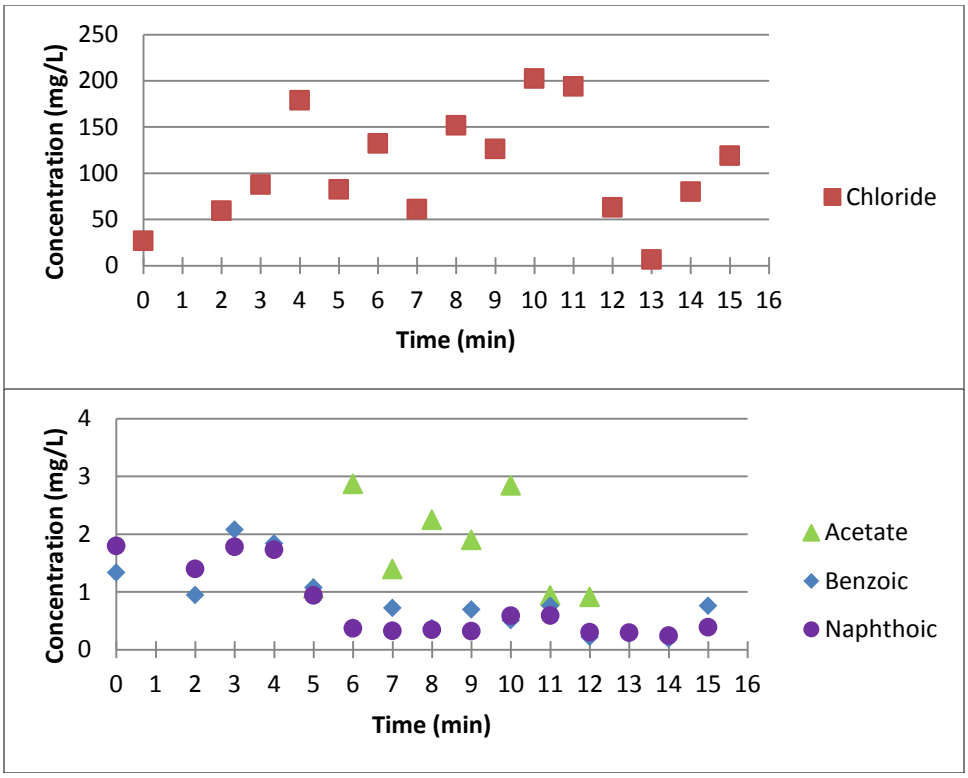

Figure 40. Time series of tracer concentrations in well T3.

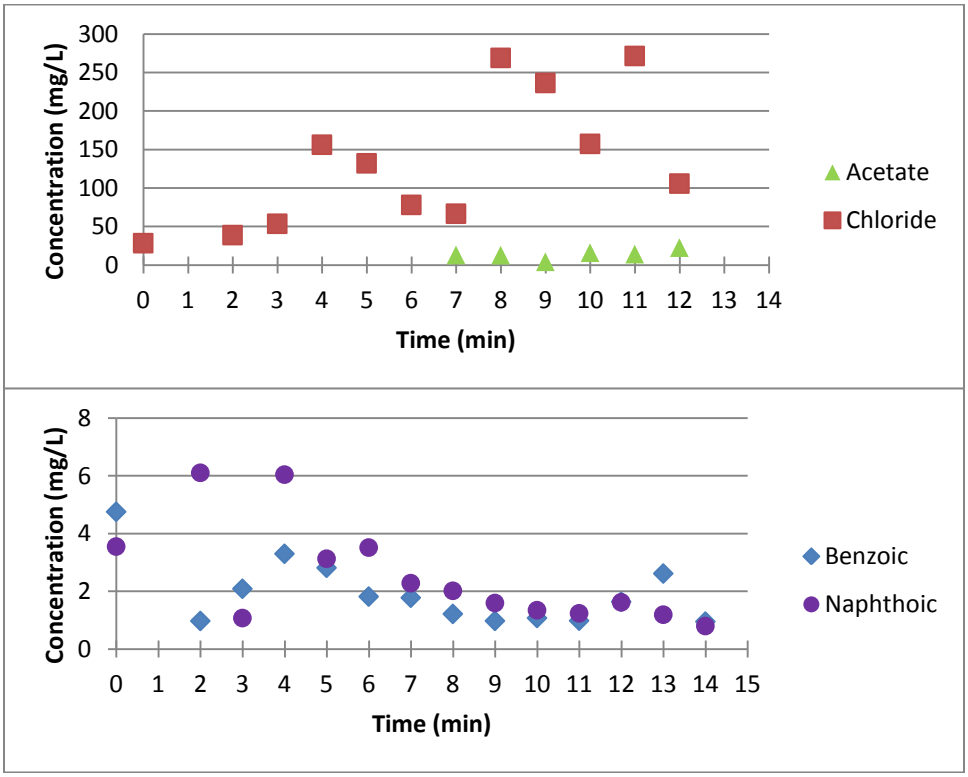

Figure 41. Time series of tracer concentrations in well 8.

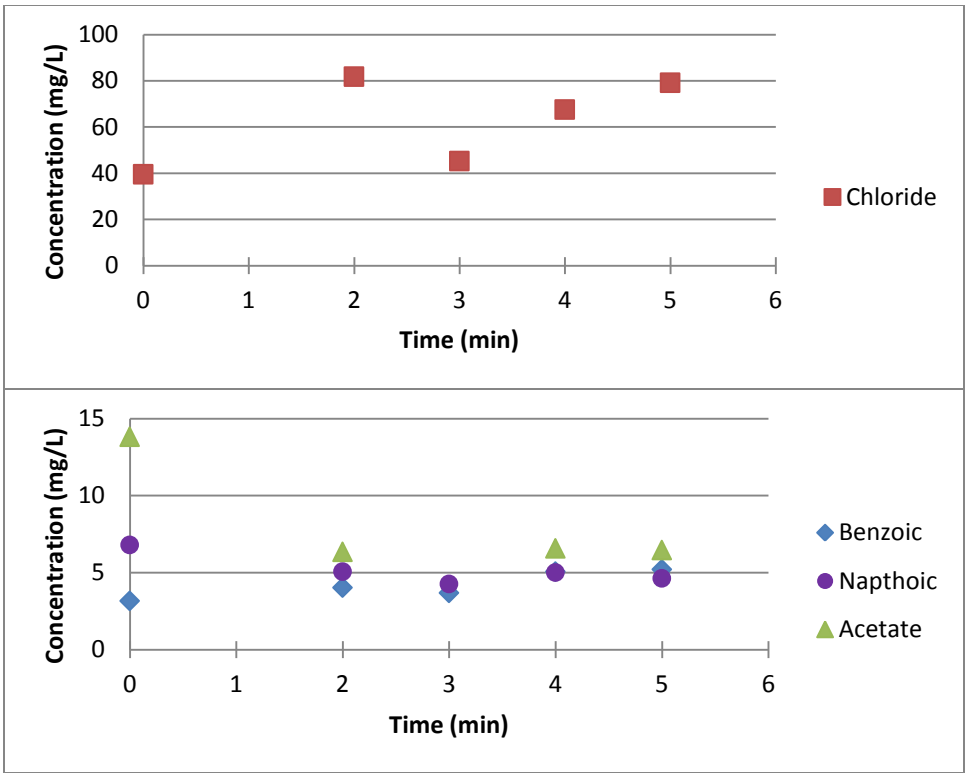

Figure 42. Time series of tracer concentrations in well 12.

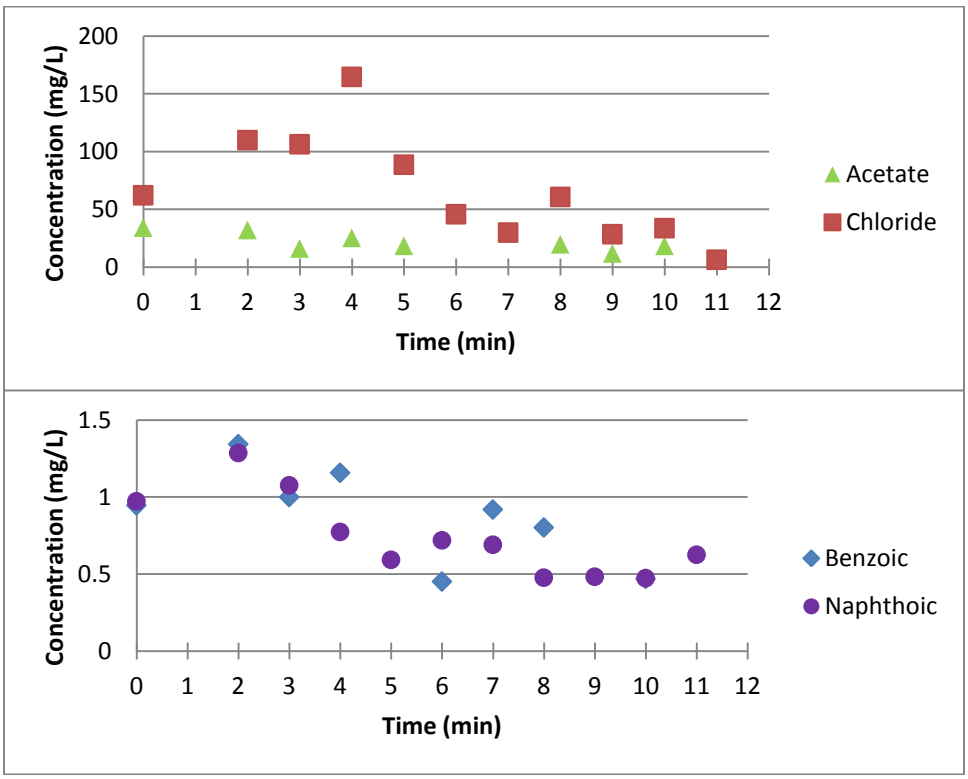

Figure 43. Time series of tracer concentrations in well 14.

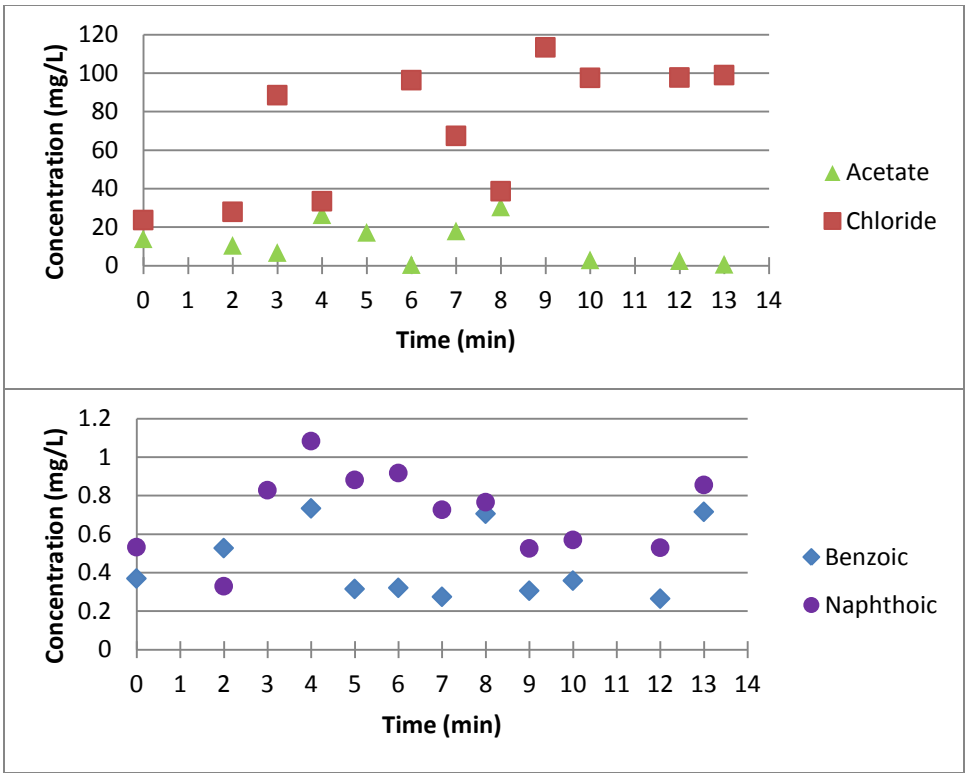

Figure 44. Time series of tracer concentrations in well 22.

APPENDIX B: FIELD SAMPLING DATA

This appendix contains data collected from the Jemez River meander field site between July 2010 and September 2011. Data collection and analytical methods are detailed in Chapter 2 and Appendix E. Sample sites S1, S3, and S12 refer to surface water samples collected in the East Fork Jemez River adjacent to wells S1, S3, and 12 respectively. All other sample sites are well locations.

Table 11. Well and surface samples collected at each sampling event.

Sample Site	7/22/2010	10/30/2010	11/13/2010	4/16/2011	5/18/2011	6/15/2011	7/19/2011	8/17/2011	9/23/2011
H2	x		x						
H3									x
S1	x	x	x	x	x	x	x	x	x
S12		x	x	x	x	x	x	x	x
S3	x	x	x	x	x	x	x	x	x
SW1	x								
T3			x	x	x	x			x
W01				x					
W02				x					x
W03		x	x	x					x
W04							x		x
W05				x					x
W06	x		x	x	x				
W07	x	x	x	x	x	x	x	x	x
W08	x	x	x	x	x	x	x	x	x
W09	x	x	x	x	x	x	x	x	x
W10	x	x	x	x	x	x	x	x	x
W11	x		x	x	x	x			x
W12									x
W13						x		x	x
W14		x	x		x	x	x	x	x
W15						x			x
W16						x	x		x
W17									x
W19					x				x
W20	x		x		x		x		x
W21					x				x
W22					x				x
W23	x	x	x						
W27									x
W29						x			
W30									x
W32									x
W33						x			
Total Samples	12	10	15	14	15	15	11	9	27

Table 12. Measurements of total organic carbon, reported in mg/L

Sample Site	7/22/10	10/30/10	11/13/10	4/16/11	5/18/11	6/15/11	7/19/11	8/17/11	9/23/11
H2	1.1		0.47						
H3									11.6
S3	2.9	1.7	0.85	1.6	1.4	1.9	2.9	4.8	3.4
S12		1.6	0.67		1.3	2.0	3.0	3.1	5.8
S1	2.6	1.7	0.92	1.5	1.3	1.7	2.9	3.6	3.7
SW1	3.4								
T3			1.9	18.4	14.8	1.1			13.1
W01				3.5					
W02				7.6					14.2
W03			6.0	6.9					15.3
W04							2.9		17.6
W05				17.0					9.0
W06			1.6	2.6	1.5				
W07			1.9	12.6	12.8	4.6	2.8	1.9	12.5
W08	6.4		9.3	7.2	7.2	4.6	1.5	1.8	14.6
W09	1.7	1.0	1.0	6.9	3.2	1.6	1.4	1.2	7.5
W10	2.8		1.3	3.5	2.3	1.8	2.4	3.1	6.3
W11	2.5		2.3	7.7	8.9	2.7			8.9
W12									5.8
W13						3.1			8.0
W14		1.7	0.88		0.50	1.1	1.2	1.1	5.5
W15						8.1			15.5
W16						2.2	2.0		8.4
W17									13.8
W19					8.3				7.0
W20			4.5		6.8		5.6		7.8
W21					5.8				13.2
W22					1.1				3.0
W23	5.3		5.02						
W27									5.3
W30									4.4
W32									10.5
W33						3.2			
Mean Stream	2.8	1.6	0.81	1.6	1.3	1.9	2.9	3.9	4.3
Mean Well	3.3	1.3	3.0	8.5	6.1	3.1	2.5	1.8	9.9

Table 13. Fluorescence Indicies (dimensionless)

Sample Site	7/22/2010	10/30/2010	11/13/2010	4/16/2011	5/18/2011	6/15/2011	7/19/2011	8/17/2011	9/23/2011
H2	1.53		1.51						
H3									1.57
S1	1.79	1.58	1.46	1.4	1.29	1.24	1.37	1.5	1.22
S12		1.52	1.35		1.5	1.25	1.37	1.5	1.47
S3	1.63	1.61	1.49	1.38	1.47	1.12	1.33	1.49	1.45
SW1	1.51								
T3			1.49	1.63	1.63				1.55
W01				1.68					
W02				1.57					1.32
W03			1.62	1.65					1.62
W04							1.44		1.53
W05				2.07					1.58
W06			1.64	1.62	1.55				
W07			1.57	1.59	1.62	1.52	1.54	1.51	1.54
W08	1.67		1.65	1.64	1.63	1.61	1.54	1.52	1.67
W09	1.67	1.53	1.5	1.67	1.65	1.35	1.35	1.36	1.42
W10	1.56		1.67	1.65	1.59	1.51	1.44	1.58	1.47
W11	1.57		1.53	1.62	1.65	1.57			1.52
W12									1.58
W13						1.63		1.54	1.48
W14		1.59	1.64		1.54	1.44	1.44	1.34	1.58
W15						1.78			1.55
W16						1.7	1.48		1.51
W17									1.81
W19					1.59				1.46
W20			1.73		1.57		1.41		1.51
W21					1.63				1.58
W22					1.66				1.54
W23	1.69		1.61						
W27									1.61
W29						1.56			
W30									1.64
W32									1.79
W33						1.89			
Mean Stream FI	1.64	1.57	1.43	1.39	1.42	1.20	1.36	1.50	1.38
Mean Wells FI	1.62	1.56	1.60	1.67	1.61	1.60	1.46	1.48	1.56

Table 14. Weight-average molecular weight (M_w) reported in log Daltons (Da).

Sample Site	6/15/2011	7/19/2011	8/17/2011	9/23/2011
H3				2.54
S1	3.24	3.08	3.12	3.11
S12	3.26	3.09	3.08	3.14
S3	3.25	3.10	3.07	3.16
T3	3.29			3.01
W02				2.85
W03				2.95
W04		3.02		3.02
W05				2.85
W07	3.32	3.08	3.05	3.00
W08	3.37	3.08	3.02	3.39
W09	3.31	3.07	3.08	3.10
W10	3.32	3.10	3.02	2.97
W11	3.3			3.11
W12	3.32			2.96
W13	3.32		3.11	3.19
W14	3.3	2.99	2.99	3.08
W15	3.33			2.97
W16	3.26	3.02		3.12
W17				2.96
W19				3.07
W20		3.08		2.93
W21				3.09
W22				3.03
W27				3.00
W30				3.00
W32				3.29
W33	3.24			
Mean Stream	3.20	3.03	3.09	3.14
Mean Wells	3.31	3.06	3.05	3.02

Table 15. Number-average molecular weight (M_n) reported in log Daltons (Da).

Sample Site	6/15/2011	7/19/2011	8/17/2011	9/23/2011
H3				2.48
S1	3.19	2.98	3.06	3.04
S12	3.22	3.02	3.01	3.08
S3	3.2	3.03	2.99	3.11
T3	3.25			2.95
W02				2.77
W03				2.88
W04		2.91		2.95
W05				2.71
W07	3.29	3.02	2.98	2.93
W08	3.36	3.03	2.94	3.69
W09	3.29	2.998	3.03	3.04
W10	3.27	3.04	2.95	2.88
W11	3.28			3.06
W12	3.3			2.9
W13	3.29		3.06	3.14
W14	3.26	2.88	2.89	3.04
W15	3.3			2.9
W16	3.21	2.94		3.07
W17				2.91
W19				3.03
W20		3.01		2.86
W21				3.04
W22				2.89
W27				2.89
W30				2.9
W32				3.49
W33	3.19			
Mean Stream	3.15	2.97	3.02	3.08
Mean Wells	3.27	2.98	2.98	2.98

Table 16. Polydispersity (M_w/M_n).

Sample Site	6/15/2011	7/19/2011	8/17/2011	9/23/2011
H3				0.98
S1	1.12	1.26	1.15	1.17
S12	1.10	1.17	1.17	1.15
S3	1.12	1.17	1.20	1.12
T3	1.10			1.15
W02				1.20
W03				1.17
W04		1.29		1.17
W05				1.38
W07	1.07	1.15	1.17	1.17
W08	1.02	1.12	1.20	
W09	1.05	1.18	1.12	1.15
W10	1.12	1.15	1.17	1.23
W11	1.05			1.12
W12	1.05			1.15
W13	1.07		1.12	1.12
W14	1.10	1.29	1.26	1.10
W15	1.07			1.17
W16	1.12	1.20		1.12
W17				1.12
W19				1.10
W20		1.17		1.17
W21				1.12
W22				1.38
W27				1.29
W30				1.26
W33	1.12			
Mean Stream	1.10	1.17	1.18	1.15
Mean Wells	1.08	1.19	1.18	1.17

Table 17. Aromaticity, as estimated by ε280, reported in percentage organic carbon.

Sample Site	7/22/2010	10/30/2010	11/13/2010	4/16/2011	5/18/2011	6/15/2011	7/19/2011	8/17/2011	9/23/2011
H2	39.4		24.7						
H3									28.5
S3	38.3	24.6	30.1	39.3	35.6	25.6	36.8	33.1	39.3
S12		28.3	37.4		38.2	25.4	36.6	46.8	25.6
S1	41.6	25.2	28.4	44.8	35.5	29.5	36.7	41.4	35.8
SW1	34.0								
T3			19.3	22.8	23.2	20.4			41.3
W01				70.4					
W02				40.0					45.2
W03			41.7	7.1					35.0
W04							98.0		36.1
W05									54.1
W06			23.2	77.2	47.6				
W07			25.2	29.6	29.8	28.8	34.5	40.8	35.4
W08			23.6	34.2	34.6	43.3	29.9	39.4	57.2
W09	52.1	62.4	37.3	40.2	55.3	17.7	32.4	57.2	36.3
W10	77.3		46.2	85.6	42.8	51.1	67.3	63.2	43.8
W11	65.4		52.5	44.5	29.8	29.9			36.5
W12									41.7
W13						40.9			50.3
W14		40.6			43.8	43.9	95.9	84.3	32.3
W15						32.1			35.7
W16						26.0	78.3		42.5
W17									36.7
W19					29.9				30.4
W20			22.3		29.2		30.8		29.3
W21					25.9				29.4
W22					32.5				32.9
W23			46.0						
W27									28.7
W29									
W30									66.7
W32									67.9
W33						20.6			
Mean Stream	39.9	23.6	31.9	42.0	32.9	22.2	32.3	41.9	31.9
Mean Well	58.5	51.5	32.9	45.1	35.4	32.2	58.4	57.0	40.6

Table 18. Loading of PARAFAC component 1, normalized to DOC concentration.

Sample Site	7/22/2010	10/30/2010	11/13/2010	4/16/2011	5/18/2011	6/15/2011	7/19/2011	8/17/2011	9/23/2011
H2	0.113		0.0894						
H3									0.0058
S3									
S12	0.113	0.0839	0.0899		0.0566	0.0177			
S1	0.113	0.0799	0.0821	0.0669	0.0757	0.0413	0.0817	0.0217	0.228
SW1		0.0966	0.111		0.0826	0.0399	0.0781	0.0348	0.133
T3		0.0815	0.0835	0.0731	0.0674	0.0398	0.0766	0.0278	0.201
W01	0.101								
W02			0.0554	0.0907	0.0873				0.208
W03				0.145					
W04				0.105					0.0066
W05			0.140	0.137					0.221
W06							0.148		0.218
W07									0.133
W08			0.157	0.114	0.119				
W09			0.139	0.111	0.116		0.199	0.270	0.188
W10	0.0567		0.104	0.107	0.107		0.239	0.0443	0.0112
W11	0.115	0.166	0.115	0.115	0.125		0.151	0.228	0.0149
W12	0.119		0.0943	0.114	0.0966	0.109	0.127	0.279	0.214
W13	0.136		0.113	0.114	0.0971	0.154			0.203
W14									0.176
W15						0.149			0.184
W16		0.130	0.172		0.141	0.151	0.238	0.0313	0.221
W17						0.177			0.170
W19						0.122	0.179		0.207
W20									0.0154
W21					0.129				0.196
W22			0.124		0.128		0.177		0.169
W23					0.126				0.187
W27					0.173				0.180
W30	0.118		0.114						
W32									0.176
Mean Stream	0.113	0.085	0.092	0.070	0.071	0.035	0.079	0.028	0.187
Mean Wells	0.110	0.148	0.118	0.115	0.120	0.137	0.182	0.170	0.145

Table 19. Loading of PARAFAC component 3, normalized to DOC concentration.

Sample Site	7/22/2010	10/30/2010	11/13/2010	4/16/2011	5/18/2011	6/15/2011	7/19/2011	8/17/2011	9/23/2011
H2	0.0705		0.0523						
H3									0.0024
S3	0.0508	0.0348	0.0427		0.0388	0.0189			
S12	0.0487	0.0349	0.0358	0.0363	0.0000	0.0220	0.0399	0.0094	0.0703
S1		0.0403	0.0494		0.0000	0.0206	0.0410	0.0153	0.0368
SW1	0.0620	0.0354	0.0399	0.0486	0.0315	0.0236	0.0380	0.0121	0.0662
T3	0.0472								
W01			0.0191	0.028	0.033				0.0687
W02				0.106					
W03				0.0376					0.0021
W04			0.0368	0.0477					0.0486
W05							0.0394		0.0415
W06									0.0059
W07			0.0448	0.0658	0.0402				
W08			0.0364	0.0368	0.0381		0.0419	0.0619	0.0300
W09	0.0134		0.0604	0.0409	0.0498		0.0564	0.0108	0.0054
W10	0.0366	0.0551	0.0302	0.0425	0.0399		0.0419	0.0681	0.0131
W11	0.0384		0.0242	0.0564	0.0607	0.0418	0.0519	0.104	0.0485
W12	0.0400		0.0284	0.0453	0.0316	0.0378			0.0331
W13									0.043
W14						0.0354			0.0325
W15		0.0476	0.128		0.0608	0.0449	0.0880	0.0096	0.0446
W16						0.0516			0.0145
W17						0.0544	0.0503		0.0590
W19									0.0033
W20					0.0286				0.0348
W21			0.0359		0.0389		0.0405		0.0288
W22					0.0341				0.0309
W23					0.0000				0.0424
W27	0.0748		0.0338						
W30									0.0335
W32									0.113
Mean Stream	0.055	0.036	0.042	0.042	0.018	0.021	0.040	0.012	0.058
Mean Wells	0.046	0.051	0.044	0.051	0.038	0.044	0.051	0.051	0.033

APPENDIX C. JEMEZ RIVER MEANDER FIELD SITE

The Jemez River meander is located within a square elk exclosure fence, 160 m on a side, on the East Fork Jemez River within the Valles Caldera National Preserve. The exclosure is located at the south end of the Valle Grande at 35.841, -106.501 in Sandoval County, New Mexico. A photo of the site appears in Figure 45.

Figure 45. Looking north at the Jemez River meander field site, Valles Caldera National Preserve. Redondito Peak is visible in the center of the frame. White standpipes denote shallow groundwater wells. Photo by Paul Gabrielsen.

The site was developed by researchers from the University of New Mexico, under Drs. Cliff Dahm and Laura Crossey, and from New Mexico Tech, under Drs. John Wilson and Michael Pullin as a research site for the New Mexico EPSCoR project "Investigating climate change impacts on New Mexico's mountain sources of water" (NSF award #0814449).

I. Shallow Groundwater Wells

Thirty-three shallow groundwater wells were installed at the site in June 2010. The wells were hand-augured and completed with a 2" PVC casing, well-rounded sand pack, and sealed with bentonite chips. A typical well construction diagram appears in Figure 46. Ten new wells were installed in June 2011.

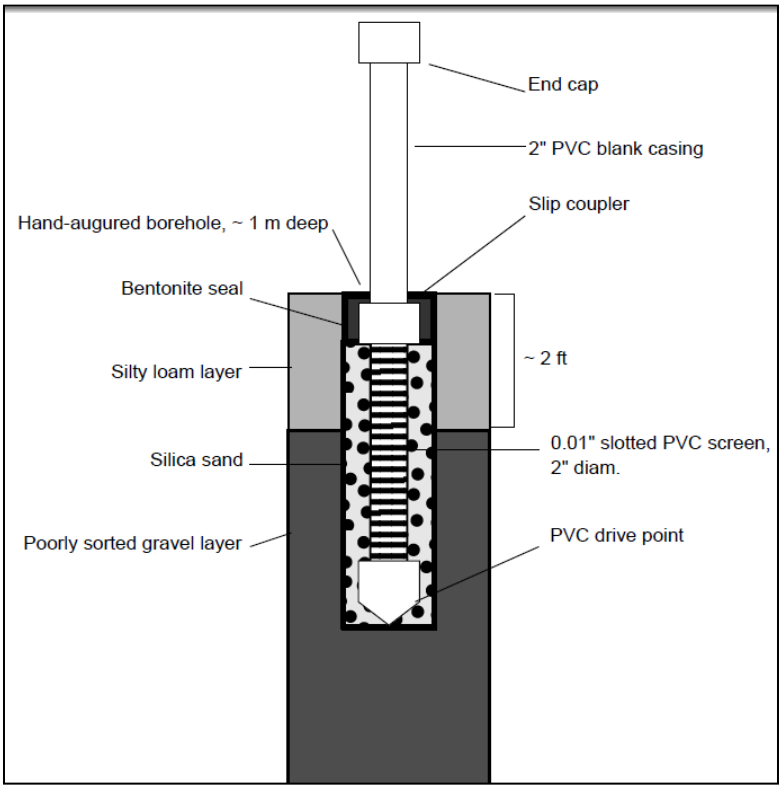

Figure 46. Typical well construction diagram for groundwater wells installed at Jemez River meander site.

HOBO dataloggers, recording pressure and temperature, were deployed in wells 2, 3, 5, 6, 12, 13, 15, 16, 17, 19, 21, 22, H1, H2, H3, H4, S5, T1, and T2. One HOBO was deployed in the atmosphere to provide atmospheric pressure correction and one was deployed mid-stream between wells S3 and S4. In June 2011, HOBOs were deployed in newly installed wells 24 – 33.

Solinst LTC leveloggers, recording pressure, temperature, and conductivity, were deployed in wells 1, 4, 7, 8, 9, 10, 11, 14, 20, 23, S1, S3, S4, and T3.

UTM coordinates of wells installed in 2010, as determined by a total station, appear in Table 20, along with well construction details. A Campbell Scientific meteorological station is installed at the meander with a net radiometer, tipping bucket rain gauge, soil moisture probes, wind gauge, and temperature and humidity probe. Weather station location appears on the site map in Figure 3, in Chapter 2.

Table 20. Well construction details for wells installed at the Jemez River meander in June 2010.

ID	Install date	x	y	Z	TWL	CH	UnderG	TSL	ESL
		m	m	m	cm	cm	Casing	cm	cm
							cm		
1	6/15/2010	364441.0	3967358.9	2583.0	232.5	79.5	153.0	107.0	97.0
2	6/15/2010	364433.5	3967374.4	2582.9	203.5	88.5	115.0	92.0	80.5
3	6/15/2010	364429.7	3967382.1	2583.1	217.5	87.0	130.5	89.0	77.5
4	6/15/2010	364425.6	3967390.4	2582.8	171.0	83.5	87.5	61.0	50.5
5	6/16/2010	364420.4	3967400.1	2583.0	203.5	76.5	127.0	97.0	85.5
6	6/15/2010	364449.1	3967363.0	2582.9	247.0	92.0	155.0	106.5	95.0
7	6/15/2010	364444.8	3967371.0	2582.8	212.0	93.5	118.5	91.0	80.5
8	6/15/2010	364441.6	3967377.4	2583.0	214.5	85.5	129.0	86.5	75.2
9	6/14/2010	364438.0	3967384.5	2583.0	199.5	90.0	109.5	81.5	70.3
10	6/15/2010	364433.1	3967392.8	2582.9	180.0	89.5	90.5	72.5	61.5
11	6/16/2010	364429.7	3967400.7	2583.0	206.0	90.0	116.0	96.5	87.0
12	6/15/2010	364456.8	3967370.8	2582.9	207.5	87.0	120.5	87.0	76.5
13	6/15/2010	364449.5	3967380.7	2582.8	183.0	85.0	98.0	73.0	62.0
14	6/14/2010	364445.8	3967385.7	2583.0	225.0	85.0	140.0	78.0	67.5
15	6/14/2010	364441.5	3967391.4	2583.0	218.0	86.0	132.0	74.0	64.5
16	6/15/2010	364439.5	3967394.2	2583.1	198.0	82.5	115.5	91.5	79.5
17	6/16/2010	364434.0	3967403.1	2583.1	208.5	91.0	117.5	92.0	82.0
19	6/15/2010	364461.5	3967384.1	2582.8	221.0	86.0	135.0	102.0	91.0
20	6/15/2010	364458.4	3967392.0	2582.9	205.0	82.0	123.0	86.5	75.5
21	6/15/2010	364454.1	3967399.7	2583.0	201.0	78.5	122.5	89.5	78.0
22	6/15/2010	364450.1	3967406.8	2583.1	198.0	87.0	111.0	82.5	72.0
23	6/15/2010	364425.7	3967381.2	2582.8	189.0	87.0	102.0	69.5	59.0
S1	5/12/2010	364398.5	3967336.3	2582.9	199.8	72.5	127.3	56.8	45.2
S2	6/15/2010	364406.1	3967340.7	2582.6	201.5	90.0	111.5	93.0	81.5
S3	6/16/2010	364440.2	3967421.8	2583.1	190.7	90.5	100.2	88.0	78.0
S4	6/16/2010	364448.7	3967423.5	2582.9	165.5	82.0	83.5	59.0	49.5
S5	6/16/2010	364454.5	3967424.2	2582.8	163.0	84.5	78.5	46.5	36.5
T1	6/16/2010	364427.3	3967418.9	2582.9	200.0	83.0	117.0	86.5	76.5
T2	6/16/2010	364423.9	3967410.4	2583.0	207.0	88.0	119.0	92.0	81.5
T3	6/16/2010	364418.2	3967418.9	2583.0	200.5	87.5	113.0	77.0	66.5
H1	6/16/2010	364414.4	3967388.1	2583.1	216.0	89.0	127.0	96.0	84.5
H2	6/16/2010	364413.1	3967378.3	2583.0	280.0	88.5	191.5	157.0	145.0
H3	6/16/2010	364419.9	3967370.3	2583.1	236.0	79.5	156.5	118.0	107.5
H4	6/16/2010	364429.2	3967366.6	2583.0	237.0	83.0	154.0	122.0	112.0

TWL = total well length
CH = casing height
TSL = total screen length
ESL = effective screen length

II. Soil Profiles

While installing new wells in June 2011, soil logs were taken at wells 24, 25, 27, 31, and 32. As described in Chapter 2, approximately the top two feet of sediment at the meander site consist of silty loam (Rodriguez & Moser, 2010). Aquifer material consists of poorly sorted gravels ranging in size from coarse sand to coarse sub-rounded gravel. Based on soil logs, the transition between silty loam and gravels occurred around 27 in. below ground surface. Full soil logs appear as Tables 21 – 25.

Table 21. Soil log for well 24, installed June 2011.

Depth (in)	Depth (cm)	Description
12	31	Clay, dark brown, organic material (roots)
16	441	Very dark brown, organic clay
25	64	Moist dark clay, sand at base w/ coarse gravel
30	76	Fine sand w/ coarse gravel, clayey mud, very moist
32	81	More gravel, incl. 2" diam. grains
36	91	2-3" diam. angular lithic grains, medium sand
39	99	same
42	107	sand becoming coarse, poorly sorted, small (2-3") cobbles

Table 22. Soil log for well 25, installed June 2011.

Depth (in)	Depth (cm)	Description
7	18	Very dark brown organic clay
13	33	Drier, crumbly fines, lighter brown
17	43	Moist fine sand, dark brown to very dark brown
22	56	wet medium sand w/ coarse gravel
25	64	Poorly sorted, fines to very coarse gravel, standing water
29	74	same
35	89	same

Table 23. Soil log for well 27, installed June 2011.

Depth (in)	Depth (cm)	Description
9	23	Silty brown dry, organic
14	36	drier, lighter brown silt
19	48	moist, silty
24	61	moist, silty, w/ coarse gravel
27	69	medium sand w/ coarse gravel
29	74	wet, sand and coarse gravel
32	81	very moist- no standing water

Table 24. Soil log for well 31, installed June 2011.

Depth (in)	Depth (cm)	Description
7	18	dark brown w/ black, silty, organic
16	41	moist and darker
22	56	transition to gravel, more moisture
28	71	water, gravel layer

Table 25. Soil log for well 32, installed June 2011.

Depth (in)	Depth (cm)	Description
5	13	Dry, light brown, silty, organic
16	41	moist silty to very fine sand, organics
21	53	dark brown to black, moist, more fine sand
30	76	more moist
36	92	wet fine sand w clay, dark brown to black
38	97	medium to coarse sand

APPENDIX D: AGENT-BASED MODEL OF DISSOLVED ORGANIC CARBON TRANSPORT AND TRANSFORMATION, CODED IN NETLOGO 4.1.3

I. Introduction

The code presented here was written by me using NetLogo 4.1.3. Implementing the code in other versions of NetLogo may require modifications. NetLogo was developed at Northwestern University, is open-source, and is available here: http://ccl.northwestern.edu/netlogo/. I strongly recommend that, before attempting to implement this code, users become familiar with the programming language of NetLogo.

To implement the code, first generate a sediment field by pressing "Initialize", then press "Go LBM" to generate the velocity field. Once the LB model finishes, then press "Make Molecules" to generate starter molecules. "Go DOC" will start the simulation. If you wish to simulate only a limited number of molecules in the simulation, enable "Tracer Mode", which will turn all starter molecules into dissolved molecules.

Further details of model function are explained as annotations in the code below.

As the Netlogo modeling environment consists of a front-end GUI (Interface Tab, see Figure 47) and lines of code (Procedures Tab, figure not shown), I first outline the interface setup, then provide the full procedure code.

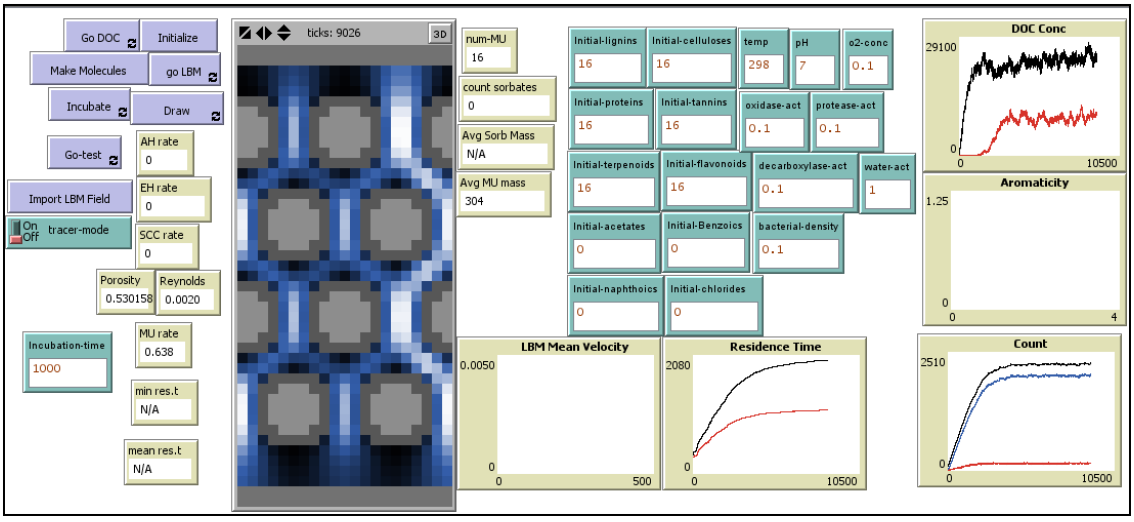

Figure 47. Screenshot of Interface tab.

II. Interface Tab

Buttons

This section is organized as follows: Display name – Commands – Forever?

Initialize – Initialize – No

go LBM – Go – Yes

Draw – draw-white –Yes

Make Molecules – make-flyers – No

Go DOC – go-doc – Yes

Incubate – Incubate – Yes

Go-test – Go-test –Yes

Import LBM Field – Import-LBM-Field – No

Monitors

All monitors are optional. These, with their accompanying reporters, are provided as an example.

Porosity – (count patches with [pcolor > 5]) / count patches

Reynolds Number – Reynolds-Number

Amide Hydrolysis Rate – sum [ct-AH] of turtles / (ticks / 360)

Ester Hydrolysis Rate – sum [ct-EH] of turtles / (ticks / 360)

Strong C=C Oxidation Rate – sum [ct-SCC] of turtles / (ticks / 360)

Microbial Uptake Rate – num-mu / (ticks / 360)

Count Sorbates – count sorbates

Avg Sorbate Mass – sum [turt-MW] of sorbates / count sorbates

Avg Microbial Uptake Mass – sum-MW-mass / num-mu

Inputs

These are the user-defined environmental and chemical conditions. Each input corresponds to a global variable. The names and ranges of each input are listed below.

Incubation-time – 0-100000 (practical limit)

Initial-lignins – 0-1000 (practical limit)

Initial-celluloses – 0-1000 (practical limit)

Initial-proteins – 0-1000 (practical limit)

Initial-tannins – 0-1000 (practical limit)

Initial-terpenoids – 0-1000 (practical limit)

Initial-flavonoids – 0-1000 (practical limit)

Initial-acetates – 0-1000 (practical limit)

Initial-benzoics – 0-1000 (practical limit)

Initial-naphthoics – 0-1000 (practical limit)

Initial-chlorides – 0-1000 (practical limit)

oxidase-act – 0-1

protease-act – 0-1

decarboxylase-act – 0-1

water-act – 0-1

Temp – 273-373

pH – 0-14

o2-conc – 0-1

World settings

Max-pxcor – 10

Max-pycor – 22

World wraps both horizontally and vertically.

Switch

Tracer-mode

Plots

This section lists the plots used to monitor metrics during simulation runs. The name of the plot and the plot pens within the plot are listed here. Plot pen properties, such as color, are user-customizable.

DOC Conc – Top, Bottom

Aromaticity – Top, Bottom

Count – dissolveds, sorbates, Total

Residence Time – Mean RT, Mean – 1 StDev

LBM Mean Velocity – default

III. Procedures Tab

Semicolons denote lines of commented code.

```
;; LBM_DOC.nlogo
;; Developed in NetLogo 4.1.3
;; Developed by Paul Gabrielsen at New Mexico Tech
;; Lattice Boltzmann computational fluid dynamics adapted from Sukop and Thorne (2007)
;; Chemical transformations adapted from Cabaniss et al., (2005)
;; May 2012

; Provides for analyzing runtime procedures to identify computationally expensive procedures
extensions [profiler]

; Definition of global variables to be used in the simulation
globals [i j ip jp in jn e1-4 e5-8 Reynolds-Number tau kinemv randseed Mt Mn Mw Zn EW Ar num-rxn
num-mu counter sum-rxn sum-mu total initial-molecules porosity Peclet Mn-Top Mn-Bottom Mw-Top
Mw-Bottom Ar-Top Ar-Bottom hatch-count sum-MW-mass dyn-visc newmass-t newmass-b oldmass-t
oldmass-b mass-balance top-conc bot-conc]

;Definition of patch-only properties
patches-own [rho ux uy u f0 f0temp f1here f2here f3here f4here f5here f6here f7here f8here whof0 whof1
whof2 whof3 whof4 whof5 whof6 whof7 whof8 feq0 feq1 feq2 feq3 feq4 feq5 feq6 feq7 feq8 sorp-site
sorp-who]

; Definition of turtle-only properties
turtles-own [f ftemp flyv Log-MW %C C %H H %N N %O O %P P %S S identity float_veloc bearing rand
turt-MW C=C Rings Phenyl-rings Alcohols Phenols Ethers Esters Ketones Aldehydes Acids Aromatic-
Acids Amines Amides RandEH Kow cond_num ct-EH ct-AH ct-AlkH ct-AlcD ct-WCC ct-SCC ct-AlcO
ct-AldO ct-D ct-MU ct-EC ct-AC  prob-EH prob-AH prob-AlkH prob-AlcD prob-WCC prob-SCC prob-
AlcO prob-AldO prob-D prob-MU prob-EC prob-AC sum-prob randbin res-time diff]

;These turtle breeds are used in Lattice Boltzmann fluid dynamics
breed [f1s f1]
breed [f2s f2]
breed [f3s f3]
breed [f4s f4]
breed [f5s f5]
breed [f6s f6]
breed [f7s f7]
breed [f8s f8]
```

```
; These breeds define the classes of molecules in the simulation space
breed [sorbates sorbate]
breed [dissolveds dissolved]

; Identifies starter molecules. The starter's identity stays with any DOC molecules that ;emit from that
starter.
breed [lignins lignin]; Identity = 1
breed [proteins protein]; Identity = 2
breed [celluloses cellulose]; Identity = 3
breed [tannins tannin]; Identity = 4
breed [terpenoids terpenoid]; Identity = 5
breed [flavonoids flavonoid]; Identity = 6
breed [chlorides chloride]; Identity = 7
breed [acetates acetate]; Identity = 8
breed [naphthoics naphthoic]; Identity = 9
breed [benzoics benzoic]; Identity = 10
; Breed of dormant molecules that have "left" the simulation space
breed [dormants dormant]

to initialize
clear-all
ask patches [set pcolor white]

; Generate first and third rows of sediment grains
ask patch -10 14 [sprout 1]
ask patch 0 14 [sprout 1]
ask turtles [ask patch-at 0 -18 [sprout 1]]
ask turtles [ask patches in-radius 4 [set pcolor black]

; Shave the "points" off the sediment grains to allow for closer packing
ask patch-at 0 4 [set pcolor white]
ask patch-at 0 -4 [set pcolor white]
ask patch-at 4 0 [set pcolor white]
ask patch-at -4 0 [set pcolor white]]
ask turtles [die]

;Generate second and fourth rows of sediment grains
 ask patch -5 5 [sprout 1]
 ask patch 5 5 [sprout 1]
ask turtles [ask patch-at 0 -18 [sprout 1]]
 ask turtles [ask patches in-radius 4 [set pcolor black]
ask patch-at 0 4 [set pcolor white]
ask patch-at 0 -4 [set pcolor white]
ask patch-at 4 0 [set pcolor white]
ask patch-at -4 0 [set pcolor white]]
ask turtles [die]

; Alternate sediment geometry: designate a porosity for a randomly spaced sediment field
;  ask patches [if random-float 1 < 0.3 [set pcolor black]]

; Alternate sediment geometry: Place sediment grains of random size throughout the simulation space
;  let count-turt 400
;  crt count-turt [set color black set size random-normal 1.25 1 set shape "circle" setxy random-xcor
random-ycor]
;  ask turtles [if size < 0 [die]]
```

```
;  ask turtles [ask patches in-radius (size / 2) [set pcolor black] die]
;  ask patches [if abs(pycor) = max-pycor - 1 [set pcolor white] if abs(pxcor) = max-pxcor - 1 [set ; pcolor white]]
;  ask patches [if pycor >= max-pycor - 3 and pycor <= max-pycor - 1 [set pcolor white]]

; Define porosity
set porosity (count patches with [pcolor > 5]) / (count patches)
; Black out top and bottom rows to create a non-periodic vertical boundary condition. The next row within this "letterbox" will serve as the boundary
ask patches with [abs(pycor) = max-pycor] [set pcolor black]
; Blacks out side columns. Use if you wish to have a non-periodic horizontal boundary condition and/or if using east and west boundary conditions.
;ask patches with [abs(pxcor) = max-pxcor] [set pcolor black]
; Designate interior patches as non-surface patches
ask patches [if all? neighbors [pcolor <= 5] [set pcolor grey]]
; Define i and j locations to be used in Lattice Boltzmann computations
set i 0 set j 0 set ip 1 set jp 1 set in -1 set jn -1
; Generate turtles at each patch to represent the directional LB densities
ask patches [sprout-f1s 1 sprout-f2s 1 sprout-f3s 1 sprout-f4s 1 sprout-f5s 1 sprout-f6s 1 sprout-f7s 1 sprout-f8s 1]

; Define initial properties
ask f1s [set f (1 / 9) ht]
ask f2s [set f (1 / 9) ht]
ask f3s [set f (1 / 9) ht]
ask f4s [set f (1 / 9) ht]
ask f5s [set f (1 / 36) ht]
ask f6s [set f (1 / 36) ht]
ask f7s [set f (1 / 36) ht]
ask f8s [set f (1 / 36) ht]
ask patches [set rho 1 set f0 (4 / 9)
if pcolor = grey [ask turtles-here [set f 0] set f0 1]]
set e1-4 1 set e5-8 (sqrt 2) set tau 1
end

to draw-white
; When activated, allows user to draw white patches, or void space
if mouse-down? [ ask patch mouse-xcor mouse-ycor[set pcolor white]]
end

to go
; Carries out Lattice Boltzmann fluid dynamics calculations. See individual processes for more details
streaming
macroscopic-variables

; Designate boundary conditions here by listing the boundary processes you wish to be active
pressure-north
pressure-south
;veloc-east
;veloc-west
equilibrium-dist-fun
collision
tick
; Test runs of the current LBM configuration stabilized within 500 ticks. If you alter LBM simulations, ensure that your simulation stabilizes within this number of ticks.
if ticks > 500 [kill-off stop]
```

```
set kinemv (1 / 3) * (tau - 1 / 2)
let meanv mean [u] of patches with [pcolor > 5]
; Determine Reynolds Number
set Reynolds-number (meanv * (2 * (max-pycor - 2))) / kinemv
let maxu max [u] of patches

; Color patches according to fluid velocity, with brighter blues indicating a higher velocity
if ticks > 1 [ask patches [if pcolor > 5[set pcolor scale-color blue u 0 maxu] ]]

;This plot monitors mean fluid velocity throughout the LBM process and provides an indicator of
stabilization.
set-current-plot "LBM Mean Velocity" set-current-plot-pen "default"
plot mean [u] of patches with [pxcor = 0]

to macroscopic-variables
; Identifies probability turtles on a given patch and transfers their directional probabilities to itself.
ask patches
[set whof1 [who] of one-of f1s-here
set whof2 [who] of one-of f2s-here
set whof3 [who] of one-of f3s-here
set whof4 [who] of one-of f4s-here
set whof5 [who] of one-of f5s-here
set whof6 [who] of one-of f6s-here
set whof7 [who] of one-of f7s-here
set whof8 [who] of one-of f8s-here
set f1here [f] of f1 whof1
set f2here [f] of f2 whof2
set f3here [f] of f3 whof3
set f4here [f] of f4 whof4
set f5here [f] of f5 whof5
set f6here [f] of f6 whof6
set f7here [f] of f7 whof7
set f8here [f] of f8 whof8]
end

to streaming
; Propagates directional probabilities in 8 directions.
ask patches [set f0temp f0]
ask f1s [set heading 90 fd 1 set ftemp f ]
ask f2s [set heading 0 fd 1 set ftemp f ]
ask f3s [set heading 270 fd 1  set ftemp f ]
ask f4s [set heading 180 fd 1  set ftemp f ]
ask f5s [set heading 45 fd sqrt 2  set ftemp f ]
ask f6s [set heading 315 fd sqrt 2  set ftemp f ]
ask f7s [set heading 225 fd sqrt 2  set ftemp f ]
ask f8s [set heading 135 fd sqrt 2  set ftemp f ]
end

to equilibrium-dist-fun
; Calculates the equilibrium distribution function for each patch, a function that will determine the new
probabilities.
ask patches[set rho f0 + f1here + f2here + f3here + f4here + f5here + f6here + f7here + f8here

; Determine fluid velocity, u, at each patch
set ux ((f1here * e1-4) + (f3here * (-1 * e1-4))+ (f5here * e1-4) + (f6here * (-1 * e1-4)) + (f7here * (-1 *
e1-4)) + (f8here * e1-4))
```

```
set uy ((f2here * e1-4) + (f3here * (0 * e1-4)) + (f4here * (-1 * e1-4)) + (f5here * e1-4) + (f6here * e1-4) +
(f7here * (-1 * e1-4)) + (f8here * (-1 * e1-4)))
set u sqrt ((ux * ux) + (uy * uy))]

; Sets velocities at boundaries to 0
ask patches [if pcolor <= 5[set rho 0 set ux 0 set uy 0 set u 0]]

; Calculates equilibrium distribution function
 ask patches
[if pcolor > 5
[let weq1 3
let weq2 (9 / 2)
let weq3 (3 / 2)
let rt0 (4 / 9)
let rt1 (1 / 9)
let rt2 (1 / 36)
let uxeq ux
let uyeq uy
; This is a gravity term. When using pressure or velocity boundaries, this term is generally not needed. Any
other external forces would incorporate into a similar term.
; - (6e-3 / rho)
let uxsq (uxeq * uxeq)
let uysq (uyeq * uyeq)
let uxuy5 uxeq + uyeq
let uxuy6 (- uxeq) + uyeq
let uxuy7 (- uxeq) + (- uyeq)
let uxuy8 uxeq + (- uyeq)
let usq uxsq + uysq
   set feq0 rt0 * (rho - (weq3 * usq))
   set feq1 rt1 * (rho + (weq1 * uxeq) + (weq2 * uxsq) - (weq3 * usq))
   set feq2 rt1 * (rho + (weq1 * uyeq) + (weq2 * uysq) - (weq3 * usq))
   set feq3 rt1 * (rho - (weq1 * uxeq) + (weq2 * uxsq) - (weq3 * usq))
   set feq4 rt1 * (rho - (weq1 * uyeq) + (weq2 * uysq) - (weq3 * usq))
   set feq5 rt2 * (rho + (weq1 * uxuy5) + (weq2 * uxuy5 * uxuy5) - (weq3 * usq))
   set feq6 rt2 * (rho + (weq1 * uxuy6) + (weq2 * uxuy6 * uxuy6) - (weq3 * usq))
   set feq7 rt2 * (rho + (weq1 * uxuy7) + (weq2 * uxuy7 * uxuy7) - (weq3 * usq))
   set feq8 rt2 * (rho + (weq1 * uxuy8) + (weq2 * uxuy8 * uxuy8) - (weq3 * usq))]]
end

to collision
; Recalculates directional probabilities based on the equilibrium distribution function
  ask patches
  [ifelse pcolor > 5
  [set f0 f0temp - (f0temp - feq0)
   ask f1 whof1 [set f ftemp - (ftemp - [feq1] of myself)]
   ask f2 whof2 [set f ftemp - (ftemp - [feq2] of myself)]
   ask f3 whof3 [set f ftemp - (ftemp - [feq3] of myself)]
   ask f4 whof4 [set f ftemp - (ftemp - [feq4] of myself)]
   ask f5 whof5 [set f ftemp - (ftemp - [feq5] of myself)]
   ask f6 whof6 [set f ftemp - (ftemp - [feq6] of myself)]
   ask f7 whof7 [set f ftemp - (ftemp - [feq7] of myself)]
   ask f8 whof8 [set f ftemp - (ftemp - [feq8] of myself)]]
  [bounceback]]
end
```

```
to bounceback
; Handles reflections of probabilities that occur at boundaries
let temp1 [f] of f1 whof1 ask f1 whof1[ set f [f] of f3 whof3] ask f3 whof3 [set f temp1]
let temp2 [f] of f2 whof2 ask f2 whof2[ set f [f] of f4 whof4] ask f4 whof4 [set f temp2]
let temp3 [f] of f5 whof5 ask f5 whof5[ set f [f] of f7 whof7] ask f7 whof7 [set f temp3]
let temp4 [f] of f6 whof6 ask f6 whof6[ set f [f] of f8 whof8] ask f8 whof8 [set f temp4]
end

to pressure-north
; Along with the following pressure boundaries, determines a constant pressure, or head, at a boundary.
 ask patches
[if pycor = max-pycor - 1
[set f0 [f0temp] of patch-at i jn
ask one-of f1s-here [set f [ftemp] of one-of f1s-at i jn]
ask one-of f2s-here [set f [ftemp] of one-of f2s-at i jn]
ask one-of f3s-here [set f [ftemp] of one-of f3s-at i jn]
ask one-of f4s-here [set f [ftemp] of one-of f4s-at i jn]
ask one-of f5s-here [set f [ftemp] of one-of f5s-at i jn]
ask one-of f6s-here [set f [ftemp] of one-of f6s-at i jn]
ask one-of f7s-here [set f [ftemp] of one-of f7s-at i jn]
ask one-of f8s-here [set f [ftemp] of one-of f8s-at i jn]
set f1here [f] of f1 whof1
set f2here [f] of f2 whof2
set f3here [f] of f3 whof3
set f4here [f] of f4 whof4
set f5here [f] of f5 whof5
set f6here [f] of f6 whof6
set f7here [f] of f7 whof7
set f8here [f] of f8 whof8
; This rho0 is the pressure term. Adjust it as necessary, but start with a small pressure gradient. If the
gradient is too high, the model will destabilize.
   let rho0 1.5
   let uy0 -1 + ((f0 + f1here + f3here + (2 * (f2here + f5here + f6here))) / rho0)
   let ru rho0 * uy0
   set f4here f2here - (2 / 3) * ru
   set f7here f5here - (1 / 6) * ru + (1 / 2) * (f1here - f3here)
   set f8here f6here - (1 / 6) * ru + (1 / 2) * (f3here - f1here)]]
end

to pressure-south
  ask patches
  [if pycor = min-pycor + 1
    [set f0 [f0temp] of patch-at i jp
    ask one-of f1s-here [set f [ftemp] of one-of f1s-at i jp]
    ask one-of f2s-here [set f [ftemp] of one-of f2s-at i jp]
    ask one-of f3s-here [set f [ftemp] of one-of f3s-at i jp]
    ask one-of f4s-here [set f [ftemp] of one-of f4s-at i jp]
    ask one-of f5s-here [set f [ftemp] of one-of f5s-at i jp]
    ask one-of f6s-here [set f [ftemp] of one-of f6s-at i jp]
    ask one-of f7s-here [set f [ftemp] of one-of f7s-at i jp]
    ask one-of f8s-here [set f [ftemp] of one-of f8s-at i jp]
  set f1here [f] of f1 whof1
  set f2here [f] of f2 whof2
  set f3here [f] of f3 whof3
  set f4here [f] of f4 whof4
  set f5here [f] of f5 whof5
```

```
  set f6here [f] of f6 whof6
  set f7here [f] of f7 whof7
  set f8here [f] of f8 whof8
    let rho0 1
    let uy0 1 - ((f0 + f1here + f3here + (2 * (f4here + f7here + f8here))) / rho0)
    let ru rho0 * uy0
    set f2here f4here + (2 / 3) * ru
    set f5here f7here + (1 / 6) * ru + (1 / 2) * (f3here - f1here)
    set f6here f8here + (1 / 6) * ru + (1 / 2) * (f1here - f3here)]]
end

to pressure-east
  ask patches
  [if pycor = min-pycor and abs pxcor < max-pxcor
    [set f0 [f0temp] of patch-at in j
    ask one-of f1s-here [set f [ftemp] of one-of f1s-at in j]
    ask one-of f2s-here [set f [ftemp] of one-of f2s-at in j]
    ask one-of f3s-here [set f [ftemp] of one-of f3s-at in j]
    ask one-of f4s-here [set f [ftemp] of one-of f4s-at in j]
    ask one-of f5s-here [set f [ftemp] of one-of f5s-at in j]
    ask one-of f6s-here [set f [ftemp] of one-of f6s-at in j]
    ask one-of f7s-here [set f [ftemp] of one-of f7s-at in j]
    ask one-of f8s-here [set f [ftemp] of one-of f8s-at in j]
  set f1here [f] of f1 whof1
  set f2here [f] of f2 whof2
  set f3here [f] of f3 whof3
  set f4here [f] of f4 whof4
  set f5here [f] of f5 whof5
  set f6here [f] of f6 whof6
  set f7here [f] of f7 whof7
  set f8here [f] of f8 whof8
    let rho0 0.5
    let ux0 (- 1) + ((f0 + f2here + f4here + (2 * (f1here + f5here + f8here))) / rho0)
    let ru rho0 * ux0
    set f3here f1here - (2 / 3) * ru
    set f7here f5here - (1 / 6) * ru + (1 / 2) * (f2here - f4here)
    set f6here f8here - (1 / 6) * ru + (1 / 2) * (f4here - f2here)]]
end

to pressure-west
  ask patches
  [if pycor = min-pycor and abs pxcor < max-pxcor
    [
      set f0 [f0temp] of patch-at ip j
    ask one-of f1s-here [set f [ftemp] of one-of f1s-at ip j]
    ask one-of f2s-here [set f [ftemp] of one-of f2s-at ip j]
    ask one-of f3s-here [set f [ftemp] of one-of f3s-at ip j]
    ask one-of f4s-here [set f [ftemp] of one-of f4s-at ip j]
    ask one-of f5s-here [set f [ftemp] of one-of f5s-at ip j]
    ask one-of f6s-here [set f [ftemp] of one-of f6s-at ip j]
    ask one-of f7s-here [set f [ftemp] of one-of f7s-at ip j]
    ask one-of f8s-here [set f [ftemp] of one-of f8s-at ip j]
  set f1here [f] of f1 whof1
  set f2here [f] of f2 whof2
  set f3here [f] of f3 whof3
  set f4here [f] of f4 whof4
```

```
  set f5here [f] of f5 whof5
  set f6here [f] of f6 whof6
  set f7here [f] of f7 whof7
  set f8here [f] of f8 whof8
    let rho0 0.1
    let ux0 1 - ((f0 + f2here + f4here + (2 * (f3here + f7here + f6here))) / rho0)
    let ru rho0 * ux0
    set f1here f3here + (2 / 3) * ru
    set f5here f7here + (1 / 6) * ru + (1 / 2) * (f4here - f2here)
    set f8here f6here + (1 / 6) * ru + (1 / 2) * (f2here - f4here)
  ]]
end

to veloc-north
; As with pressure boundaries, these conditions designate constant velocity, or constant flux boundaries.
 ask patches  [if pycor = max-pycor - 1
    [set f0 [f0temp] of patch-at i jn
    ask one-of f1s-here [set f [ftemp] of one-of f1s-at i jn]
    ask one-of f2s-here [set f [ftemp] of one-of f2s-at i jn]
    ask one-of f3s-here [set f [ftemp] of one-of f3s-at i jn]
    ask one-of f4s-here [set f [ftemp] of one-of f4s-at i jn]
    ask one-of f5s-here [set f [ftemp] of one-of f5s-at i jn]
    ask one-of f6s-here [set f [ftemp] of one-of f6s-at i jn]
    ask one-of f7s-here [set f [ftemp] of one-of f7s-at i jn]
    ask one-of f8s-here [set f [ftemp] of one-of f8s-at i jn]
  set f1here [f] of f1 whof1
  set f2here [f] of f2 whof2
  set f3here [f] of f3 whof3
  set f4here [f] of f4 whof4
  set f5here [f] of f5 whof5
  set f6here [f] of f6 whof6
  set f7here [f] of f7 whof7
  set f8here [f] of f8 whof8
  ; uy0 is the velocity term. Again, high velocities can lead to instabilities in the model
    let uy0 -0.1
    let rho0 ((f0 + f1here + f3here + (2 * (f2here + f5here + f6here))) / (1 + uy0))
    let ru rho0 * uy0
    set f4here f2here - (2 / 3) * ru
    set f7here f5here - (1 / 6) * ru + (1 / 2) * (f1here - f3here)
    set f8here f6here - (1 / 6) * ru + (1 / 2) * (f3here - f1here)]]
end

  to veloc-south
  ask patches
  [if pycor = min-pycor + 1
    [set f0 [f0temp] of patch-at i jp
    ask one-of f1s-here [set f [ftemp] of one-of f1s-at i jp]
    ask one-of f2s-here [set f [ftemp] of one-of f2s-at i jp]
    ask one-of f3s-here [set f [ftemp] of one-of f3s-at i jp]
    ask one-of f4s-here [set f [ftemp] of one-of f4s-at i jp]
    ask one-of f5s-here [set f [ftemp] of one-of f5s-at i jp]
    ask one-of f6s-here [set f [ftemp] of one-of f6s-at i jp]
    ask one-of f7s-here [set f [ftemp] of one-of f7s-at i jp]
    ask one-of f8s-here [set f [ftemp] of one-of f8s-at i jp]
  set f1here [f] of f1 whof1
  set f2here [f] of f2 whof2
```

```
  set f3here [f] of f3 whof3
  set f4here [f] of f4 whof4
  set f5here [f] of f5 whof5
  set f6here [f] of f6 whof6
  set f7here [f] of f7 whof7
  set f8here [f] of f8 whof8
    let uy0 -0.1
    let rho0 ((f0 + f1here + f3here + (2 * (f4here + f7here + f8here))) / (1 - uy0))
    let ru rho0 * uy0
    set f2here f4here + (2 / 3) * ru
    set f5here f7here + (1 / 6) * ru - (1 / 2) * (f1here - f3here)
    set f6here f8here + (1 / 6) * ru - (1 / 2) * (f3here - f1here)]]
end

to veloc-east
  ask patches
  [if pxcor = max-pxcor - 1 and abs pxcor < max-pxcor
    [set f0 [f0temp] of patch-at in j
    ask one-of f1s-here [set f [ftemp] of one-of f1s-at in j]
    ask one-of f2s-here [set f [ftemp] of one-of f2s-at in j]
    ask one-of f3s-here [set f [ftemp] of one-of f3s-at in j]
    ask one-of f4s-here [set f [ftemp] of one-of f4s-at in j]
    ask one-of f5s-here [set f [ftemp] of one-of f5s-at in j]
    ask one-of f6s-here [set f [ftemp] of one-of f6s-at in j]
    ask one-of f7s-here [set f [ftemp] of one-of f7s-at in j]
    ask one-of f8s-here [set f [ftemp] of one-of f8s-at in j]
  set f1here [f] of f1 whof1
  set f2here [f] of f2 whof2
  set f3here [f] of f3 whof3
  set f4here [f] of f4 whof4
  set f5here [f] of f5 whof5
  set f6here [f] of f6 whof6
  set f7here [f] of f7 whof7
  set f8here [f] of f8 whof8
    let ux0 0
    let rho0 ((f0 + f2here + f4here + (2 * (f1here + f5here + f8here))) / (1 + ux0))
    let ru rho0 * ux0
    set f3here f1here - (2 / 3) * ru
    set f7here f5here - (1 / 6) * ru + (1 / 2) * (f2here - f4here)
    set f6here f8here - (1 / 6) * ru + (1 / 2) * (f4here - f2here)]]
end

to veloc-west
  ask patches
  [if pxcor = min-pxcor + 1 and abs pxcor < max-pxcor
    [set f0 [f0temp] of patch-at ip j
      ask one-of f1s-here [set f [ftemp] of one-of f1s-at ip j]
    ask one-of f2s-here [set f [ftemp] of one-of f2s-at ip j]
    ask one-of f3s-here [set f [ftemp] of one-of f3s-at ip j]
    ask one-of f4s-here [set f [ftemp] of one-of f4s-at ip j]
    ask one-of f5s-here [set f [ftemp] of one-of f5s-at ip j]
    ask one-of f6s-here [set f [ftemp] of one-of f6s-at ip j]
    ask one-of f7s-here [set f [ftemp] of one-of f7s-at ip j]
    ask one-of f8s-here [set f [ftemp] of one-of f8s-at ip j]
  set f1here [f] of f1 whof1
  set f2here [f] of f2 whof2
```

```
  set f3here [f] of f3 whof3
  set f4here [f] of f4 whof4
  set f5here [f] of f5 whof5
  set f6here [f] of f6 whof6
  set f7here [f] of f7 whof7
  set f8here [f] of f8 whof8
    let ux0 0
    let rho0 ((f0 + f2here + f4here + (2 * (f3here + f7here + f6here))) / (1 - ux0))
    let ru rho0 * ux0
    set f1here f3here + (2 / 3) * ru
    set f5here f7here + (1 / 6) * ru - (1 / 2) * (f2here - f4here)
    set f8here f6here + (1 / 6) * ru - (1 / 2) * (f4here - f2here)]]
end

to kill-off
; Once the LBM calculations are complete, the directional probability turtles must be cleared away
ask turtles [die]
; Creates a four patch wide buffer zone between top and bottom boundaries, again ensuring a non-periodic
boundary condition.
ask patches [if abs(pycor) >= max-pycor - 1 [set pcolor 4]]
; Sets surfaces to a gray color, enhancing surface visibility
ask patches [if pcolor = black [set pcolor 3]]
end

to make-flyers
; Generates starter molecules using user-defined starter molecule amounts defined on the Interface tab
  clear-turtles
  clear-all-plots
  reset-ticks
  set num-mu 0
  set sum-MW-mass 0
  create-lignins Initial-lignins [set color orange set identity 1]
  create-proteins Initial-proteins [set color violet set identity 2]
  create-celluloses Initial-celluloses [set color lime set identity 3]
  create-tannins Initial-tannins [set color red set identity 4]
  create-terpenoids Initial-terpenoids [set color magenta set identity 5]
  create-flavonoids Initial-flavonoids [set color yellow set identity 6]
  create-acetates Initial-acetates [set color black set identity 8]
  create-benzoics Initial-benzoics [set color black set identity 9]
  create-naphthoics Initial-naphthoics [set color black set identity 10]
  create-chlorides Initial-chlorides [set color brown set identity 7]
set Initial-molecules count lignins + count proteins + count celluloses + count tannins + count terpenoids +
count flavonoids + count acetates + count benzoics + count naphthoics
; Place starter molecules at the very top of the simulation space, randomly distributed.
ask turtles [setxy random-xcor max-pycor - 1.51 set shape "circle" set size 0.5]

; Define starting chemical properties of starter molecules
ask proteins [set C 240 set H 382 set N 60 set O 76 set C=C 15 set Rings 5 set Phenyl-rings 5 set Alcohols
10 set Amides 54]
ask lignins [set C 400 set H 402 set O 81 set C=C 160 set Rings 40 set Phenyl-rings 40 set Alcohols 2 set
Phenols 1 set Ethers 79]
ask celluloses [set C 360 set H 602 set O 301 set Rings 60 set Alcohols 182 set Ethers 119]
ask tannins [set C 14 set H 10 set O 9 set C=C 6 set rings 2 set phenyl-rings 2 set alcohols 5 set phenols 5
set esters 1 set acids 1 set aromatic-acids 1]
ask terpenoids [set C 20 set H 30 set O 2 set C=C 2 set rings 3 set acids 1]
```

```
ask flavonoids [set C 15 set H 12 set O 6 set C=C 6 set rings 3 set phenyl-rings 2 set alcohols 4 set phenols
3 set ethers 1 set ketones 1]
ask acetates [set C 2 set H 3 set O 2 set acids 1 ]
ask benzoic [set C 7 set H 6 set O 2 set phenyl-rings 1 set acids 1]
ask naphthoics [set C 14 set H 12 set O 2 set phenyl-rings 2 set acids 1]
; Define dynamic viscosity, which will be used later to define diffusivities
set dyn-visc 1000 * (2.414e-5 * 10 ^ (247.8 / (temp - 140)))
; Define log molecular weight of turtles, dependant on elemental composition, also set turtle size
proportional to molecular weight
ask turtles
[if breed != chlorides [set Log-MW log ((C * 12.011) + (H * 1.008) + (N * 14.007)
    + (O * 15.999)) 10 set size (Log-MW / 4)]]
ask chlorides [set diff (1.38e-5 * 40000)]  ; units of diffusifity are lu^2/ts
end

to import-LBM-field
; To obviate the need for regenerating the LBM velocity field repeatedly, you can import the previously
;generated field. A critical step if you want to perform BehaviorSpace simulations. To generate this file,
;initialize the simulation, run a Lattice Boltzmann simulation, and at its conclusion use the command
;export-world “LBMGrid20x10.csv” in the command line.
import-world "LBMGrid20x10.csv"
end

to go-doc
; These algorithms govern DOC transport and transformation. For more details on each, see the individual
processes
; Tracer mode turns all starters into dissolveds.
  if tracer-mode = true [ask turtles [if breed != sorbates and breed != dormants[set breed dissolveds set color
cyan set shape "circle"]]]
  hatch-source
  move-dissolveds
  refineRandEH
  calc-properties
  sorb
  calc-prob
; This command determines the time scale of chemical reactions, which is 0.1 hr, where 1 tick = 1 sec
 if ticks mod 360 = 0 [determine-if-rxn]
  desorb
  sink
  new-weight
  histo-MW-Sorb
  tick
; Track residence time of molecules
  ask turtles [if breed = dissolveds or breed = sorbates or breed = chlorides [set res-time res-time + 1]]
; Vary length of simulation here.
if ticks > 99999 [stop]
end

to incubate
; If desired, this feature can incubate starter molecules for a predetermined number of ticks and then change
them back into starter molecules,
; creating an "evolved" set of starters.
ifelse ticks < incubation-time
[ ask turtles [set breed dissolveds]
  refineRandEH
  calc-properties
```

```
  calc-prob
  ask turtles [if Log-MW < 3 and C > 0[set prob-MU Bacterial-density * ((O / C) + 0.002 * (P + N)) * ( 0.1
- (1e-4 * (10 ^ Log-MW)))]]
if ticks mod 360 = 0 [determine-if-rxn]
  new-weight
  histo-MW-Sorb tick]
 ; Changes incubated molecules back to starters
 [ ask turtles [if identity = 1 [set breed lignins]
     if identity = 2 [set breed proteins]
     if identity = 3 [set breed celluloses]
     if identity = 4 [set breed tannins]
     if identity = 5 [set breed terpenoids]
     if identity = 6 [set breed flavonoids]
     if identity = 8 [set breed acetates]
     if identity = 9 [set breed naphthoics]
     if identity = 10 [set breed benzoics]]
   set initial-molecules count turtles]
end

  to hatch-source
; This algorithm governs the release of DOC molecules from starter molecules
  let rand4 random (Initial-molecules + 1)
  ask lignins [if rand4 = who [hatch-dissolveds 1[set color cyan set shape "circle" set res-time 0 set heading
180 fd 1]]]
  ask proteins [if rand4 = who [hatch-dissolveds 1[set color cyan set shape "circle" set res-time 0 set
heading 180 fd 1]]]
  ask celluloses [if rand4 = who [hatch-dissolveds 1[set color cyan set shape "circle" set res-time 0 set
heading 180 fd 1]]]
  ask tannins [if rand4 = who [hatch-dissolveds 1[set color cyan set shape "circle" set res-time 0 set heading
180 fd 1]]]
  ask terpenoids [if rand4 = who [hatch-dissolveds 1[set color cyan set shape "circle" set res-time 0 set
heading 180 fd 1]]]
  ask flavonoids [if rand4 = who [hatch-dissolveds 1[set color cyan set shape "circle" set res-time 0 set
heading 180 fd 1]]]
  ask acetates [if rand4 = who [hatch-dissolveds 1[set color cyan set shape "circle" set res-time 0 set
heading 180 fd 1]]]
  ask benzoics [if rand4 = who [hatch-dissolveds 1[set color cyan set shape "circle" set res-time 0 set
heading 180 fd 1]]]
  ask naphthoics [if rand4 = who [hatch-dissolveds 1[set color cyan set shape "circle" set res-time 0 set
heading 180 fd 1]]]
end

to move-dissolveds
; Advects molecules, incorporating diffusion
; Each molecule takes its x and y velocity vectors from the patch it's standing on. X and y vectors of
random size, normally distributed and proportional to diffusivity,
; are added to the patch velocity vectors.
ask turtles [if breed = dissolveds or breed = chlorides [let xdiff random-normal 0 sqrt(2 * diff) let ydiff
random-normal 0 sqrt (2 * diff) let ux-here [ux] of patch-here let uy-here [uy] of patch-here
    let xadv ux-here + xdiff let yadv uy-here + ydiff if ux-here != 0 or uy-here != 0 [set flyv sqrt((xadv ^ 2) +
(yadv ^ 2)) set heading atan xadv yadv]]]
; These lines prevent molecules from moving through a solid and will set a molecule as dormant if it arrives
at the bottom of the simulation space
ask turtles [if breed = dissolveds or breed = chlorides [ifelse patch-ahead flyv = min-pycor [if ycor <
0[setxy xcor min-pycor set breed dormants set color 52 set sum-prob 0]]
 [if [pcolor] of patch-ahead flyv > 5 [ fd flyv]]]]
```

```
end

to refineRandEH
; The random number RandEH is used to determine the proportion of mass of daughter molecules produced by splitting reactions.
; This process ensures that the ratio is in the range prescribed.
ask dissolveds [set RandEH random 100]
ask dissolveds [if RandEH < 50 [set RandEH RandEH + 50]] ask dissolveds [if RandEH > 80 [set RandEH RandEH - 20]]
ask dissolveds [set RandEH (RandEH / 100)]
end

to calc-prob
; Calculates reaction probabilities for each molecule
  ask turtles
  [if breed = dissolveds or breed = sorbates
   [if Log-MW < 3 and C > 0[set prob-MU Bacterial-density * ((O / C) + 0.002 * (P + N)) * ( 0.1 - (1e-4 * (10 ^ Log-MW)))]
    set prob-AldO Aldehydes * (5e9 * ((O2-Conc / 1000) * oxidase-act * (2.718281828 ^ ((-50)/(8.314e-3 * temp)))))
    set prob-EH Esters * water-act * (6e5) * (2.718281828 ^ ((-60)/(8.314e-3 * temp))) * (1 + 1e4 * (10 ^ (-(pH))) + 3e8 * (10 ^ (-(14 - pH))))
    set prob-AH Amides * 6e6 * (2.718281828 ^ ((-50)/(8.314e-3 * temp))) * ((10 ^ (-(pH))) + 10 * (10 ^ (-(14 - pH))) + protease-act)
    set prob-AlkH (C=C * water-act * 2e13 * (2.718281828 ^ ((-80)/(8.314e-3 * temp))) * (10 ^ (-(pH))))
    set prob-AlcD (Alcohols * 10 ^ 12 * (2.718281828 ^ ((-80)/(8.314e-3 * temp))) * (10 ^ (-(pH))))
    set prob-WCC (C=C * (5e9 * (O2-Conc / 1000) * oxidase-act * (2.718281828 ^ ((-50)/(8.314e-3 * temp)))))
    set prob-SCC (C=C * (1e9 * (O2-Conc / 1000) * oxidase-act * (2.718281828 ^ ((-50)/(8.314e-3 * temp)))))
   ifelse O > C [set prob-AlcO 0.0000001] [set prob-AlcO Alcohols * (5e9 * (O2-Conc / 1000) * oxidase-act * (2.718281828 ^ ((-50)/(8.314e-3 * temp))))]
    set prob-D Acids * ((10 ^ (-(pH))) / (1e-4 + (10 ^ (-(pH))))) * 5e7 * decarboxylase-act * (2.718281828 ^ ((-50)/(8.314e-3 * temp)))
   if Acids > 0
[ifelse (any? other dissolveds with [Alcohols > 1]) [set prob-EC (Acids * (10 ^ (-(pH))) * 5e10 * (2.718281828 ^ ((-60)/(8.314e-3 * temp))))][set prob-EC 0.00000001]]
    if Aldehydes > 0
[ifelse (any? other dissolveds with [Aldehydes > 1 or Ketones > 1])
  [set prob-AC (Acids * ((10 ^ (-(pH))) + (10 ^ (-(14 - pH)))) * 1e10 * (2.718281828 ^ ((-50)/(8.314e-3 * temp))))
  ][set prob-AC 0.000000001]]]]
end

to determine-if-rxn
; Determines whether a molecule undergoes a reaction based on the sum of its reaction probabilities
ask turtles  [if breed = dissolveds or breed = sorbates
  [  set sum-prob prob-EH + prob-AH + prob-AlkH + prob-AlcD + prob-WCC + prob-SCC + prob-AlcO + prob-AldO + prob-D + prob-MU + prob-EC + prob-AC
    set randbin random-float 1
  if randbin <= sum-prob[run-rxns]]]
end

to run-rxns
; Determines which reaction proceeds based on reaction probabilities
; Unlike the other processes, the microbial utilization procedure removes a molecule from the simulation.
```

```
if randbin <= prob-MU
[if any? patches with [pcolor <= 4] in-radius 1 [set num-mu num-mu + 1 set sum-MW-mass sum-MW-mass + turt-MW die ]]
if randbin > prob-MU and randbin <= prob-MU + prob-AldO [oxidize-aldehyde]
if randbin > prob-MU + prob-AldO and randbin <= prob-MU + prob-AldO + prob-EH [ester-hydrolysis]
if randbin > prob-MU + prob-AldO + prob-EH and randbin <= prob-MU + prob-AldO + prob-EH + prob-AH [amide-hydrolysis]
if randbin > prob-MU + prob-AldO + prob-EH + prob-AH and randbin <= prob-MU + prob-AldO + prob-EH + prob-AH + prob-AlkH [alkene-hydration]
if randbin > prob-MU + prob-AldO + prob-EH + prob-AH + prob-AlkH and randbin <= prob-MU + prob-AldO + prob-EH + prob-AH + prob-AlkH + prob-AlcD [alcohol-dehydration]
if randbin > prob-MU + prob-AldO + prob-EH + prob-AH + prob-AlkH + prob-AlcD and randbin <= prob-MU + prob-AldO + prob-EH + prob-AH + prob-AlkH + prob-AlcD + prob-WCC [weak-C=C]
if randbin > prob-MU + prob-AldO + prob-EH + prob-AH + prob-AlkH + prob-AlcD + prob-WCC and randbin <= prob-MU + prob-AldO + prob-EH + prob-AH + prob-AlkH + prob-AlcD + prob-WCC + prob-SCC [strong-C=C]
if randbin > prob-MU + prob-AldO + prob-EH + prob-AH + prob-AlkH + prob-AlcD + prob-WCC + prob-SCC and randbin <= prob-MU + prob-AldO + prob-EH + prob-AH + prob-AlkH + prob-AlcD + prob-WCC + prob-SCC + prob-AlcO [alcohol-oxidation]
if randbin > sum-prob - prob-AC - prob-EC - prob-D and randbin <= sum-prob - prob-AC - prob-EC [decarboxylation]
if randbin > sum-prob - prob-AC - prob-EC and randbin <= sum-prob - prob-AC [ester-condensation]
if randbin > (sum-prob - prob-AC) [aldol-condensation]
end

to go-test
; This is a test algorithm to evaluate a flow field
ask turtles [set breed dissolveds]
ask turtles [set heading 90 fd [ux] of patch-here
  set heading 0 fd [uy] of patch-here]
end

to sorb
; Sorption process
  ask patches
  [if pcolor < 4 and sorp-site = 0 and any? dissolveds in-radius 1
  [ask one-of dissolveds in-radius 1 [if random-float 1 < (0.99 * (1 / (1 + (2.718281828 ^ (((10 ^ Log-MW) - 8000) / 5000)))) + 0.01 )
    [set color red set breed sorbates set shape "circle"setxy [pxcor] of myself [pycor] of myself]] ]]
; The binary sorp-site property ensures that sorption sites are exclusive and only one molecule can occupy a sorption site.
  ask patches [if any? sorbates-here [set sorp-site 1]]
  ask patches [if not any? sorbates-here [set sorp-site 0]]
  end

to desorb
; Desorption process
  ask patches [if sorp-site = 1 [ask sorbates-here
  [if random-float 1 < (0.89 * (2.718281828 ^ ((- (10 ^ Log-MW) / 2000)) + 0.01 ))
  [move-to one-of neighbors with [pcolor > 5] set color cyan  set breed dissolveds set shape "circle"]]]]
  end

; Sets dormant the molecules that reach the end of the simulation space
to sink ask turtles [ if ycor <= min-pycor + 2 [set breed dormants set color 52 set sum-prob 0]] end
```

```
; The following processes are chemical transformation processes

to oxidize-aldehyde set O O + 1 set Acids Acids + 1 set Aldehydes Aldehydes - 1 set ct-AldO ct-AldO + 1
end

to ester-hydrolysis
; To maintain chemical plausibility, the elemental composition of rings, ketones, aldehydes, acids, and
amides are preserved in splitting reactions
  let splittable-C C - (Rings * 6) - Ketones - Aldehydes - Acids - Amides
  let splittable-C=C C=C - (Phenyl-rings * 3)
  let splittable-H H - (Rings * 5) - Alcohols - Aldehydes - Acids
  let splittable-O O - Alcohols - Ketones - Aldehydes - (Acids * 2) - Amides
  let splittable-N N - Amines - Amides
set ct-EH ct-EH + 1 set H H + 2 set O O + 1 hatch 1 [set Log-MW round(Log-MW * (1 - RandEH)) set C
round(splittable-C * (1 - RandEH)) set H round(splittable-H * (1 - RandEH)) set N round(splittable-N * (1
- RandEH))
    set O round(splittable-O * (1 - RandEH)) set P round(P * (1 - RandEH)) set S round(S * (1 - RandEH))
set C=C round(splittable-C=C * (1 - RandEH)) set Rings round(Rings * (1 - RandEH))
    set Phenyl-rings round(Phenyl-rings * (1 - RandEH)) set Alcohols round((Alcohols * (1 - RandEH))) +
1 set Phenols round(Phenols * (1 - RandEH)) set Ethers round(Ethers * (1 - RandEH)) set Esters
round(Esters * (1 - RandEH))
    set Ketones round(Ketones  * (1 - RandEH)) set Aldehydes round(Aldehydes * (1 - RandEH)) set Acids
round(Acids * (1 - RandEH)) set Aromatic-Acids round(Aromatic-Acids  * (1 - RandEH)) set Amines
round(Amines * (1 - RandEH))
    set Amides round(Amides * (1 - RandEH))
    set C C + (Rings * 6) + Ketones + Aldehydes + Acids + Amides
    set C=C C=C + (Phenyl-rings * 3)
    set H H + (Rings * 5) + Alcohols + Aldehydes + Acids
    set O O + Alcohols + Ketones + Aldehydes + (Acids * 2) + Amides
    set N N + Amines + Amides]
set Log-MW Log-MW * RandEH set C round(splittable-C * RandEH) set H round(H * RandEH) set N
round(N * RandEH)
    set O round(O * RandEH) set P round(P * RandEH) set S round(S * RandEH) set C=C round(C=C *
RandEH) set Rings round(Rings * RandEH)  set Phenyl-rings round(Phenyl-rings * RandEH)
    set Alcohols round(Alcohols * RandEH) set Phenols round(Phenols * RandEH) set Ethers round(Ethers
* RandEH) set Esters round(Esters * RandEH) set Ketones round(Ketones  * RandEH)
    set Aldehydes round(Aldehydes * RandEH) set Acids round(Acids * RandEH) + 1 set Aromatic-Acids
round(Aromatic-Acids  * RandEH) set Amines round(Amines * RandEH) set Amides round(Amides *
RandEH)
    set C C + (Rings * 6) + Ketones + Aldehydes + Acids + Amides
    set C=C C=C + (Phenyl-rings * 3)
    set H H + (Rings * 5) + Alcohols + Aldehydes + Acids
    set O O + Alcohols + Ketones + Aldehydes + (Acids * 2) + Amides
    set N N + Amines + Amides
end

to amide-hydrolysis
  let splittable-C C - (Rings * 6) - Ketones - Aldehydes - Acids - Amides
  let splittable-C=C C=C - (Phenyl-rings * 3)
  let splittable-H H - (Rings * 5) - Alcohols - Aldehydes - Acids
  let splittable-O O - Alcohols - Ketones - Aldehydes - (Acids * 2) - Amides
  let splittable-N N - Amines - Amides
set ct-AH ct-AH + 1 set H H + 2 set O O + 1 hatch 1 [set Log-MW round(Log-MW * (1 - RandEH)) set C
round(splittable-C * (1 - RandEH)) set H round(splittable-H * (1 - RandEH)) set N round(splittable-N * (1
- RandEH))
```

```
    set O round(splittable-O * (1 - RandEH)) set P round(P * (1 - RandEH)) set S round(S * (1 - RandEH))
set C=C round(splittable-C=C * (1 - RandEH)) set Rings round(Rings * (1 - RandEH))
    set Phenyl-rings round(Phenyl-rings * (1 - RandEH))
    set Alcohols round((Alcohols * (1 - RandEH))) set Phenols round(Phenols * (1 - RandEH)) set Ethers
round(Ethers * (1 - RandEH)) set Esters round(Esters * (1 - RandEH))
    set Ketones round(Ketones  * (1 - RandEH))
    set Aldehydes round(Aldehydes * (1 - RandEH)) set Acids round(Acids * (1 - RandEH)) + 1 set
Aromatic-Acids round(Aromatic-Acids  * (1 - RandEH)) set Amines round(Amines * (1 - RandEH))
    set Amides round(Amides * (1 - RandEH))
    set C C + (Rings * 6) + Ketones + Aldehydes + Acids + Amides
    set C=C C=C + (Phenyl-rings * 3)
    set H H + (Rings * 5) + Alcohols + Aldehydes + Acids
    set O O + Alcohols + Ketones + Aldehydes + (Acids * 2) + Amides
    set N N + Amines + Amides]
set Log-MW Log-MW * RandEH set C round(splittable-C * RandEH) set H round(H * RandEH) set N
round(N * RandEH)
    set O round(O * RandEH) set P round(P * RandEH) set S round(S * RandEH) set C=C round(C=C *
RandEH) set Rings round(Rings * RandEH)  set Phenyl-rings round(Phenyl-rings * RandEH)
    set Alcohols round(Alcohols * RandEH) set Phenols round(Phenols * RandEH) set Ethers round(Ethers
* RandEH) set Esters round(Esters * RandEH) set Ketones round(Ketones  * RandEH)
    set Aldehydes round(Aldehydes * RandEH) set Acids round(Acids * RandEH) set Aromatic-Acids
round(Aromatic-Acids  * RandEH) set Amines round(Amines * RandEH) + 1 set Amides round(Amides *
RandEH)
    set C C + (Rings * 6) + Ketones + Aldehydes + Acids + Amides
    set C=C C=C + (Phenyl-rings * 3)
    set H H + (Rings * 5) + Alcohols + Aldehydes + Acids
    set O O + Alcohols + Ketones + Aldehydes + (Acids * 2) + Amides
    set N N + Amines + Amides
end

to alkene-hydration set C=C C=C - 1 set Alcohols Alcohols + 1 set H H + 2 set O O + 1 set ct-AlkH ct-
AlkH + 1 end

to alcohol-dehydration set H H - 2 set O O - 1 set Alcohols Alcohols - 1 set C=C C=C + 1 set ct-AlcD ct-
AlcD + 1 end

to weak-C=C set H H + 2 set O O + 2 set Alcohols Alcohols + 2 set C=C C=C - 1 set ct-WCC ct-WCC + 1
end

to strong-C=C
set O O + 2 set Aldehydes Aldehydes + 2 set C=C C=C - 1 set ct-SCC ct-SCC + 1
 if C=C > 0 [ifelse random-float 1 < (Phenyl-rings * 3) / C=C [set Rings Rings - 1] [splitC=C]]
  end

; carries out the splitting component of strong C=C oxidation
to splitC=C
  let splittable-C C - (Rings * 6) - Ketones - Aldehydes - Acids - Amides
  let splittable-C=C C=C - (Phenyl-rings * 3)
  let splittable-H H - (Rings * 5) - Alcohols - Aldehydes - Acids
  let splittable-O O - Alcohols - Ketones - Aldehydes - (Acids * 2) - Amides
  let splittable-N N - Amines - Amides
hatch 1 [set Log-MW round(Log-MW * (1 - RandEH)) set C round(splittable-C * (1 - RandEH)) set H
round(splittable-H * (1 - RandEH)) set N round(splittable-N * (1 - RandEH))
    set O round(splittable-O * (1 - RandEH)) set P round(P * (1 - RandEH)) set S round(S * (1 - RandEH))
set C=C round(splittable-C=C * (1 - RandEH)) set Rings round(Rings * (1 - RandEH))
    set Phenyl-rings round(Phenyl-rings * (1 - RandEH))
```

```
    set Alcohols round((Alcohols * (1 - RandEH))) set Phenols round(Phenols * (1 - RandEH)) set Ethers
round(Ethers * (1 - RandEH)) set Esters round(Esters * (1 - RandEH))
    set Ketones round(Ketones  * (1 - RandEH))
    set Aldehydes round(Aldehydes * (1 - RandEH)) set Acids round(Acids * (1 - RandEH)) set Aromatic-
Acids round(Aromatic-Acids  * (1 - RandEH)) set Amines round(Amines * (1 - RandEH))
    set Amides round(Amides * (1 - RandEH))
    set C C + (Rings * 6) + Ketones + Aldehydes + Acids + Amides
    set C=C C=C + (Phenyl-rings * 3)
    set H H + (Rings * 5) + Alcohols + Aldehydes + Acids
    set O O + Alcohols + Ketones + Aldehydes + (Acids * 2) + Amides
    set N N + Amines + Amides]
set Log-MW Log-MW * RandEH set C round(C * RandEH) set H round(H * RandEH) set N round(N *
RandEH)
    set O round(O * RandEH) set P round(P * RandEH) set S round(S * RandEH) set C=C round(C=C *
RandEH) set Rings round(Rings * RandEH)  set Phenyl-rings round(Phenyl-rings * RandEH)
    set Alcohols round(Alcohols * RandEH) set Phenols round(Phenols * RandEH) set Ethers round(Ethers
* RandEH) set Esters round(Esters * RandEH) set Ketones round(Ketones  * RandEH)
    set Aldehydes round(Aldehydes * RandEH) set Acids round(Acids * RandEH) set Aromatic-Acids
round(Aromatic-Acids  * RandEH) set Amines round(Amines * RandEH) set Amides round(Amides *
RandEH)
set C C + (Rings * 6) + Ketones + Aldehydes + Acids + Amides
    set C=C C=C + (Phenyl-rings * 3)
    set H H + (Rings * 5) + Alcohols + Aldehydes + Acids
    set O O + Alcohols + Ketones + Aldehydes + (Acids * 2) + Amides
    set N N + Amines + Amides
end

to alcohol-oxidation
set H H - 2 set Alcohols Alcohols - 1 set ct-AlcO ct-AlcO + 1
ifelse random-float 1 < 0.4 [set Ketones Ketones + 1][set Aldehydes Aldehydes + 1]
end

to decarboxylation set C C - 1 set O O - 2 set Acids Acids - 1 set ct-D ct-D + 1 end

; Condensation reactions depend on the presence of another molecule with certain functional groups.
; When condensing, the two molecules combine properties.
to ester-condensation
  if (any? other dissolveds with [Alcohols > 1])
[set cond_num [who] of one-of other dissolveds with [Alcohols > 1]
set Log-MW log-MW + [log-MW] of turtle cond_num
set C C + [C] of turtle cond_num
set H H - 2 + [H] of turtle cond_num
set N N + [N] of turtle cond_num
set O O + 1 + [O] of turtle cond_num
set P P + [P] of turtle cond_num
set S S + [S] of turtle cond_num
set C=C C=C + [C=C] of turtle cond_num
set Rings Rings + [Rings] of turtle cond_num
set Phenyl-rings Phenyl-rings + [Phenyl-rings] of turtle cond_num
set Alcohols Alcohols - 1 + [Alcohols] of turtle cond_num
set Phenols Phenols + [Phenols] of turtle cond_num
set Ethers Ethers + [Ethers] of turtle cond_num
set Esters Esters + 1 + [Esters] of turtle cond_num
set Ketones Ketones + [Ketones] of turtle cond_num
set Aldehydes Aldehydes + [Aldehydes] of turtle cond_num
set Acids Acids - 1 + [Acids] of turtle cond_num
```

```
set Aromatic-Acids Aromatic-Acids + [Aromatic-Acids] of turtle cond_num
set Amines Amines + [Amines] of turtle cond_num
set Amides Amides + [Amides] of turtle cond_num
set ct-EC ct-EC + 1
ask turtle cond_num
[die]]
end

to aldol-condensation
  if (any? other dissolveds with [Aldehydes > 0 or Ketones > 0])
[set cond_num [who] of one-of other dissolveds with [Alcohols > 1 or Ketones > 1]
set Log-MW log-MW + [log-MW] of turtle cond_num
set C C + [C] of turtle cond_num
set H H + [H] of turtle cond_num
set N N + [N] of turtle cond_num
set O O + [O] of turtle cond_num
set P P + [P] of turtle cond_num
set S S + [S] of turtle cond_num
set C=C C=C + [C=C] of turtle cond_num
set Rings Rings + [Rings] of turtle cond_num
set Phenyl-rings Phenyl-rings + [Phenyl-rings] of turtle cond_num
set Alcohols Alcohols + [Alcohols] of turtle cond_num
set Phenols Phenols + [Phenols] of turtle cond_num
set Ethers Ethers + [Ethers] of turtle cond_num
set Esters Esters + [Esters] of turtle cond_num
set Ketones Ketones + [Ketones] of turtle cond_num
set Aldehydes Aldehydes + [Aldehydes] of turtle cond_num
set Acids Acids + [Acids] of turtle cond_num
set Aromatic-Acids Aromatic-Acids + [Aromatic-Acids] of turtle cond_num
set Amines Amines + [Amines] of turtle cond_num
set Amides Amides + [Amides] of turtle cond_num
set ct-AC ct-AC + 1
ask turtle cond_num
[die]]
end

to new-weight
; Calculates new molecular weights and diffusivities
  ask turtles
[if breed != chlorides and identity != 7 [set Log-MW log ((C * 12.011) + (H * 1.008) + (N * 14.007)
    + (O * 15.999)) 10
  set size (Log-MW / 5)]]
; Diffusivity calculation found in Schwarzenbach and Gschwend (1993)
ask turtles [if breed != chlorides and identity != 7[let vol (C * 16.5) + (H * 2) + (O * 5.5) + (N * 5.7) + (S *
17) - ((rings + phenyl-rings) * 20.2)
set diff (13.26e-5 / ((dyn-visc ^ 1.14) * (vol ^ 0.589))) * 40000 set peclet [u] of patch-here / diff]] ;
diffusivity units: lu^2 / ts
end

to calc-properties
; Calculates analytical metrics: Hydrophobicity, molecular weight averages, and Aromaticity
  ask turtles
  [set turt-MW (10 ^ Log-MW)
    if C > 0
 ; Hydrophobicity
  [set Kow ((-1.53) + (sqrt(C) * 1.32) + ((H / C) * 0.518)
```

```
    + ((O / C) * (-4.88))
    + ((Acids / C) * 5.16)
    + ((Aromatic-acids / C) * 6.27)
    + ((Alcohols / C) * (-1.98)) + ((Phenols / C) * 0.633)
    + ((Aldehydes / C) * 1.092) + ((Ketones / C) * (-2.58))
    + ((Amines / C) * (-6.25)) + ((Amides / C) * (-5.95))
    + ((Esters / C) * 3.37))]]

; Molecular weight averages
 let Mt-Top sum [turt-MW] of dissolveds with [ycor > (max-pycor - 8) and ycor < (max-pycor - 2)]
 let Mt-Bottom sum [turt-MW] of dissolveds with [ycor < (min-pycor + 8) and ycor > (min-pycor + 2)]
 let ct-top count dissolveds with [ycor > (max-pycor - 8) and ycor < (max-pycor - 2)]
 let ct-bottom count dissolveds with [ycor < (min-pycor + 8) and ycor > (min-pycor + 2)]
 if ct-top > 0 [ set Mn-Top Mt-Top / ct-top]
 if ct-bottom > 0 [set Mn-Bottom Mt-Bottom / ct-bottom]
 let Mt-Top-sq sum [turt-MW ^ 2] of dissolveds with [ycor > (max-pycor - 8) and ycor < (max-pycor - 2)]
 let Mt-Bot-sq sum [turt-MW ^ 2] of dissolveds with [ycor < (min-pycor + 8) and ycor > (min-pycor + 2)]
 if ct-top > 0 [   set Mw-Top Mt-Top-sq / Mt-Top]
 if ct-bottom > 0 [set Mw-Bottom Mt-Bot-sq / Mt-Bottom]

; Aromaticity
if ct-top > 0 [  set Ar-Top (2 * sum [C=C] of dissolveds with [ycor > (max-pycor - 8) and ycor < (max-
pycor - 2)]) / sum [C] of dissolveds with [ycor > (max-pycor - 8) and ycor < (max-pycor - 2)]]
if ct-bottom > 0 and sum [C] of dissolveds with [ycor < min-pycor + 8] > 0 [ set Ar-Bottom (2 * sum
[C=C] of dissolveds with [ycor < (min-pycor + 8) and ycor > (min-pycor + 2)]) / sum [C] of dissolveds
with [ycor < (min-pycor + 8) and ycor > (min-pycor + 2)]]
end

to histo-MW-Sorb
; Plot count of turtles in simulation space
  set-current-plot "Count”
  set-current-plot-pen "dissolveds" plot count dissolveds
  set-current-plot-pen "sorbates" plot count sorbates
  set-current-plot-pen "total" plot (count turtles - count dormants)

; Plot mean residence time of molecules
  set-current-plot "Residence Time"
  set-current-plot-pen "Mean RT"
  if count dormants > 1 [plot mean [res-time] of dormants]
  set-current-plot-pen "Mean - 1 StDev"
  if count dormants > 1 [plot (mean [res-time] of dormants) - (standard-deviation [res-time] of dormants)]

; Plot DOC concentrations
set-current-plot "DOC Conc"
let vol-top count patches with [pycor > (max-pycor - 8) and pycor  < (max-pycor - 2) and pcolor > 7]
let vol-bottom count patches with [pycor < (min-pycor + 8) and pycor > (min-pycor + 2) and pcolor > 7]
set-current-plot-pen "Top"
set top-conc (sum [turt-MW] of dissolveds with [ycor > (max-pycor - 8) and ycor < (max-pycor - 2)]) / vol-
top
plot top-conc
set-current-plot-pen "Bottom"
set bot-conc (sum [turt-MW] of dissolveds with [ycor < (min-pycor + 8) and ycor > (min-pycor + 2)]) / vol-
bottom
plot bot-conc
end
```

APPENDIX E: METHODOLOGICAL NOTES

This appendix contains methods details too extensive to include in Chapter 2.

I. Combustion Analysis

Following the August 17, 2011 sampling trip, filtered turbid material from well 8 was combusted to determine organic carbon content. Approximately 100 mL of sample water was filtered through each of four 0.7 µm Whatman GF/F glass fiber filters. These filters were weighed, dried overnight at 110°C, weighed again, combusted at 450°C in a muffle furnace overnight, and weighed a final time. Percent organic carbon was determined as:

$$\left(1 - \frac{(W_{dr} - W_{cl}) - (W_{co} - W_{cl})}{W_{dr} - W_{cl}}\right) \times 100$$

W_{dr} = weight of dried filter, W_{co} = weight of combusted filter, and W_{cl} = weight of clean filter.

II. DOC Concentration Analysis

Most samples were analyzed for total organic carbon on an OI 9210E total carbon analyzer by reagentless electrochemical oxidation and NDIR CO_2 detection. Samples from the August and September 2011 sampling events were analyzed on a Shimadzu TOC-VCSH by Pt catalyzed combustion at 680°C and NDIR CO_2 detection and after acidification and sparging to remove inorganic carbon.

Each sample for TOC analysis was previously filtered to 0.2 µm (0.7 µm prior to Jun 15, 2011) and stored in precombusted glass TOC vials, capped with either Parafilm or a cap with a Teflon septum. Calibration curves for the OI 9210E instrument were generated using TOC standards of 0, 0.25, 0.5, 5, 15, 25, and 30 ppm.

KNO_3 was used as the total nitrogen standard on the Shimadzu TOC-VCSH. HCl was used to remove inorganic carbon from samples.

III. Field Sampling Protocol

Some procedures were adapted from the USGS National Field Manual for the Collection of Water Quality Data (US Geological Survey, variously dated).

At each field sampling well, the cap was removed and depth to water measured using a Solinst water level meter. The in-situ pressure transducer was removed and acid-washed Tygon sample tubing inserted to approximately 6 inches above the bottom of the well.

A Masterflex peristaltic sampling pump was set to a low flow rate, approximately 0.1 L/min, as estimated during each sampling event. The well was purged for ten minutes according to low-flow sampling procedures, as described in Chapter 2.

After the purge period, the outflow tubing was inserted to the bottom of a clean, precombusted glass bottle and the bottle was filled from the bottom up. The bottle was allowed to overflow before tubing was removed. The process was repeated for a clean, acid-washed Nalgene bottle.

Samples were immediately placed on ice in a cooler. Outflow tubing was decontaminated by rinsing with MilliQ water. When all wells had been sampled, water levels were re-measured and the pressure transducers replaced.

Filtration protocol is outlined in Chapter 2.

IV. High-Pressure Liquid Chromatography

High Pressure Size Exclusion Chromatography (HP-SEC) used a Waters Protein-Pak 125 silica column with a 2 µM KH_2PO_4 + 0.1 N NaCl eluent buffered to pH 6.8 using 1 M NaOH. This eluent was filtered to 0.2 µm. The flow rate was 1 mL/min and the detector wavelength was 230 nm. We used polystyrene sulfonate standards of peak molecular weight 15800, 6430, and 5180 Da along with salicylic acid, as calibration standards.

V. Absorbance Data Post-Processing

Absorbance was measured on a Shimadzu UV-2550 UV-Vis Spectrophotometer from 200 to 700 nm with a step size of 1 nm, using a 1 cm quartz cuvette. Data were copied and pasted from UV-Vis software into a Microsoft Excel spreadsheet. Molar absorptivity at 280 nm (ε280) was calculated from absorbance data as follows.

Derivation of ε280 begins with the Beer-Lambert Law,

$$A = \varepsilon c l$$

where A = absorbance in absorbance units, ε the molar absorptivity in L mol^{-1} cm^{-1}, c the concentration of the analyte in moles per liter, and l the pathlength, 1 cm in this case. Rearranging the Beer-Lambert Law yields the following equation for ε280, using the measurement of absorbance at 280 nm and the TOC concentration in the sample.

$$\varepsilon 280 = \frac{A_{280}}{(Moles\ C\ L^{-1}) * 1\ cm}$$

ε280 is correlated to aromaticity (r^2 = 0.90) by the following equation (Chin et al., 1994).

$$Aromaticity = 0.05 * \varepsilon 280 + 6.74$$

ε280 is also correlated to weight-average molecular weight (in Daltons) by the following equation (ibid.).

$$M_w = 3.99 * \varepsilon 280 + 490$$

Absorbance data were used to calculate the inner filter effect (IFE) correction factor (McKnight et al., 2001) applied to fluorescent excitation-emission matrices (EEMs).

$$IFE = 10^{-A(total)}$$

where

$$A(total) = A_{excit} * 0.5\ cm + A_{emiss} * 0.5\ cm$$

where A_{excit} = absorbance at the excitation wavelength and A_{emiss} = absorbance at the emission wavelength. 0.5 cm is considered the effective path length within the sample cuvette.

APPENDIX F: THREE-COMPONENT PARALLEL FACTOR ANALYSIS MODEL FITTED TO JEMEZ RIVER MEANDER FLUORESCENCE DATA

I. Introduction

Parallel factor analysis (PARAFAC) is a statistical decomposition technique used to derive unique components that explain the variation in a three-dimensional matrix sample. It is used in this study (and further described in Chapter 2) to analyze fluorescence of DOC samples taken at the Jemez River meander field site.

The three-component model was developed using 310 samples taken between July 2010 and December 2011. Blank samples were omitted from the sample set as outliers. Samples W8 from July 22, 2010, W5b from April 16, 2011, EFB from July 19, 2011, and Push-Pull Input from September 23, 2011 (see Appendix A) were also omitted from the sample set as outliers.

The three-component model fitted to experimental data is provided here in table form and accompanied by graphical visualizations of these components.

II. Component Vectors

Table 26. Component (Cpt) excitation vectors

λ (nm)	Cpt 1	Cpt 2	Cpt 3
230	0.0434	0	0.115
235	0.0581	0	0.115
240	0.0740	0	0.115
245	0.0851	0.00960	0.116
250	0.0931	0.0361	0.125
255	0.0986	0.0694	0.141
260	0.105	0.0967	0.160
265	0.109	0.119	0.178
270	0.111	0.134	0.195
275	0.111	0.141	0.212
280	0.112	0.141	0.227
285	0.117	0.136	0.241
290	0.125	0.131	0.252
295	0.134	0.124	0.256
300	0.149	0.118	0.260
305	0.165	0.117	0.263
310	0.183	0.117	0.264
315	0.203	0.119	0.262
320	0.221	0.123	0.256
325	0.239	0.130	0.245
330	0.255	0.138	0.224
335	0.270	0.150	0.195
340	0.282	0.165	0.156
345	0.286	0.182	0.115
350	0.281	0.200	0.0691
355	0.265	0.216	0.0289
360	0.237	0.227	0.00500
365	0.204	0.235	0
370	0.173	0.236	0
375	0.142	0.233	0
380	0.116	0.230	0
385	0.0914	0.220	0
390	0.0678	0.212	0
395	0.0462	0.208	0
400	0.0254	0.196	0
405	0.00774	0.176	0.00158
410	0	0.162	0.00393
415	0	0.143	0.00270
420	0	0.129	0.00275
425	0	0.111	0.00321
430	0	0.0987	0.00333
435	0	0.0884	0.00278
440	0	0.0811	0.00135
445	0	0.0717	0
450	0	0.0699	0

Table 27. Component (Cpt) emission vectors

λ (nm)	Cpt 1	Cpt 2	Cpt 3
250	0	0	0.000708
255	0	0	0.00142
260	0	0	0.00255
265	0	0	0.00453
270	0	0	0.00663
275	0	0	0.00995
280	0	0	0.0147
285	0	0	0.0227
290	0	0	0.0332
295	0	0	0.0509
300	0	0	0.0703
305	0	0	0.0878
310	0	0	0.103
315	0	0	0.114
320	0	0	0.124
325	0	0	0.134
330	0	0	0.143
335	0	0	0.153
340	0	0	0.165
345	0	0	0.184
350	0.00531	0	0.199
355	0.0208	0	0.206
360	0.0404	0	0.210
365	0.0644	0	0.210
370	0.0871	0	0.215
375	0.111	0	0.220
380	0.134	0	0.228
385	0.157	0	0.234
390	0.181	0	0.236
395	0.208	0	0.232
400	0.235	0	0.220
405	0.261	0	0.202
410	0.274	0.0171	0.185
415	0.279	0.0412	0.169
420	0.278	0.0689	0.153
425	0.272	0.0979	0.138
430	0.263	0.126	0.123
435	0.251	0.151	0.111
440	0.238	0.171	0.100
445	0.223	0.192	0.0889
450	0.207	0.208	0.0822
455	0.188	0.222	0.0764
460	0.169	0.233	0.0734
465	0.152	0.240	0.0686
470	0.132	0.245	0.0737
475	0.116	0.246	0.0684
480	0.0969	0.245	0.0703
485	0.0816	0.241	0.0721
490	0.0691	0.237	0.0706
495	0.0562	0.231	0.0727
500	0.0458	0.222	0.0720
505	0.0363	0.212	0.0688
510	0.0281	0.200	0.0670
515	0.0215	0.187	0.0668
520	0.0170	0.172	0.0645
525	0.0107	0.160	0.0638
530	0.00780	0.146	0.0610
535	0.004841	0.133	0.0571
540	0.00219	0.121	0.0556
545	0.000794	0.109	0.0502
550	0	0.0969	0.0465
555	0	0.0859	0.0375
560	0	0.0751	0.0354

Table 27 -- Continued

565	3.12E-05	0.0656	0.0245
570	0	0.0569	0.0234
575	0.00196	0.0478	0.0111
580	0.00171	0.0414	0.0115
585	0.00266	0.0347	0.000936
590	0.00294	0.0295	0.00155
595	0.00236	0.0251	0
600	0	0.0194	0

III. Figures of Components

Two-Dimensional Representation

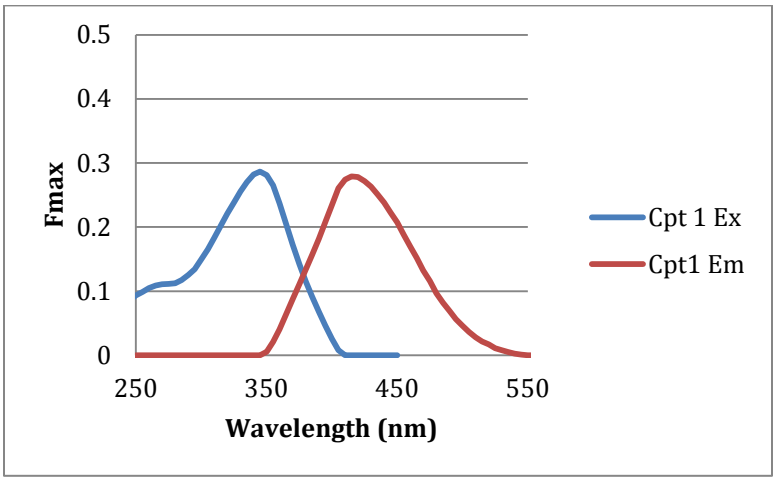

Figure 48. Excitation and emission vectors of component 1.

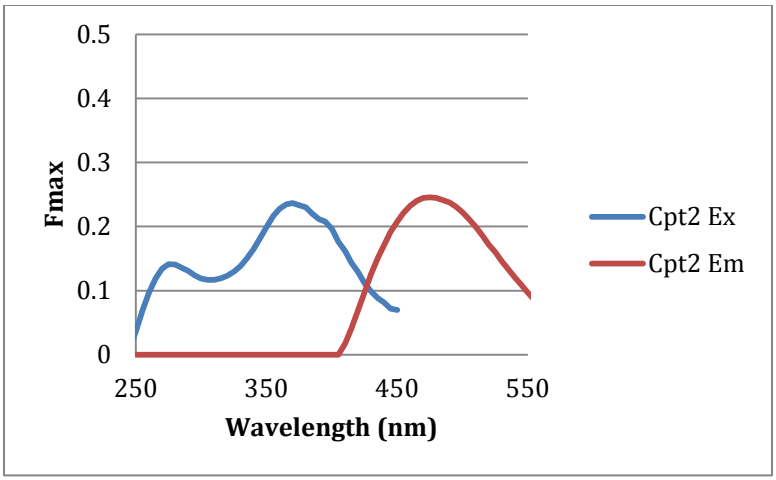

Figure 49. Excitation and emission vectors of component 2.

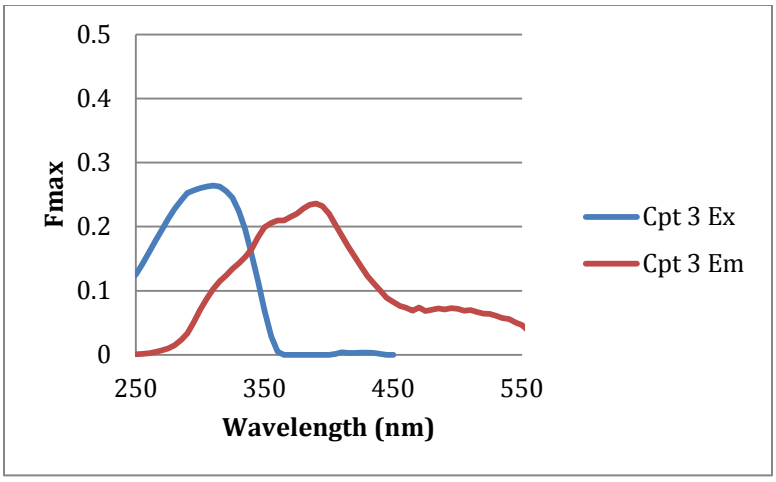

Figure 50. Excitation and emission vectors of component 3.

Three-Dimensional Renderings

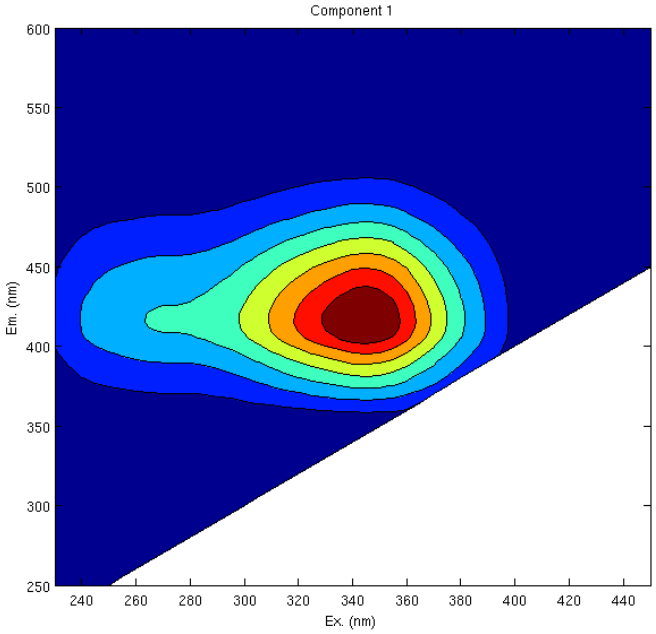

Figure 51. Component 1 rendered as an excitation-emission matrix (EEM).

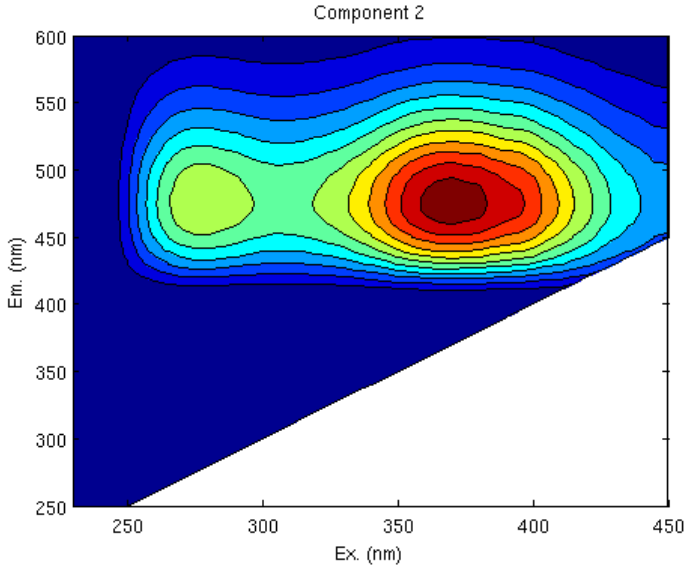

Figure 52. Component 2 rendered as an EEM.

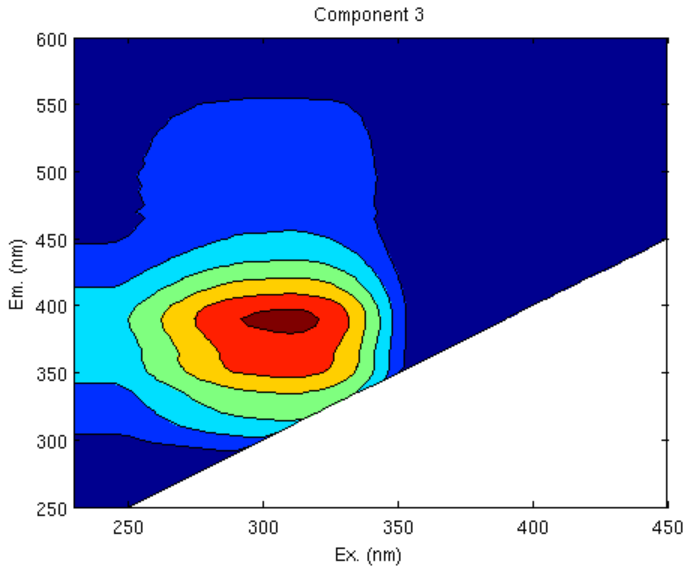

Figure 53. Component 3 rendered as an EEM.

REFERENCES CITED

Aerts, R., and F.S. Chapin III, 2000. The mineral nutrition of wild plants revisited: A re-evaluation of processes and patterns. In Advances in Ecological Research, Vol. 30, A.H. Fitter & D.G. Raffaelli, eds. Academic Press.

Ågren, A., I. Buffam, M. Berggren, K. Bishop, M. Jansson, H. Laudon, 2008. Dissolved organic carbon characteristics in boreal streams in a forest-wetland gradient during the transition between winter and summer. Journal of Geophysical Research 113, G03031.

Ainsworth, E.A., S.P. Long, 2005. What have we learned from 15 years of free-air CO_2 enrichment (FACE)? A meta-analytic review of the responses of photosynthesis, canopy. New Phytol. 165, 351–371.

Amon, R.M.W, R. Benner, 1996. Bacterial utilization of different size classes of dissolved organic matter. Limnology and Oceanography 41, 41-51.

Andrews, J.A., R. Matamala, K.M. Westover, W.H. Schlesinger, 2000. Temperature effects on the diversity of soil heterotrophs and the $\delta^{13}C$ of soil-respired CO_2. Soil Biology & Biogeochemistry 32, 699-706.

Arthurs, L., P.A. Maurice, X. Xiang, R. Kennedy, G.R. Madey. 2004. "Agent-based stochastic simulation of natural organic matter adsorption and mobility in soils." Oral presentation, Eleventh International Symposium on Water-Rock Interaction. Saratoga Springs, New York. June 2004.

Baghoth, S.A., S.K. Sharma, G.L. Amy, 2011. Tracking natural organic matter (NOM) in a drinking water treatment plant using fluorescence excitation-emission matrices and PARAFAC. Water Research 45,797-809.

Baker, M.A., C.N. Dahm, H.M. Valett, 1999. Acetate retention and metabolism in the hyporheic zone of a mountain stream. Limnology and Oceanography 44, 1530-1539.

Baker, M.A., H.M. Valett, C.N. Dahm, 2000. Organic carbon supply and metabolism in a shallow groundwater ecosystem. Ecology 81, 3133-3148.

Bartschat, B.M., S.E. Cabaniss, F.M.M. Morel, 1992. Oligoelectrolyte model for cation binding by humic substances. Environmental Science & Technology, 26, 284-294.

Boano, F., A. Demaria, R. Revelli, L. Ridolfi. 2010. Biogeochemical zonation due to intrameander hyporheic flow. Water Resources Research 46, W02511.

Bonabeau, E., 2002. Agent-based modeling: Methods and techniques for simulating human systems. Proceedings of the National Academy of Sciences of the United States of America 99, 7280 – 7287.

Bowen, B., 1996. Rainfall and climate variation over a sloping New Mexico plateau during the North American monsoon. Journal of Climate 9, 3432-3442.

Boyer, E.W, G.M. Hornberger, K.E. Bencala, D.M. McKnight, 1996. Overview of a simple model describing variation of dissolved organic carbon in an upland catchment. Ecological Modeling 86, 183 – 188.

Boyle, E.A., J.M. Edmond, E.R. Sholkovitz, 1977. The mechanism of iron removal in estuaries. Geochimica et Cosmochimica Acta, 41, 1313–1324.

Brooks, P.D., D.M. McKnight, K.E. Bencala, 1999. The relationship between soil heterotrophic activity, soil dissolved organic carbon (DOC) leachate, and catchment-scale DOC export in headwater catchments. Water Resources Research 35, 1895-1902.

Brooks, P.D., M.M. Lemon, 2007. Spatial variability in dissolved organic matter and inorganic nitrogen concentrations in a semiarid stream, San Pedro River, Arizona. Journal of Geophysical Research, 112, G03S05.

Brooks, P.D., P.A. Haas, A.K. Huth, 2007. Seasonal variability in the concentration and flux of organic matter and inorganic nitrogen in a semiarid catchment, San Pedro River, Arizona. Journal of Geophysical Research 112, G03S04.

Cabaniss, S.E., 2008. Quantitative structure-property relationships for predicting metal binding by organic ligands. Environmental Science & Technology 42, 5210-5216.

Cabaniss, S.E., G. Madey, L. Leff, P.A. Maurice, R. Wetzel, 2005. A stochastic model for the synthesis and degradation of natural organic matter. Part I. Data structures and reaction kinetics. Biogeochemistry 76, 319-347.

Cabaniss, S.E., G. Madey, L. Leff, P.A. Maurice, R. Wetzel. 2007. A stochastic model for the synthesis and degradation of natural organic matter. Part II. Molecular property distributions. Biogeochemistry, 86, 269-286.

Cabaniss, S.E., P. Maurice, G. Madey, 2007. A stochastic model for the synthesis and degradation of natural organic matter. Part III: Modeling Cu(II) complexation. Applied Geochemistry 22, 1646-1658.

Cabaniss, S.E., Q. Zhou, P.A. Maurice, Y-P. Chin, G.R. Aiken, 2000. A log-normal distribution model for the molecular weight of aquatic fulvic acids. Environmental Science & Technology 34, 1103-1109.

Cardenas, M.B., 2009. Stream-aquifer interactions and hyporheic exchange in gaining and losing sinuous streams. Water Resources Research 45, W06429.

Cassiani, G., L.F. Burbery, M. Giustiniani, 2005. A note on in situ estimates of sorption using push-pull tests. Water Resources Research 41, W03005.

Chapelle, F.H., P.M. Bradley, D.J. Goode, C. Tiedeman, P.J. Lacombe, K. Kaiser, R. Benner, 2009. Biochemical indicators for the bioavailability of organic carbon in ground water. Ground water 47, 108-121.

Chappelle, F.H. 1993. Ground-water Microbiology and Geochemistry. John Wiley & Sons, New York, NY. 424 pp.

Chin, Y-P., G. Aiken, E. O'Loughlin, 1994. Molecular weight, polydispersity, and spectroscopic properties of aquatic humic substances. Environmental Science & Technology 28, 1853-1858.

Chiou, C.T., R.I. Malcolm, T.I. Brinton, D.E. Kile, 1986. Water solubility enhancement of some organic pollutants and pesticides by dissolved humic and fulvic-acids. Environmental Science & Technology, 20, 502-508.

Coble, P.G., 1996. Characterization of marine and terrestrial DOM in seawater using excitation-emission matrix spectroscopy. Marine Chemistry 51, 325-346.

Cory, R.M., D.M. McKnight, 2005. Fluorescence spectroscopy reveals ubiquitous presence of oxidized and reduced quinones in dissolved organic matter. Environmental Science & Technology 39, 8142-8149.

Dahm, C.N., M.A. Baker, D.I. Moore, J.R. Thibault, 2003. Coupled biogeochemical and hydrological responses of streams and rivers to drought. Freshwater Biology 48, 1219-1231.

Davis, J.A, J.O. Leckie, 1978. Effects of adsorbed complexing ligands on trace metal uptake by hydrous oxides. Environmental Science & Technology, 12, 1309–1315.

Deng, Y.W., and W. Stumm, 1994. Reactivity of aquatic iron(III) oxyhydroxides: Implications for redox cycling of iron in natural waters. Applied Geochemistry 9, 23 – 36.

Di Toro, D.M., H.E. Allen, H.L. Bergman, J.S. Meyer, P.R. Paquin, R.C. Santore, 2001. Biotic ligand model of the acute toxicity of metals. 1. Technical basis. Environmental Toxicology and Chemistry 20, 2383-2396.

Elder, D.J.E., D.J. Kelly, 1994. The bacterial degradation of benzoic acid and benzenoid compounds under anaerobic conditions- Unifying trends and new perspectives. FEMS Microbiology Reviews 13, 441-468.

Fellman, J.B., E. Hood, R.G.M. Spencer, 2010. Fluorescence spectroscopy opens new windows into dissolved organic matter dynamics in freshwater ecosystems: A review. Limnology and Oceanography 55, 2452-2462.

Fetter, C.W. 2001. *Applied Hydrogeology*. Prentice-Hall, Upper Saddle River, NJ. 598 pp.

Findlay, S., D. Strayer, C. Goumbala, K. Gould, 1993. Metabolism of streamwater dissolved organic carbon in the shallow hyporheic zone. Limnology and Oceanography 38, 1493-1499.

Fischer, H., F. Kloep, S. Wilzcek, M.T. Pusch, 2005. A river's liver – microbial processes within the hyporheic zone of a large lowland river. Biogeochemistry 76, 349-371.

Goff F, Gardner J.N., 1994. Evolution of a mineralized geothermal system, Valles Caldera, New Mexico. Economic Geology 89: 1803–1832.

Goff, F., Gardner, J.N., Reneau, S.L., Goff, C.J., 2005. Preliminary geologic map of the Redondo Peak quadrangle, Sandoval County, New Mexico. N.M. Bureau Geology & Mineral Res, Open-file Geol. Map OF-GM-111, scale 1:24,000.

Gomez, J.D. and J.L. Wilson, 2011 "Flow dynamics and connectivity of meandering streams and shallow aquifers: an observational study in northern New Mexico." Poster, AGU Fall Meeting, Dec 2011.

Grimm, V., E. Revillia, U. Berger, F. Jeltsch, W.M.Mooij, S.F. Railsback, H.H.Thulke, J. Weiner, T. Weigand, D.L. DeAngelis, 2005. Pattern-oriented modeling of agent-based complex sustems: Lessons from ecology. Science 310, 987 – 991.

Groffman, A.R., L.J. Crossey, 1999. Transient redox regimes in a shallow alluvial aquifer. Chemical Geology 161, 415 – 442.

Hansch. C., A. Leo and D. Hoekman. 1995. Exploring QSAR. Hydrophobic, Electronic, and Steric Constants. ACS Professional Reference Book. Washington, DC: American Chemical Society.

Hedin, L.O., J.C. von Fischer, N.E. Ostrom, B.P. Kennedy, M.G. Brown, G.P. Robertson, 1998. Thermodynamic constraints on nitrogen transformations and other biogeochemical processes at soil-stream interfaces. Ecology 79, 684-703.

Helms, J.R., A. Stubbins, J.D. Richie, E.C. Minor, D.J. Kieber, K. Mopper, 2008. Absorption spectral slopes and slope ratios as indicators of molecular weight, source, and

photobleaching of chromophoric dissolved organic matter. Limnology and Oceanography 53, 955-969.

Hering, J.G., F.M.M. Morel, 1988. Humic acid complexation of calcium and copper. Environmental Science & Technology, 22, 1234-1237.

Hornberger, G.M, K.E. Bencala, D.M. McKnight, 1994. Hydrological controls on dissolved organic carbon during snowmelt in the Snake River near Montezuma, Colorado. Biogeochemistry 25, 147-165.

Huang, J., J.A. Christ, M.N. Goltz, 2010. Analytical solutions for efficient interpretation of single-well push-pull tracer tests. Water Resources Research 46, W08538.

InciWeb Incident Information System, http://inciweb.org/incident/2385/ , updated 8/3/2011, accessed 1/5/2012.

Ishii, S.K.L., T.H. Boyer, 2012. Behavior of reoccurring PARAFAC components in fluorescent dissolved organic matter in natural and engineered systems: A critical review. Environmental Science & Technology 46, 2006 – 2017.

Istok, J.D., J.A. Field, M.H. Schroth, 2001. In situ determination of subsurface microbial enzyme kinetics. Ground Water 39, 348-355.

Jennings, N.R., 2001. An agent-based approach for building complex software systems. Communications of the ACM 44, 35 – 41.

Johnson, M.S., E.G. Couto, M. Abdo, J. Lehmann, 2011. Fluorescence index as an indicator of dissolved organic carbon quality in hydrologic flowpaths of forested tropical watersheds. Biogeochemistry 105, 149-157.

Kanokkantapong, V., T.F. Marhaba, B. Panyapinyophol, P. Pavasant, 2006. FTIR evaluation of functional groups involved in the formation of haloacetic acids during the chlorination of raw water. Journal of Hazardous Materials B136, 188-196.

Kaplan, L.A. J.D. Newbold. 2000. Surface and subsurface dissolved organic carbon. pp. 237-258 In: Streams and Ground Waters, J.B. Jones and P.J. Mulholland, eds. Academic Press.

Kiersch, K., J. Kruse, K-U. Eckhardt, A. Fendt, T. Streibel, R. Zimmerman, G. Broll, P. Leinweber. 2012. Impact of grassland burning on soil organic matter as revealed by a synchrotron- and pyrolysis-mass spectrometry-based multi-methodological approach. Organic Geochemistry 44, 8 – 20.

Kim, Y., M. Azizan, J. Istok, L. Semprini, 2006. Field push-pull test protocol for aerobic cometabolism of chlorinated aliphatic hydrocarbons. Oregon State University, prepared for Environmental Security Technology Certification Program, U.S. Air Force.

Klapper, L., D.M. McKnight, J.R. Fulton, E.L. Blunt-Harris, K.P. Nevin, D.R. Lovley, P.G. Hatcher, 2002. Fulvic acid oxidation state detection using fluorescence spectroscopy. Environmental Science & Technology 36, 3170-3175.

Kleikemper, J., S.A. Pombo, M.H. Schroth, W.V. Sigler, M. Pesaro, J. Zeyer, 2005. Activity and diversity of methanogens in a petroleum hydrocarbon-contaminated aquifer. Applied and Environmental Microbiology 71, 149 – 158.

Kostrzeski J.M., P.D. Brooks, 2005. Quantifying the effects of vegetation and water source on water quality in three watersheds in Valles Caldera National Preserve, New Mexico. EOS Trans. AGU, 86(52), Fall Meet. Suppl., Abstract H31B-1312.

Kothawala, D.N., R.D. Evans, P.J. Dillon, 2006. Changes in the molecular weight distribution of dissolved organic carbon within a Precambrian shield stream. Water Resources Research 42, W05401.

Kothawala, D.N., T.R. Moore, W.H. Hendershot, 2009. Soil properties controlling the adsorption of dissolved organic carbon to mineral soils. Soil Science Society of America Journal 73, 1831 – 1842.

Langmuir, D. 1997. Aqueous Environmental Geochemistry. Prentice-Hall, Upper Saddle River, NJ. 600 pp.

Li, Y., E.J. LeBoeuf, 2010. Investigation of transport- and sorption-related factors on the removal of hydrophobic organic compounds in heterogeneous soils using a hierarchical modeling approach. Transp. Porous Med. 84, 319-333.

Liu, F., R. Parmenter, P.D. Brooks, M.H. Conklin, R.C. Bales, 2008. Seasonal and interannual variation of streamflow pathways and biogeochemical implications in semiarid, forested catchments in Valles Caldera, New Mexico. Ecohydrology 1, 239-252.

Lovely, D.R., E.J.P. Phillips, 1988. Novel mode of microbial energy metabolism: Organic carbon oxidation coupled to dissimilatory reduction of iron or manganese. Applied and Environmental Microbiology 54, 1472-1480.

Lutz, B.D., E.S. Bernhardt, B.J. Roberts, R.M. Cory, P.J. Mulholland, 2012. Distinguishing dynamics of dissolved organic matter components in a forested stream using kinetic enrichments. Limnology and Oceanography 57, 76-89.

Lyons, M.M., F.C. Dobbs. 2012. Differential utilization of carbon substrates by aggregate-associated and water-associated heterotrophic bacterial communities. Hydrobiologia 686, 181-193.

Manizza, M., M.J. Follows, S. Dutkiewicz, J.W. McClelland, D. Menemenlis, C. N. Hill, A. Townsend-Small, B.J. Peterson, 2009. Modeling transport and fate of riverine

dissolved organic carbon in the Arctic Ocean. Global Biogeochemical Cycles, 23, GB4006.

Maurice, P.A., S.E. Cabaniss, J. Drummond, E. Ito, 2002. Hydrogeochemical controls on the variations in chemical characteristics of natural organic matter at a small freshwater wetland. Chemical Geology 187, 59-77.

McKnight, D.M., E.W. Boyer, P.K. Westerhoff, P.T. Doran, T. Kulbe, D.T. Anderson, 2001. Spectrofluorometric characterization of dissolved organic matter for indication of precursor organic material and aromaticity. Limnology and Oceanography 46, 38-48.

Michalzik, B., E. Tipping, J. Mulder, J.F. Gallardo Lancho, E. Matzner, C.L. Bryant, N. Clarke, S. Lofts, M.A. Vicente Esteban, 2003. Modelling the production and transport of dissolved organic carbon in forest soils. Biogeochemistry, 66, 241-264.

Mishra, A.K., 1997. Reactive Transport in Chemically and Physically Heterogeneous Porous Media: Effect of Non-Equilibrium Linear Sorption. PhD Dissertation, New Mexico Institute of Mining and Technology, Socorro, NM, 217 pp.

Mladenov, N., D.M. McKnight, S.A. Macko, M. Norris, R.M. Cory, L. Ramberg, 2007. Chemical characterization of DOM in channels of a seasonal wetland. Aquatic Sciences 69, 456-471.

Mobed, J.J., S.L. Hemmingsen, J.L. Autry, L.B. McGown, 1996. Fluorescence characterization of IHSS humic substances: Total luminescence spectra with absorbance correction. Environmental Science & Technology 30, 3061-3065.

Mopper, K., Z. Feng, S.B. Bentjen, R.F. Chen, 1996. Effects of cross-flow filtration in the absorption and fluorescence properties of seawater. Marine Chemistry 55, 53 – 74.

Morales, V.L., W. Zhang, B. Gao, L.W. Lion, J.J. Bisogni, Jr., B.A. McDonough, T.S. Steenhuis, 2011. Impact of dissolved organic matter on colloid transport in the vadose zone: Deterministic approximation of transport deposition coefficients from polymeric coating characteristics. Water Research 45, 1691-1701.

Morrice, J.A., C.N. Dahm, H.M. Valett, P.V. Unnikrishna, M.E. Campana, 2000. Terminal electron accepting processes in the alluvial sediments of a headwater stream. Journal of the North American Benthological Society 19, 593 – 608.

New Mexico Environment Department, 2006. Final approved total maximum daily load for the Jemez River watershed, Valles Caldera National Preserve, boundaries to headwaters. 207 pp.

Onstad, G.D., D.E. Canfield, P.D. Quay, J.I. Hedges, 2000. Sources of particulate organic matter in rivers from the continental USA: Lignin phenol and stable carbon isotope compositions. Geochimica et Cosmochimica Acta 64, 3539 – 3546.

Pan, B., P. Ning, B. Xing, 2009. Part V- sorption of pharmaceuticals and personal care products. Environmental Science & Pollution Research 16, 106-116.

Parker, S.R., S.R. Poulson, M.G. Smith, C.L. Weyer, K.M. Bates, 2010. Temporal variability in the concentration and stable carbon isotope composition of dissolved inorganic and organic carbon in two Montana, USA rivers. Aquatic Geochemistry 16, 61 – 84.

Phillips, E.H., 2004. Collapse and resurgence of the Valles caldera, Jemez Mountains, New Mexico: 40Ar/39Ar age constraints on the timing and duration of resurgence and ages of megabreccia blocks. M.S. thesis, N.M. Institute of Mining and Technology, Socorro, N.M. 200 pp.

Pullin, M.J., C. Anthony, P.A. Maurice, 2007. Effects of iron on the molecular weight distribution, light absorption, and fluorescence properties of natural organic matter. Environmental Engineering Science 24, 987 – 997.

Pullin, M.J., C.A. Progress, P.A. Maurice, 2004. Effects of photoirradiation on the adsorption of dissolved organic matter to goethite. Geochimica et Cosmochimica Acta 68, 3643-3656.

Pullin, M.J., S.E. Cabaniss, 1995. Rank Analysis of the pH Dependent Synchronous Fluorescence Spectra of Six Standard Humic Substances, Environmental Science and Technology, 29, 1460-1467.

Puls, R.W., M.J. Barcelona, 1996. Low-flow (minimal drawdown) ground-water sampling procedures. USEPA Office of Research and Development. 12 pp.

Robertson, A.P., J.O. Leckie, 1999. Acid/Base, copper binding, and Cu^{2+}/H^{+} exchange properties of a soil humic acid, an experimental and modeling study. Environmental Science & Technology, 33, 786-795.

Rodriguez, M., and E. Moser, 2010. Hydrology – Existing Condition Report. Valles Caldera Trust, 21 pp.

Schwarzenbach, R.P., P.M. Gschwend. 1993. Environmental Organic Chemistry. John Wiley & Sons, New York, NY.

Smith, R.L., R.A. Bailey, C.S. Ross, 1970. Geologic map of the Jemez Mountains, New Mexico. Misc. Geol. Invest. Map. I-571.

Sobczak, W.V., S. Findlay, 2002. Variation in bioavailability of dissolved organic carbon among stream hyporheic flowpaths. Ecology 83, 3194 – 3209.

Sobczak, W.V., S. Findlay, S. Dye, 2003. Relationships between DOC bioavailability and nitrate removal in an upland stream: An experimental approach. Biogeochemistry 62, 309 – 327.

Stanford, J.A., J.V. Ward, 1988. The hyporheic habitat of river ecosystems. Nature 335, 64 – 65.

State of New Mexico, 2005. Potential Effects of Climate Change on New Mexico. Agency Technical Working Group. 47 pp.

Stedmon, C. A., S. Markager, and R. Bro, 2003. Tracing dissolved organic matter in aquatic environments using a new approach to fluorescence spectroscopy. Marine Chemistry, 82, 239 – 254.

Stedmon, C.A., R. Bro, 2008. Characterizing dissolved organic matter fluorescence with parallel factor analysis: a tutorial. Limnology and Oceanography: Methods 6, 1-6.

Stedmon, C.A., S. Markager, 2005. Resolving the variability in dissolved organic matter fluorescence in a temperate estuary and its catchment using PARAFAC analysis. Limnology and Oceanography 50, 686-697.

Sukop, M. C. & D. T. Thorne, Jr, 2005. Lattice Boltzmann Modeling: An Introduction for Geoscientists and Engineers. (2nd Ed.) Springer, New York, NY. 172 p.

Thiele-Bruhn S., T. Seibicke, H.R. Schulten, P. Leinweber, 2004. Sorption of sulfonamide pharmaceutical antibiotics on whole soils and particle-size fractions. Journal of Environmental Quality 33, 1331–1342.

Thurman, E.M. 1985. Amount of Organic Carbon in Natural Waters, in Organic Geochemistry of Natural Waters, Nijhoff/Junk, p. 7-65.

Tonina, D., J.M. Buffington, 2007. Hyporheic exchange in gravel-bed rivers with pool-riffle morphology: Laboratory experiments and three-dimensional modeling. Water Resources Research 43, W01421.

Tonina, D., J.M. Buffington, 2009. Hyporheic exchange in mountain rivers I: Mechanics and environmental effects. Geography Compass 3, doi: 10.1111/j.1749-8198.2009.00226.x

Tosiani, T., W. Melendez, F. Vivas, 2006. Modeling humic acids transport in a bauxite profile: Los Pijiguaos, Venezuela. Journal of Geochemical Exploration, 88, 246-248.

Triska, F.J., V.C. Kennedy, R.J. Avanzino, G.W. Zellweger, K.E. Bencala, 1989. Retension and transport of nutrients in a 3rd-order stream in northwestern California – Hyporheic processes. Ecology 70, 1893 – 1905.

U.S. Environmental Protection Agency. 2012. Estimation Programs Interface Suite™ for Microsoft® Windows, v 4.10. United States Environmental Protection Agency, Washington, DC, USA.

U.S. Geological Survey, variously dated, National field manual for the collection of water-quality data: U.S. Geological Survey Techniques of Water-Resources Investigations, book 9, chaps. A1-A9, available online at http://pubs.water.usgs.gov/twri9A.

U.S. Global Change Research Program (2009), "Regional Climate Impacts: Southwest" in Global Climate Change Impacts in the United States. 129-134.

vallescaldera.com, "85% of Las Conchas Fire now contained; smoldering blaze dampened by moisture, causing flash flood threat." July 22, 2011. http://vallescaldera.com/archives/date/2011/07, accessed 1/5/2012.

Van Horn, D.J., R.L. Sinsabaugh, C.D. Takacs-Vesbach, K.R. Mitchell, C.N. Dahm, 2011. Response of heterotrophic stream biofilm communities to a gradient of resources. Aquatic Microbial Ecology 64, 149-161.

Volk, C.J., C.B. Volk, L.A. Kaplan, 1997. Chemical composition of biodegradable dissolved organic matter in streamwater. Limnology & Oceanography 42, 39 – 44.

Weishaar, J.L., G.R. Aiken, B.A. Bergamaschi, M.S. Fram, R. Fujii, K. Mopper, 2003. Evaluation of specific ultraviolet absorbance as an indicator of the chemical composition and reactivity of dissolved organic carbon. Environmental Science & Technology 37, 4702-4708.

Wetzel, R.G. 1992. Gradient-dominated ecosystems - sources and regulatory functions of dissolved organic-matter in fresh-water ecosystems. Hydrobiologia, 229, 181-198.

Wetzel, R.G. 1995. Death, detritus, and energy-flow in aquatic ecosystems. Freshwater Biology, 33, 83-89.

Wilensky, U. 1999. NetLogo. http://ccl.northwestern.edu/netlogo/. Center for Connected Learning and Computer-Based Modeling, Northwestern University. Evanston, IL. (Accessed 2 Mar 2012).

Wong, J.C.Y., D.D. Williams, 2009. Sources and seasonal patterns of dissolved organic matter (DOM) in the hyporheic zone. Hydrobiologia 647, 99-111.

Wroblicky, G.J., M.E. Campana, H.M. Valett, C.N. Dahm, 1998. Seasonal variation in surface-subsurface water exchange and lateral hyporheic area of two stream-aquifer systems. Water Resources Research 34, 317-328.

Young, D.F., B.R. Munson, T.H. Okiishi, 2004. A Brief Introduction to Fluid Mechanics (3rd ed.) John Wiley and Sons, Inc., Hoboken, NJ. 533 pp.

Zarnetske, J. P., R. Haggerty, S. M. Wondzell, and M. A. Baker (2011), Dynamics of nitrate production and removal as a function of residence time in the hyporheic zone, Journal of Geophysical Research 116, G01025, doi:10.1029/2010JG001356.

Zhou, Q., S.E. Cabaniss, P.A. Maurice, 2000. Considerations in the use of high-pressure size exclusion chromatography (HPSEC) for determining molecular weights of aquatic humic substances. Water Research 34, 3505-3514.

Zhou, Q.H., P.A. Maurice, S.E. Cabaniss. 2001. Size fractionation upon adsorption of fulvic acid on goethite: Equilibrium and kinetic studies. Geochimica et Cosmochimica Acta 65, 803-812.

Zou, Q, X. He, 1997. On pressure and velocity boundaries for the lattice Boltzmann BGK model. Physics of Fluids 9, 1591-1598.